Identifying Genes in Wheat Involved in Soil Erosion

Zoë Kitching

Faculty of Life Sciences
The University of Bristol

Supervisors: Prof Claire Grierson, Dr Emily R Larson
and Prof Keith Edwards

A dissertation submitted to the University of Bristol
in accordance with the requirements for award of
the degree of MSc(R) in the Faculty of Life Sciences.

November 2022
Word count: 20171

Abstract

Soil erosion threatens global food security by reducing crop yields. Thus it is essential that we develop crops with traits that can limit soil erosion rates. Plant roots play an important role in stabilising soil and reducing erosion. Recently, work is beginning to elucidate the mechanisms by which they do this using in vitro assays and model plant species. However, the traits that underpin root-soil cohesion in crop species have not yet been characterised in detail. This is mainly due to the difficultly in phenotyping roots and the lack of effective assays. Here I present a novel uprooting assay for measuring root-soil cohesion in wheat (*Triticum aestivum*). This work also provides wheat mutant lines for genes that may effect root-soil cohesion and genetic constructs to investigate the wheat gene *TaXTH23* in model plant species. The uprooting assay revealed that uprooted soil per root length does not change between growth stage (GS) 10 and GS11 but significantly increases at GS13. It also showed that uprooted soil mass increased linearly with root length density (RLD) at all growth stages. This work also successfully identified and crossed wheat TILLING and deletion lines to generate mutants for two genes of interest whose orthologs affected root-substrate cohesion in *Arabidopsis thaliana* and expressed the wheat gene *TaXTH23* in the model plant species *A. thaliana*. The uprooting assay developed could help identify traits that affect root-soil cohesion and reduce soil erosion.

Declaration

I declare that the work in this dissertation was carried out in accordance with the requirements of the University's Regulations and Code of Practice for Research Degree Programmes and that it has not been submitted for any other academic award. Except where indicated by specific reference in the text, the work is the candidate's own work. Work done in collaboration with, or with the assistance of, others, is indicated as such. Any views expressed in the dissertation are those of the author.
SIGNED:

DATE: 18/11/22

Acknowledgements

I would like to thank my supervisors Prof. Claire Grierson, for her invaluable supervision and support, Dr. Emily Larson for all her time, advice and support in the lab and throughout the year and Prof. Keith Edwards, this could not have happened with out his expertise and advice in all things wheat. I would also like to thank the generous support of Bristol Centre for Agricultural Innovation who funded my work. Additionally, I am very grateful to Dr Alice Baillie, Dr Beth Eldridge and Bryony Gardener who generously provided their advice, materials and excellent lab company. I am also very grateful to my fellow MSc students, inhabitants of 94 Cranbrook Road and parents for their unwavering supporting.

Contents

1 Introduction **4**
- 1.1 Soil erosion . . . 4
- 1.2 Soil Erosion Mitigation . . . 5
- 1.3 Measuring the effect of roots on soil erosion . . . 6
  - 1.3.1 Hydraulic flume . . . 7
  - 1.3.2 Uprooting . . . 8
- 1.4 Role of Exudates in Root-Soil Cohesion . . . 9
  - 1.4.1 Direct Effects of Exudates on Root-Soil Cohesion . . . 10
  - 1.4.2 Indirect effect of exudates on root-soil cohesion . . . 13
- 1.5 Aims . . . 14

2 Materials and Methods **15**
- 2.1 Bacterial Strains and Plant Lines . . . 15
- 2.2 Breeding Wheat Mutant Lines . . . 15
  - 2.2.1 Mutant Line Selection . . . 15
  - 2.2.2 Genotyping Parental Lines . . . 17
  - 2.2.3 TILLING Parental Line Genotyping by Sequencing . . . 17
  - 2.2.4 Deletion Line Genotyping . . . 21
  - 2.2.5 Wheat Mutant Line Crossing . . . 22
- 2.3 Development of Novel Soil Erosion Assay for Wheat . . . 25
  - 2.3.1 Soil Composition Analysis . . . 25
  - 2.3.2 Making Uprooting Anchors for Wheat Seedlings . . . 25
  - 2.3.3 Development of a Wheat Uprooting Protocol . . . 25
  - 2.3.4 Uprooting Wheat Seedlings . . . 27
- 2.4 Cloning *XTH23* and Expression in Model Plant Species . . . 32
  - 2.4.1 Genotyping of *xth23 A. thaliana* Mutant Line . . . 32
  - 2.4.2 RT-PCR of *xth23* Mutant Line . . . 33
  - 2.4.3 Stable and Transient Expression of *TaXTH23* in Model Plant Species . . . 37
  - 2.4.4 Microbiology Methods . . . 38

2.4.5 Molecular Biology Methods 40
2.4.6 Transformation of Model Plant Species with *A. tumefaciens* . 42
2.4.7 Microscopy 43
2.4.8 Plant Materials, Growth Conditions and Medium 43

3 Results **44**
3.1 Breeding of Wheat Mutant Lines 44
3.1.1 Genotyping Deletion Lines by PCR 45
3.1.2 Progeny of Deletion Line Crosses are Double *TaXTH23* Mutants 48
3.1.3 Genotyping *TaATH6* Mutant TILLING Lines 49
3.2 Developing a Soil Erosion Assay for Wheat 54
3.2.1 Soil Composition Analysis 54
3.2.2 Development of Uprooting Methods 55
3.2.3 Uprooting Wheat Seedlings at Different Growth Stages 57
3.3 Stable and Transient Expression of *TaXTH23* in Model Plant Species 62
3.3.1 Gateway Cloning of *XTH23* 62
3.3.2 The *xth23 Arabidopsis thalina* Mutant is Homozygous but not a Knockout 70

4 Discussion **74**
4.1 Uprooting of Wheat Seedlings as an Assay for Identifying Traits which Influence Soil Erosion Rates. 74
4.2 Breeding Mutant Wheat Lines 77
4.3 Expression of *XTH23* in Model Species 81
4.4 Conclusions 83

5 Appendix **85**

Abbreviations

Abbreviation	Full Name
°C	Degrees Celsius
35S / CaMV35S	Cauliflower Mosaic Virus 35S Promoter
ABC transporter	ATP-Binding Cassette transporter
ATH6	*ATP Binding Cassette Transporter 2 Homolog 6*
ATP	Adenosine TriPhosphate
AtXTH19	*Arabidopsis thaliana Xyloglucan Endotransglycoslyase 19 gene*
AtXTH23	*Arabidopsis thaliana Xyloglucan Endotransglycoslyase 23 gene*
bp	Base Pairs
C terminus	Carboxyl-terminus
Cad	Cadenza wheat
cDNA	Complimentary DNA
cm	Centimetre
Col-0	Columbia-0 ecotype
CRISPR	Clustered Regularly Interspaced Short Palindromic Repeats
d	Days
d.p.	Decemal Place
DNA	Deoxyribose Nucleic Acid
EF1α	*Elongation factor 1-alpha gene*
EMS	Ethyl MethaneSulfonate
g	Grams
gDNA	Genomic DNA
Gent	Gentamicin
GFP	Green Fluorescent protein
GmR	*Gentamicin Resistance Gene*
GS	Growth Stage
GUS	*Beta-glucuronidase gene*
h	Hours
HMW	High Molecular Weight
kb	Kilobases

km	Kilometre
LB	Luria Broth
LB primer	Left Border primer
m	Metre
mg	Milligram
min	Minutes
ml	Millilitre
mm	Millimetre
mRNA	Messenger RiboNucleic Acid
MS	Murashige and Skoog basal Media
n	Sample size
N terminus	Amino-terminus
NASC	Nottingham Arabidopsis Stock Centre
ng	Nanograms
nm	Nanometre
p	P value
PB buffer	Phosphate Buffer
PCR	Polymerase Chain Reaction
PDR2	phosphate deficiency response 2 gene
PE buffer	Phosphate Ethanol Buffer
pro	Native Promoter
PTFE	PolyTetraFluoroEthylene
R^2	Coefficient of determination
RD	Root Density
RFP	Red Fluorescent protein
RL	Root Length
RLD	Root Length Density
RNA	RiboNucleic Acid
RNAi	RNA interference
RSAD	Root Surface Area Density
RT-PCR	Reverse Transcription Polymerase Chain Reaction
s	Seconds
s.f.	Significant Figures
SpR	*Spectinomycin Resistance gene*
Spec	Spectinomycin
t	T test statistic value
T-DNA	Transfere DNA
T-test	Hypothesis Test Statistic
TaATH6	*Triticum aestivum ATP Binding Cassette Transporter 2 Homolog 6*

TAE	Tris-Acetate-Ethylenediaminetetraacetic acid
TALENs	Transcription Activator-Like Effector Nucleases
Taq	Thermus Aquaticus DNA polymerase
TaXTH19	*Triticum aestivum Xyloglucan Endotransglycoslyase 19 gene*
TaXTH23	*Triticum aestivum Xyloglucan Endotransglycoslyase 23 gene*
TILLING	Targeting Induced Local Lesions in Genomes
V	Volts
w/v	Weight/volume %
WT	Wild Type
x g	Gravity
XTH	Xyloglucan Endotransglycoslyase
μ	Mean
μg	Microgram
μl	Microlitre
μmol	Micromole

Chapter 1

Introduction

1.1 Soil erosion

We live in a world where human survival is intrinsically linked to the soil. Over 99% of our food is dependent on it, with only 0.3% coming from rivers and oceans [1]. Thus, looking after soil is essential for human well-being. However, much of the world's soil is under threat from soil erosion, with 80% of agricultural land experiencing moderate to severe rates [1]. This issue should be of the highest priority as it severely impacts food security and has toppled civilisations before like the Mayans and Mesopotamians [2]. Soil erosion is one of the physical mechanisms by which soil is degraded and is characterised as the detachment, transportation, and deposition of soil particles [2]. Causal factors of soil erosion include both natural and agricultural processes. In agricultural systems, soil erosion is primarily driven by rainwater, although in some places wind also contributes [3]. Rainwater can detach soil particles in several ways, including raindrops hitting the surface of the soil, over land and through flow. These processes degrade soil by reducing soil depth, removing organic matter and nutrients, and decreasing its water storage capacity. With climate change fuelling a more vigorous hydrological cycle that creates stronger, longer, and more frequent storms, rates of soil erosion are only predicted to increase. Estimates vary from 10% to 66% but either way are unsustainable and will severely affect global food security by reducing crop yields [4, 5].

Soil erosion reduces crop yields by mechanically damaging crops and reducing the soil's nutrient content, water-holding capacity, and biodiversity [1]. Eventually, this leads to the soil becoming so degraded it is no longer agriculturally productive. The degraded land is then abandoned, reducing the amount of available fertile land for crop production. Reduction of global yields could have serious implications for food security, which is already under pressure from a growing population. Currently, global

yields are predicted to be outstripped by demand before 2050 [6]. Further expansion into natural ecosystems is also not a sustainable solution as 38% of the world's land mass is already covered by agriculture [7, 8].

In addition to compromising agriculture, soil erosion causes a host of other issues. The main economic costs associated with soil erosion are often downstream from the site of erosion and, in the UK alone is over £1 billion a year [9]. Soil erosion increases the sediment and pollutants in water systems, which directly affects human well-being by reducing drinking water quality and increasing flood risks through the build-up of sediments in urban drains, rivers and canals [9, 10]. Moreover, sediments and agricultural runoff indirectly affect human well-being by damaging freshwater and ocean ecosystems. Increased sediments, nutrients and pollutants in water systems reduce their biodiversity by harming aquatic organisms and promoting algal blooms that release toxins and cause anoxia, reducing the aquatic ecosystem's ability to provide essential ecosystem services [10].

1.2 Soil Erosion Mitigation

Although soil erosion is driven by the weather the expansion of intensive agriculture has played a huge role in increasing global rates of soil erosion. Intensive agricultural practices such as tilling, tree and hedge removal, and drainage improvements, along with heavy machinery and monocultures all work to increase soil erosion rates by increasing over land flow and disturbing the soil. Other influences on the rate of soil erosion include slope angle, soil type, the force of the erosive agent, and vegetative cover, all of which are largely out of farmers' control, except for the vegetative cover. Thus, most soil conservation techniques aim to reduce soil erosion by protecting the soil with a biomass cover [3]. These techniques work by intercepting raindrops before they hit the soil surface to reduce their ability to detach soil particles and by slowing over land flow, reducing its capacity to transport the detached soil particles and encouraging the water to infiltrate the soil. Techniques that reduce soil erosion by using a biomass cover include no-tillage, mulches, cover crops and agroforestry. Many of these practices cost money to implement and result in a yield loss. Thus, farmers have little incentive to carry them out [10] and other solutions are needed that do not require drastic changes in agricultural techniques or compromise crop yields.

Genetic improvements to crops to enhance soil erosion-reducing traits could be one such solution. The breeding and engineering of genetically enhanced crops have been successful in other areas and are thought to have entirely counterbalanced the effects of climate change on crop yields since the 1980s [11]. The genetic improvement of crops also does not require changes to agricultural techniques and has lower investment costs [10]. Bread wheat, *Triticum aestivum* is a pertinent target crop to

reduce global soil erosion as it covers the greatest land mass of any other crop. It also provides a large part of our nutrition accounting for approximately 20% of human calories and protein consumption [11] making it highly relevant to food security.

The greatest potential for reducing soil erosion through genetic improvements lies in root phenotypes. Many studies have looked at the importance of vegetation cover on soil erosion rates, but Zhou et al. [12] and De Baets et al. [13] have shown that plant roots hold far greater potential to reduce soil erosion rates. They estimated that 95% of a plant's ability to reduce erosion by over land flow could be attributed to the roots. Additionally, above-ground organs have been optimised for increased yields and therefore any changes in their morphology to reduce soil erosion would be likely to negatively affect yields [11]. Therefore, identifying and targeting root traits should be prioritised over above ground traits in the context of reducing soil erosion.

The remainder of this chapter will focus on methods for identifying plant traits that reduce soil erosion and the role of exudates in reducing soil erosion rates in the context of cereals, with a focus on wheat.

1.3 Measuring the effect of roots on soil erosion

Roots are thought to reduce soil erosion in a variety of ways: physical reinforcement, by enmeshing soil particles that increase friction and the tensile strength of the soil; increasing water infiltration by reinforcing pores and creating channels for water to run down; and increasing aggregate stability directly through sticky root secretions or indirectly by modifying soil chemistry within the microbiome.

Studies on the effects roots have on soil erosion are relatively few compared to the number of those on above-ground plant cover, mainly due to the difficulty in observing root traits directly and the lack of effective proxies [14]. It is harder still to understand the underlying biology and physiology as a myriad of interconnected factors contribute to soil cohesion. Most studies have compared species with different root morphologies to identify traits that affect soil erosion or root-soil cohesion. Investigations of root morphology have included root length density (RLD)[15–18], root surface area density (RSAD)[18], root length (RL) [19] and root density (RD) [17]. RLD and RSAD are key measurements of root morphology, RLD is the length of roots in a given volume of soil whereas RSAD is the root surface area in a given volume of soil, generally a m^3. The effect of plant roots RLD on soil erosion and root-soil cohesion has generally been studied using 1. hydraulic flume assays and 2. uprooting assays.

1.3.1 Hydraulic flume

Hydraulic flume assays use a flume in the lab to mimic over land flow events on a sample of root-soil composite. They are effective ways of measuring the effect plants have on soil erosion, as important physical and biological variables and confounding factors can be controlled and measured. Physical factors that need to be taken into consideration include soil type [20], soil compaction [2], water content [21], slope angle [22], and critically the force applied to the soil by the water (shear stress)[13, 21, 23]. Biological factors such as plant species, planting density, above-ground cover, and the microbiome also must be considered when investigating root-soil cohesion and soil erosion. The higher level of control provided by the hydraulic flume assay compared to field studies allows a more detailed analysis of the role of plant traits in soil erosion without all the background noise. To date, hydraulic flume investigations have focused on identifying plant species and their morphological traits that have the potential to reduce soil erosion and restore degraded lands [13, 15, 17, 18, 24]. All have focused on uncultivated plant species except Li et al., who investigated the role of wheat seedling surface cover [21]. Through species comparisons of soil detachment and morphological traits, studies generally agree that amongst the measured morphological root traits, RLD and RSAD have the greatest impact on soil detachment rates under concentrated water flow events. Furthermore, De Baets et al. [13], Hao et al. [17] and Wang et al. [15] all found a negative exponential relationship between RLD and soil detachment, with increasing RLD between 0 and 400 km/m^3 resulting in large decreases in soil detachment. In Wang et al. [15] and De Baets et al. [13], soil detachment was reduced to nearly 0 at RLDs greater than approximately 200 and 400 km/m^3 , respectively. RLD ranged from 10 to 30 km/m^3 in Hao et al [17] which still resulted in significant decreases in soil erodibility. This suggests that a small enhancement in root morphology could drastically reduce soil erosion rates.

Other findings from hydraulic flume studies showed that fibrous roots are better than tap root systems and perennial species are better than annuals at reducing soil erosion and should, therefore, be used for land regeneration and soil and water conservation [15, 18]. However, these conclusions were drawn from comparisons of only a few species. Xu et al. [18] only compared one perennial species with one annual species, while Wang et al. [15] compared only ten, five fibrous root and five tap root systems, all from the same habitat. Thus, it is unconvincing to conclude that all tap root systems and all perennials are better at reducing soil erosion. Indeed, some grass pioneer species with fibrous roots may actually be at an advantage not enforcing soil cohesion as unstable soil could exclude competitors [25].

Though the hydraulic flume studies provide useful findings. In the context of restoring degraded land, many of the studies do not consider the differences in root exudates and microbiomes between species, both of which affect root-soil cohesion

and, therefore, probably influence soil erosion rates [24]. To date, only one study has used the hydraulic flume to measure soil erosion rates for crop species [21]. Li et al. [21] carried out a hydraulic flume experiment on wheat but focused on the role of above-ground cover. However, they found that soil moisture levels before the concentrated flow event offset any effect of the wheat seedling above-ground cover. It is well known that above-ground cover affects soil erosion rates. The hydraulic flume assay's inability to detect changes in plant cover, indicates that it may not be sensitive enough and/or contain too much noise to identify underlying biological traits that affect soil erosion. The hydraulic flume assay also requires a relatively high input of time, space and resources compared to uprooting.

1.3.2 Uprooting

Uprooting is when a plant is pulled out of the soil substrate. In natural and agricultural systems, this process is generally experienced as lodging and weeding. Lodging is when the stem is permanently toppled to a horizontal position and is generally caused by high winds. Experimental uprooting is generally carried out by exerting an upwards force on the base of the plant and can help assess simple hypotheses about root-soil cohesion. Uprooting also has relevance in other areas such as lodging, no-till farming and weed removal. Thus far, only two studies have investigated uprooting in cereals, which is surprising given the loss of cereal crop yields due to lodging. Ennos [19] uprooted wheat plants and Edmaier et al., [20] investigated oat, *Avena sativa*. Ennos [19] uprooted three seven day old and four three week old seedlings at 5 mm/min to investigate the root's ability to resist lodging. This work showed that at seven days old the wheat seedlings' roots snapped off in the soil and that older plants had stronger and stiffer roots than younger ones increasing their resistance to uprooting. This study however applied the vertical uprooting force to the shoot which broke before the roots, and it is also not clear what soil or moisture content was used. Edmaier et al., [20] investigated the relationship between uprooting force and root architecture and soil variables. He also found that older plants had a greater resistance to uprooting. Additionally, this study showed a linear relationship between maximum uprooting force and root length and an exponential relationship between uprooting work done and root length, which was repeated in *A. thaliana* by Denbigh [25]. The effects of soil moisture and sediment size on uprooting forces were also investigated, both of which significantly effected uprooting forces. Together work by Ennos [19] and Edmaier et al. [20] show that uprooting cereals can be a powerful tool to investigate mechanical and architectural root traits and highlight important confounding factors.

Other crop species investigated using uprooting include sunflower [26], carrot [27], and onion [28]. Sunflower has been uprooted to investigate traits that could influence

susceptibility to lodging which it is particularly vulnerable due to its large heavy flowers [26]. Carrots and onions need to be uprooted for harvesting and therefore identifying traits which reduce uprooting force in these species may reduce energy required to harvest them [27, 28]. Non-crop species have included a variety of grass weeds [29, 30] and *A. thaliana* [16, 25, 28]. Model wood and rubber roots have also been uprooted to evaluate mechanical effects of root structures on soil stability [31]. However, it is debatable whether model wooden or rubber roots act in a similar way to real living ones. All the studies generally agree that older, more dense root systems and longer tap roots are better at resisting uprooting than young, dispersed root systems and species with short tap roots. Uprooting in the cereals could be a useful way to identify root traits that affect root-substrate cohesion, with implications for reducing soil erosion and lodging. However, Ennos [19] clamped the wheat seedlings around the base of the stem and found that the leaves consistently broke before the roots and hypothesized that this was an adaptation to grazing. Thus, uprooting by clamping the shoot is not appropriate for trying to measure root-soil cohesion. All the methods for uprooting use clamp or rope attached to the stem of the plant, except for De Beats et al. [16], who used a metal washer beneath the rosette of the *A. thaliana* plant to anchor it to the machine applying the uprooting force. Using a metal washer would not uproot wheat seedlings as they would slip through the hole of the washer but modifying the methods and finding a different shaped anchor could result in an effective uprooting assay for wheat. Furthermore, De Baets et al. [16] showed that the uprooting resistance of *A. thaliana* mutants was an effective proxy for soil erosion, as root hair-less mutants that were less resistant to uprooting than the wild type (WT) also had higher rates of soil erosion in a hydraulic flume experiment.

1.4 Role of Exudates in Root-Soil Cohesion

Root morphology is known to affect soil erosion rates in many species and has been investigated using many different methods and has focused on slope stabilisation and soil conservation. However, Hawkesford [11] reported that any changes to root architecture may not be beneficial in agricultural systems as plants are grown at very high densities. The high density of plants means there is little room for increases in root density or length and investment into larger, denser root systems may actually be disadvantageous. Enhancing root exudation, however, could also result in reduced soil erosion rates, as exudates have been shown to affect soil properties and root-substrate cohesion [32–35]. Exudates are compounds secreted from plant roots that help plants interact with and adapt to their environment (reviewed in [36, 37]). Their role in plant function is clearly important, as plants exude up to 20% of their fixed carbon [37], with the greatest proportion being polysaccharide-derived sugars, amino acids

and organic acids [38]. Exudates are involved in a wide variety of functions including water and nutrient uptake [39, 40], pathogen defence [41], the attraction of beneficial microbes, root lubrication [42] and plant-plant interactions [43]. Root exudates are important in facilitating multiple essential plant functions in the rhizosphere but the specific exudates and their function in the rhizosphere are poorly characterised. The following section will summarise the evidence that root exudates are also involved in root-soil cohesion, an important root function which helps anchor plants to the soil.

1.4.1 Direct Effects of Exudates on Root-Soil Cohesion

Role of Polysaccharide Exudates in Soil Cohesion

Recent studies have shown that exudates have soil adhesive properties that can directly change soil cohesion and stability[32, 35, 38, 44]. Akhtar et al. [32] used nitrocellulose sheets to immobilise spots of high molecular weight (HMW) exudates from maize, barley, wheat, pea, tomato and liverwort. The amount of soil that stuck to each spot was then quantified, which showed that soil adhered to the exudates for all the species at exudates masses between 50 and 10 µg. Wheat HMW exudates were found to be the most adhesive, which was consistent with findings for wheat and maize in Galloway et al. [34] and barley in Galloway et al. [33], both of which found that HMW exudates could adhere to soil in vitro. Galloway et al. [32] treated the HMW exudate spots with periodate oxidation, which depolymerises polysaccharides into shorter chain oligosaccharides [45]. After this treatment the amount of soil that adhered to the spots significantly decreased, indicating that it was the polysaccharides that were responsible for the soil adhesion. To test whether wheat roots naturally secreted high enough concentrations of exudates to adhere to soil particles, wheat seedlings were applied to nitrocellulose sheets for two hours and removed before the sheet was covered with soil. When the nitrocellulose sheet was washed, soil stuck to where the roots had been, indicating that the seedlings had secreted enough polysaccharide exudates in two hours to adhere soil particles. Work by Naveed et al. [38] has also shown that maize exudates can stabilise soil particles; however, conversely, they found that barley exudates dispersed soil particles. This suggests that the ability of exudates to bind soil particles may be species specific, which would not be surprising given that exudate composition and function are known to differ between species, developmental stage, and environment [37, 46]. Analysis of wheat HMW exudate composition with gas chromatography-mass spectrometry found that the polysaccharides xyloglucan and heteroxylan, and the glycoproteins arabinogalactan protein and extensin were the most abundant [34]. These results suggest that these polysaccharides may be the most important in exudate function and therefore also root-soil cohesion.

Of the tested polysaccharides present in exudates, xyloglucan seems to play the largest role in root-soil cohesion in vitro [32, 34]. Xyloglucans are hemicellulose polysaccharides with a $\beta 1-4$ linked d-glucan backbone and xylose side residues [47, 48]. In the cell wall, xyloglucans cross-link with cellulose microfibrils and are thought to strengthen the cell wall [48]. Analysis of wheat, maize and barley exudate composition has identified xyloglucan as one of the main components [33, 34]. Immunocytochemistry and cytochemical staining have shown that xyloglucan creates a dense fibrous network in the rhizosphere by crossing-linking with other polysaccharides such as heteroxylan and arabinogalactan [49]. This fibrous network of xyloglucan encloses border cells in the rhizosphere of pea plants. In wheat, exuded xyloglucan is distinct from that in the cell wall, indicating that it has a specific function and is not just released from the degradation of the root cap and border cells [34]. Its functions are thought to vary from stabilising other exudate compounds to entrapping border cells and preventing pathogen penetration [49]. Work by Akhtar et al. [32] has also shown that xyloglucan has soil-binding properties. When compared to other plant polysaccharides, xyloglucan was one of the stickiest. Overall, the work discussed so far suggests that exuded xyloglucan is the main polysaccharide involved in root-soil cohesion, as it is one of the most abundant polysaccharides in root exudates, creates a fibrous network of linked polysaccharides in the rhizosphere and can adhere soil particles in vitro. This makes xyloglucan exudation a potential target for altering root-soil cohesion. Although the findings discussed here must be taken with some caution because they used commercially available xyloglucans and HMW exudates from hydroponically grown plants. Whether hydroponically grown plants produce similar quantities and composition of exudates as plants grown in soil is currently unknown due to the challenge of extracting exudates from soil-grown plants .

The Role of Protein Exudates in Root-Soil Cohesion

Root exudates also contain many proteins; however, literature on their role in root-soil cohesion is limited. A few studies have identified proteins that have adhesive properties in the climbing plant species, English ivy (*Hedera helix*), but have not been investigated in the context of soil cohesion [50]. Protein exudates have not yet been shown to have soil adhesive properties, but some have been identified that can modify root-substrate cohesion by altering exudate composition and structure. So far, the proteins that have been identified are ATP binding cassette (ABC) transporters and xyloglucan endotransglycosylases (XTHs) proteins [35, 51].

ABC transporters

High molecular weight exudates must be transported from inside root cells out to the rhizosphere [52]. The mechanisms by which roots export exudates into the rhizosphere have not yet been fully characterised. Recently, the ABC transporter *pdr2* mutant was shown to have altered exudate composition when compared with WT [52]. Most ABC transporters are membrane intrinsic active pumps that require ATP to function. They can transport a wide variety of carbon compounds, including lipids phytohormones, carboxylates, chlorophyll catabolites and also heavy metals [53]. There are many members of the ABC transporter gene family in plants, some of which are essential for abiotic and biotic stress responses and development. Recent work by Eldridge et al. [35] found that the ABC transporter mutants *pdr2* and *abcg43* were much less likely to detach from an agar growth medium under centrifugal force than WT (0.38 and 0.36 times, respectively). This indicates that they had enhanced root-substrate cohesion and shows that by targeting ABC transporters, root-substrate cohesion can be altered. Other similar ABC transporters such as *ATH6* have also been identified as potential modifiers of root exudate composition and conveniently a wheat double mutant TILLING (targeting induced local lesions in genomes) line has a been identified by [54], making it quicker and easier to test the effects of an ABC transporter on root exudate composition in a relevant crop species.

Xyloglucan Endotransglycosylases

XTHs are a group of glycosylase enzymes that cleave and re-join xyloglucan fibres and hydrolyse them [47, 48]. This ability to cut and stick xyloglucan fibres allows XTHs to remodel the cell wall and facilitate cell expansion [55]. The XTHs are encoded by a multi-gene family which consists of 33 members in *A. thaliana,* 29 in rice and >57 in wheat [56–58]. Many of the family members exhibit temporally and spatially specific expression patterns and are important in several plant physiological processes, including germination [59], plant defence [60] and fruit ripening [61]. *XTH23* and *XTH19* are both highly expressed in plant roots and are specifically involved in lateral root development and salt stress responses in *A. thaliana* [62, 63]. Xu et al. [18] showed that *xth23* and *xth19* mutants had reduced lateral root formation and increased sensitivity to salt stress, whilst constitutive over-expression led to enhanced lateral root formation and resistance to salt stress. This study also demonstrated that *XTH23* and *XTH19* expression is controlled by the brassinosteroid pathway, as they were both directly downstream of the transcription factor *BES1*.

XTH23 and *XTH19* may also play a role in root-soil cohesion and the XTH23 protein has been identified in root exudates [51]. *XTH19* on the other hand was not, though this may have been as exudates were collected from plants between three

and four weeks old and *XTH19* may be specifically expressed in young seedlings. Whether the XTHs alter root-substrate cohesion was investigated by Pulumbo [51] using the centrifuge assay from Eldridge et al. [35] and *xth A. thaliana* mutants. Both *xth23* and *xth19* resisted detachment compared to WT, indicating that the mutants had increased root-substrate cohesion. This was also not down to changes in root hair length or density, both of which are known to affect root substrate cohesion, as the mutants did not differ from WT in these phenotypes [16, 35]. Thus, *XTH23* and *XTH19* probably alter root-substrate cohesion by altering xyloglucans in the rhizosphere, which changes the polysaccharide matrix. Therefore, these genes may be a good target for enhancing soil erosion rates in crop species. This led Mahony [54] to identify orthologs of *A. thaliana (At)XTH23* and *AtXTH19* in crop species, including wheat. Further investigation is needed to determine whether the orthologs in wheat have the same function as in *A. thaliana*.

1.4.2 Indirect effect of exudates on root-soil cohesion

Exudates may also be able to indirectly affect root-soil cohesion by changing the function and structure of the rhizobiome, which is composed of microorganisms associated with plant roots [37, 52]. Secreting a tailored cocktail of exudates, plants could encourage microbes in the rhizobiome to produce adhesive compounds. They could also attract beneficial microbes and repel pathogens to change the composition and structure of the rhizobiome. In turn, changing the chemical composition of the rhizosphere and potentially the stability of the soil. The rhizobiome is sensitive to the exudates a plant secretes as shown in Badri et al. [52]. This study showed that an *A. thaliana* mutant for the ABC transporter *pdr2* had an altered exudate profile with fewer sugars and more phenolics. The *pdr2* mutants also had an altered fungal and bacterial rhizobiome, with more beneficial nitrogen-fixing and plant growth-promoting bacteria.

Wheat exudates have also been shown to modify the rhizobiome. When Shi et al. [64] applied wheat root exudates to bare soil, the abundance of bacteria in a variety of groups significantly increased. When added to another species rhizosphere, wheat root exudates increased the abundance of most bacterial groups tested and decreased others [64]. Taken together, Badri *et al.*[65] and Shi *et al.*[64] showed that plant root exudates can change the structure and composition of the rhizobiome in species- and genotype-specific ways. Whether changes in the rhizobiome can alter soil cohesion has not been directly tested but there is emerging evidence that it may be possible.

Both mycorrhizal fungi and rhizobacteria have the potential to alter soil cohesion and stability. Mycorrhizal fungi create a mycelium network in the soil that could help enmesh soil particles physically and chemically as, like plants, they also release polysaccharides into the soil. Indeed, the fungal polysaccharide chitosan was shown

to have soil-adhesive properties by Akhtar et al. [32]. This study also showed the bacterial polysaccharide xanthan had soil-adhesive properties and both chitosan and xanthan were more adhesive to soil than xyloglucan at the same concentrations. However, whether the polysaccharides are present in the same concentrations used in Akhtar et al. [32] and persist in the soil is not clear.

1.5 Aims

The amount of research on the effect of roots on soil stability, especially root exudates, is limited due to the difficulty in observing the roots in situ. Recent work is beginning to elucidate some of the underlying components involved in root-soil cohesion using high throughput assays like the soil adhesion assay by Akhtar et al. [32] and the centrifuge assay by Eldridge et al. [35]. These studies have shown that exudates have the potential to change root-soil and root-substrate cohesion. Testing these findings in crop species such as wheat remains difficult. Existing assays for cereal crop species are currently limited to hydraulic flume or field studies, which require high input of materials and do not control for confounding variables such as the rhizobiome. This work firstly aims to adapt an existing uprooting assay to provide a lab-based, high throughput proxy for soil erosion to identify traits that affect root-soil cohesion in wheat. Secondly, I aimed to breed appropriate wheat mutant lines to validate that ABC transporters and XTHs involved in root-substrate adhesion in *A. thaliana* are also responsible for root adhesion in wheat that can be used in the modified uprooting assay. Finally, I wanted to investigate the localisation and function of the wheat *XTH23* in model plant species.

Chapter 2

Materials and Methods

2.1 Bacterial Strains and Plant Lines

Details of plant seed stocks and bacterial strains are given in the relevant sections below.

2.2 Breeding Wheat Mutant Lines

2.2.1 Mutant Line Selection

TILLING and deletion lines are great alternatives to insertional mutagenesis and modern transformation techniques to generate mutant lines. Wheat in particular is difficult to transform as it has a large genome with a high copy number [66]. This study used TILLING and deletion collections to identify mutants for the genes of interest.

Gene Expression Analysis

RNA-seq expression data was acquired for each homeolog of *TaXTH23* and *TaATH6* from wheat-expression.com. Expression data from studies of Chinese spring wheat grown under normal conditions were collated. The mean expression across tissues collected from each homeolog and the percentage contribution of the homeolog to the transcripts per million were calculated. The percentage contribution of each homeolog was plotted on a ternary plot in Origin (Originlabs, Northampton, Massachusetts, USA).

Identification of TILLING Lines with STOP Gained Mutations in *TaATH6*

TILLING lines with STOP gained mutations in the gene *TaATH6* were identified and using EnsemblPlant and from Mahony [54]. Homozygous lines with STOP gained mutations at the start of the gene were prioritised. Selected TILLING lines were ordered from SeedStor (John Innes Centre, Norwich, UK, Version 2.03) and are summarised in table 2.1. Two lines with a STOP gained mutation in the A genome homeolog were ordered in case one had a background mutation that severely affected development.

Table 2.1: Summary of *Taath6* TILLING lines ordered from SeedStor

Line	Homeolog of mutation	Genome	Parental genotype	Mutation	Consequence
Cad0110	TraesCS1A02G343000	A	hom	TGG->TGA	STOP gained
Cad0679	TraesCS1A02G343000	A	het	TGG->TGA	STOP gained
Cad1704	TraesCS1B02G356200	B	hom	TGG->TGA	STOP gained
Cad1704	TraesCS1D02G345200	D	het	CAA->TAA	STOP gained

het = heterozygous, hom= homozygous

Deletion Line Identification for *TaXTH23* Mutants

For *TaXTH23*, there was only one TILLING line available, Cad1588. This line had gained a STOP codon in the D homeolog of *TaXTH23*, TraesCS7D02G419900. Therefore, a complete knockout of *TaXTH23* could not be bred using TILLING lines and so deletion lines were investigated instead. Appropriate deletion lines were identified using the TGCA Browser Deletions on `wheat-deletion.cyverseuk.org`. Two lines for each desired genotype were selected with the smallest number of deletions to reduce the chance of deleterious background mutations. The lines selected are summarised in table 2.2.

Table 2.2: Summary of *Taxth23* deletion lines ordered from SeedStor.

Line	Gene deleted	Expected genotype	Deletion size (bp)
J3-6	TraesCS7D02G419900	AABBdd	10800000
J5-46	TraesCS7D02G419900	AABBdd	9100000
J1-72	TraesCS7A02G427600	aaBBDD	252506235
J8-18	TraesCS7A02G427600	aaBBDD	3900000
J3-62	TraesCS7B02G327700	AAbbDD	5237500
J4-64	TraesCS7B02G327700	AAbbDD	3012500

bp= base pairs

2.2.2 Genotyping Parental Lines

Genomic DNA Extraction from TILLING and Deletion Lines

For both Tilling and deletion lines, genomic DNA (gDNA) was extracted from 3 cm long leaf samples of two-week-old wheat seedlings following the protocol described in Edwards et al. (1991) [67]. After collection, each leaf sample was placed in a freezer at $-80°C$ with two stainless steel ball bearings in a 2 ml microfuge tube. The tissue was lysed using the Genogrinder at max speed for 3 min. After lysis, 600 µl heated (55 $°C$) extraction buffer was added to each leaf sample, shaken by invertion, and then incubated at 55 $°C$ for 10 min. The samples were then cooled to room temperature and 300 µl 6 M ammonium acetate was added to precipitate proteins from the samples. The precipitated proteins were removed by centrifugation at 21,100 $\times$ g for 10 min. A 600 µl aliquot of the supernatant from each sample was recovered and added to 550 µl isopropanol and mixed by inverting 6 times. The samples were left at room temperature for 5 min for the DNA to precipitate, then centrifuged at 21,100 $\times$ g for 10 min to pellet the DNA. The supernatant was removed, and the samples were re-centrifuged for 30 s to aid the removal of the residual supernatant, which was also removed by pipetting. Finally, the pelleted DNA was resuspended in 100 µl TE buffer by vortexing, incubated at $50°C$ for 10 min, and vortexed again. The extracted gDNA was stored at $4°C$.

2.2.3 TILLING Parental Line Genotyping by Sequencing

Homeolog Specific Primer Design

Homeolog-specific primers were designed to amplify 500-600 base pair (bp) regions around the STOP gained mutation. To make primers homeolog-specific, a single nucleotide polymorphism specific to each homeolog was identified by eye from homeolog alignments in the multiple alignment program Clustral Omega and visualised in the Unipro bioinformatic software UGENE. The homeolog-specific primers had a corresponding single nucleotide polymorphism at the 3' end to stall the DNA polymerase and prevent elongation. Homeolog-specific primers are shown in table2.3. The homeolog DNA sequences were obtained from the genome browser EnsemblPlant.

PCR Amplification of *TaATH6* Homeologs from TILLING Lines

Two 25 µl PCR reactions were set up for each plant in the TILLING line Cad1704, one with the B homeolog-specific primers and the other with D homeolog-specific primers. The PCR reaction components are shown in table 2.4 and the conditions are summarised in table 2.5 and 2.6 for the B and D homeolog respectively.

Table 2.3: Summary of TaATH6 homeolog-specific primers used to amplify regions around DNA lesions for genotyping TILLING lines by sequencing.

Primer name	Associated Gene	Genome	Line	F/R	Nucleotide Sequence (5'-3')	Predicted product length (bp)
Cad0110 F	TraesCS1A02G343000.2	A	Cad0110	F	GAGTATGGCCTTGATCTAATGA	611
Cad0110 R				R	CTCCACAGGTTATTTCTTGAC	
Cad0679 F	TraesCS1A02G343000.2	A	Cad0679	F	GGTGATTTTAGAGTGTTTTCG	570
Cad0679 R				R	CAAGGCTATCCTTATTTGTGC	
Cad1704 B F1	TraesCS1B02G356200	B	Cad1704	F	CCCTCGCGTACCTACTAATC	519
Cad1704 B R2				R	GCATTTCTACTCCACTTCCC	
Cad1704 D F1	TraesCS1D02G345200.1	D	Cad1704	F	GCTTTGTTGCTTGAATGTTT	628
Cad1704 D R1				R	TCGCAATAGTGCAATGGG	

F= forward and R= reverse

The TILLING lines Cad0110 and Cad0679 25 µl PCR reactions were run with A homeolog specific primers. The PCR reaction components and conditions are summarised in tables 2.4 and 2.7 respectively. All PCR products were stored at $4°C$ until purification and sequencing.

Table 2.4: PCR components for a 25 µl reaction used to amplify regions containing mutations in *TaATH6* for the TILLING lines Cad0110, Cad0769 and Cad1704.

Component	Volume (µl)
Template DNA	1.5
hot star Taq plus MM	12.5
Forward primer	1
Reverse primer	1
Nuclease free water	9

MM= master mix

Table 2.5: Summary of PCR conditions used to amplify regions around mutation in *TaATH6* B homeolog in the TILLING line Cad1704.

Stage	Temperature (°C)	Time
Initial denaturisation	95	5min
	95	30s
X35	57	30s
	72	1min
Final extension	72	10min
Hold	4	-

Table 2.6: Summary of PCR conditions used to amplify regions around mutation in *TaATH6* D homeolog in the TILLING line Cad1704.

Stage	Temperature (°C)	Time
Initial denaturisation	95	5min
	95	45s
X35	50	45s
	72	1min
Final extension	72	10min
Hold	4	-

Table 2.7: Summary of PCR conditions used to amplify regions around mutation in *TaATH6* homeologs in the TILLING lines Cad0110 and Cad0679

Stage	Temperature (°C)	Time
Initial denaturisation	95	5min
	95	30s
X35	55	30s
	72	1min
Final extension	72	10min
Hold	4	-

Gel Electrophoresis

Gel electrophoresis was carried out on all PCR products to ensure the desired fragment had been amplified and that the primers were homeolog specific. For each PCR reaction 7 µl was run on 1 % (w/v) agarose gel made using 1X TAE buffer. Runs where at 90 V for 50 min. For Cad1704 B reactions, 4 µl purple 6X gel loading dye was added to the wells before loading the PCR products. The first well of each agarose gel was loaded with 5 µl Quick-Load Purple 2-Log DNA Ladder (New England Biolabs), which was used as a size reference. The gels were observed with a Blue-LED-Transilluminator (Vilber Fusion Pulse) and imaged with the software EvolutionCapture.

PCR Product Purification

PCR products were purified for sequencing using the QIAGEN QIAquick PCR Purification Kit. The remaining PCR products not run on the agarose gel (20 µl) were transferred to fresh 1.5 ml microfuge tubes and 100 µl phosphate buffer (PB) was added to the PCR samples and mixed by vortexing for 5 s. Then, the samples were transferred to QIAGEN spin columns in collection tubes and centrifuged at 21,100

$\times$ g for 60 s. The flow through was discarded and the DNA was washed with 750 µl phosphate ethanol (PE) buffer followed by centrifuging at 21,100 $\times$ g for 60 s and the flow through was discarded. Then, the QIAGEN spin columns were dried by further centrifugation at 21,100 $\times$ g for 60 s. The spin columns were transferred to fresh 1.5 ml microfuge tubes for DNA collection and 30 µl of sterile distilled water was added. The columns were then incubated for 1-5 min at room temperature, then centrifuged at 21,100 $\times$ g for 1 min to elute the DNA. The eluted purified PCR products were stored at $-20°C$.

Sequencing Reactions

Sanger sequencing of the Cad1704 *TaATH6* B homeolog fragment was carried out in the Edwards Lab at The University of Bristol using the Applied Biosystems BigDye sequencing Kit. For each Cad1704 plant sample, forward and reverse sequencing reactions were set up in PCR tubes with the reagents and quantities shown in table 2.8. The sequencing reactions were placed in a thermocycler under the conditions provided in table 2.9.

Table 2.8: Components of one sequencing reaction for sequencing Cad1704 plants for the B genome mutation

Component	Volume (µl)
BigDye sequencing reaction mix	2 µl
Sequencing buffer	1µl
Forward/ Reverse primer	1µl
Template PCR product	3µl
Sterile Distilled water	3µl
Final reaction volume	10µl

Table 2.9: Sequencing reaction conditions used in sequencing Cad1704 plants for the B genome mutation

Step		Temperature (°C)	Time
Initial Denaturation		94	30s
Denaturation		96	10s
Annealing	X30	50	5s
Extension		60	4m
Hold		4	-

Sequencing Reaction Product Purification

For each sequencing reaction 10 µl was recovered and transferred to a fresh 1.5 ml microfuge tube. Then 10 µl of sterile distilled water, 5 µl 125 mM EDTA and 60 µl 100% ethanol were added to each reaction and mixed by brief vortexing. The samples were then centrifuged at 21,100 $\times$ g for 10 min before the supernatant was removed by pipetting. The pellet was washed by adding 100 µl 75% ethanol and then centrifuged again at 21,100 $\times$ g for 10 min. The ethanol was then removed by pipetting and the pellet was dried in a vacuum. After drying, the pellet was resuspended in 20 µl formamide loading buffer and each sample was loaded into a 96-well microtitre plate for sequencing.

Sanger Sequencing

Both forward and reverse Sanger sequencing reactions of Cad1704 B homeolog were run and read by the Applied Biosystems™ 3500 Series Genetic Analyzer.

Plants from the other lines (Cad0679, Cad0110 and Cad1704 D) were sequenced using the Eurofins genomics tubseq service. For each plant, a 17 µl sequencing reaction was set up containing 15 µl purified DNA at 5 ng/µl and 2 µl corresponding forward primer (10 µM) used in the PCR amplification (table 2.3).

DNA Sequence Analysis

Sequencing chromatograms were viewed in the software SnapGene. The quality of each sequencing run was checked, and the locus of the DNA lesion was identified, allowing the genotype to be determined.

2.2.4 Deletion Line Genotyping

PCR Amplification of *TaXTH23* Homeologs

As in 2.2.1. homeolog-specific primers were designed manually for genotyping deletion lines and are summarised in 2.10. PCR reactions of 25 µl were set up for each plant with the components summarised in table 2.4. Lines with different genotypes were used as positive controls against each other. The PCR conditions used to genotype the deletion lines are summarised in table 2.11. PCR products 10 µl were run on 1% (w/v) agarose gel for 50 min at 90 V (see section 2.2.3).

Table 2.10: Summary of TaXTH23 homeolog specific primers used to genotype deletion lines by PCR and gel electrophoresis.

Primer name	Associated Gene	Genome	Line	F/R	Nucleotide Sequence (5'-3')	Predicted product length (bp)
TaXTH23D F	TraesCS7D02G419900	D	J3-6 & J5-46	F	CACTTCACTCAGTAGCAGCTA	389
TaXTH23D R				R	ATACGGAAATGGCAACGA	
TaXTH23A F	TraesCS7A02G427600	A	J1-72 & J8-18	F	TCCAAGAGCGAGTACCTG	1059
TaXTH23A R				R	ACCATCCCACAGAGCTTC	
TaXTH23B F	TraesCS7B02G327700	B	J3-62 & J4-64	F	CCACGGCATTTACTACGC	553
TaXTH23B R				R	CCGATGAACTGCGACTGT	

Table 2.11: PCR reaction conditions used to genotype deletion lines.

Step		Temperature (°C)	Time
Initial Denaturation		95	5min
Denaturation	X35	95	30s
Annealing		54	1min
Extension		72	1:15min
Final extension		72	10
Hold		4	-

2.2.5 Wheat Mutant Line Crossing

Crossing Methods

Once spikes on the desired lines had fully emerged from the flag leaf by 2-3 inches but before anthers had matured and released any pollen (GS59), they were emasculated following the methods described in Wheat Training How to Cross Wheat guide (2018) and as instructed by Professor Keith Edwards. Firstly, spikelets at the tip and the base of the spike were removed using scissors. Then, the middle floret of each spikelet was removed using forceps. The top third of each floret was cut off horizontally with scissors to aid anther removal and pollination. Finally, all the anthers from each floret were pulled out with forceps and a plastic sheath was placed over the emasculated spikes to prevent pollination from undesired sources.

Once the stigma had matured, the emasculated spikes were pollinated each day for 3-5 days by brushing anthers containing mature pollen against the stigma.

TILLING Line Crossing Scheme

The homozygous double knockout individuals from the TILLING line Cad1704 were emasculated and crossed with individuals from the Cad0110 line, of which all individuals were homozygous for the A genome mutation. This produced F1 seeds that are expected to be heterozygous for each of the homeologs. A full crossing scheme

for the breeding of triple knockout mutants for *TaATH6* from the parental TILLING lines Cad1704 and Cad0110 is shown in 2.1

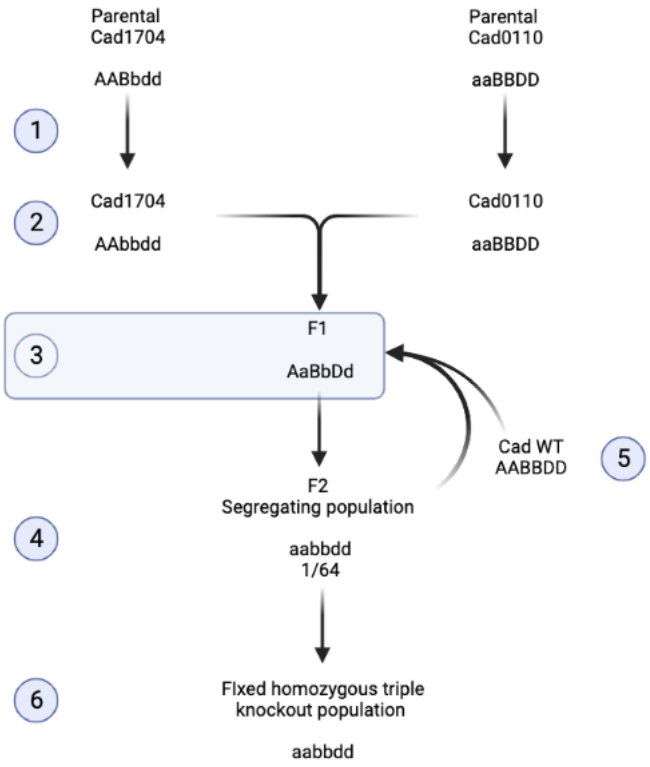

Figure 2.1: TILLING line crossing scheme to generate an *Taath6* near isogenic line (NILs). The blue box shows the position of the current work. (1) Parental lines genotyped and selfed producing (2) Seeds attained from SeedStor, which were grown up, genotyped by sequencing and crossed to produce F1 seeds (3). F1 should be selfed producing a segregating F2 population (4). F2 should be genotyped to identify triple homozygous mutants. (5) triple homozygous mutants should be back-crossed with a non-mutagenized line. (6) After multiple generations of back-crossing triple homozygous mutants should be selfed to produce a NILs population.

Deletion Line Crossing Scheme

The deletion lines J1-72, J8-18, J3-6, and J5-46 were crossed with the pollen donor line J4-64. This produced seeds that are expected to be double heterozygous mutants for the *TaXTH23* gene. The full crossing scheme to produce triple homozygous mutants for the gene *TaXTH23* is shown in fig. 2.2.

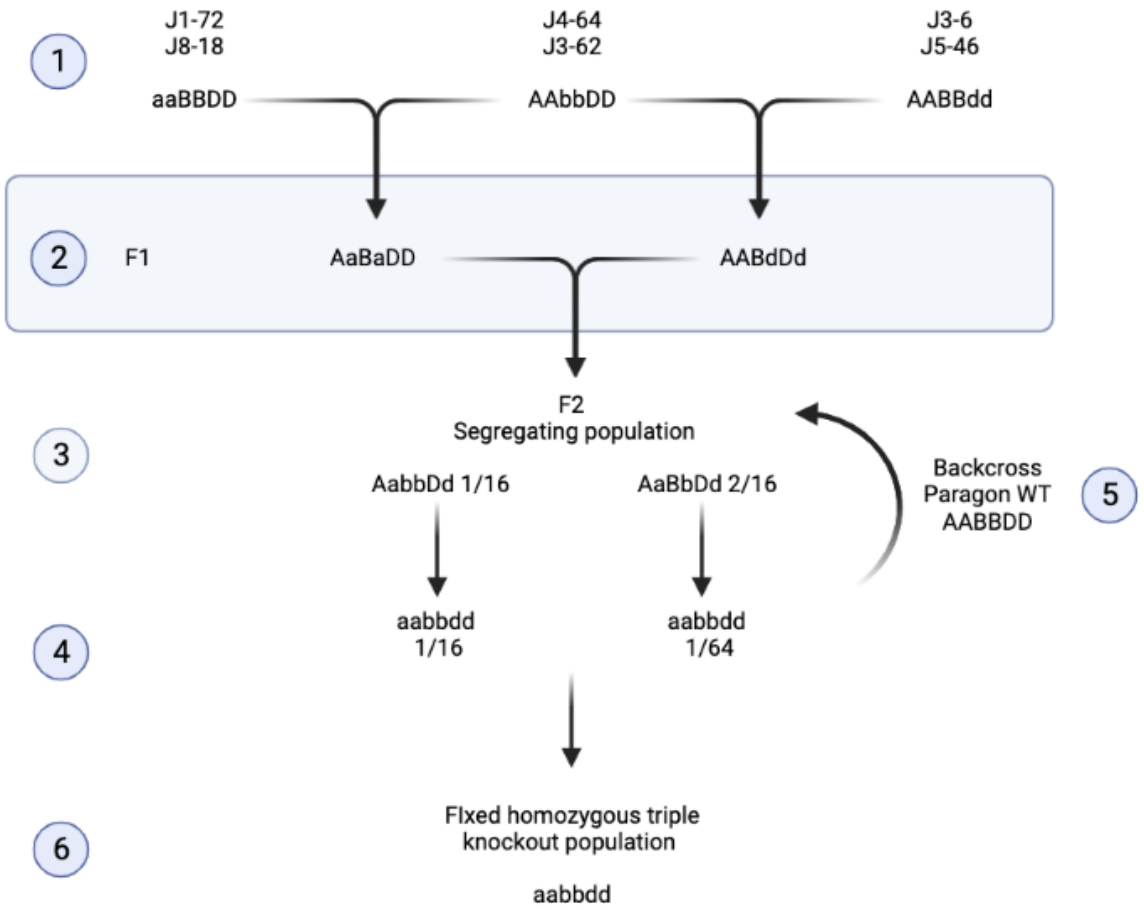

Figure 2.2: Deletion line crossing scheme to generate *xth23* mutant line. (1) Deletion lines were attained from Seedstor, genotyped by PCR and crossed. (2) The cross resulted in F1 mutant progeny. This generation should be crossed to produce an F2 segregating population (3). F2 should be genotyped and appropriate mutants selfed to produce triple knockouts (4). These triple knockouts should be backcrossed to a non-mutagenised Paragon line (5). Multiple backcrosses to reduce the background load should result in triple homozygous *xth23* mutant population (6).

Wheat Growth Conditions

All wheat plants used in this section were grown in a greenhouse under natural light conditions in Sinclair potting compost.

2.3 Development of Novel Soil Erosion Assay for Wheat

2.3.1 Soil Composition Analysis

The soil used throughout the uprooting assay development was bulk bought and described as a sandy loam. To confirm that the soil was sandy loam and had a consistent composition across bags, soil composition was analysed using a laser particle analyser.

Firstly, soil samples were taken from 5 separate bags and sieved to 2 mm to remove gravel particles. The samples were dried in a 60°C oven for 3 days to remove all water content. Then the organic content was burnt off by baking the samples at 375°C for 1 day, to reduce disruption of the laser particle analyser. This also allowed the organic content of the soil to be determined by weighing the samples before and after the baking.

The soil sample size composition was measured using a laser particle analyser, Mastersizer 3000E (Malvern Panalyical, Malvern, Worcestershire, UK), which measures the particle size distribution at regular intervals. For each soil sample, the particle size composition was taken at five consecutive time points. The mean percentage of silt, sand and clay was calculated from these time points for each sample to approximate the particle size composition of each sample. Data were collected using the Mastersizer 3000E software and analysed in Microsoft Excel.

2.3.2 Making Uprooting Anchors for Wheat Seedlings

Making Uprooting Anchors

Modified P1000 pipette tips used to uproot the wheat seedlings were made using a sharp razor blade and a ruler to remove 5 mm from the end. Then a 1.2 mm x 40 mm blunt fill needle heated with a Bunsen burner was used to poke three evenly spaced holes 5 mm from the top of the pipette tip. These holes were used to attach 12 cm lengths of 1 mm diameter, stiff garden wire. The wire was attached by looping the wire through the hole and then twisting it with itself. The outside of the modified pipette tips were sprayed with PTFE lubricant spray before use.

2.3.3 Development of a Wheat Uprooting Protocol

Growing Wheat Seedlings for Uprooting

Preliminary work was done to investigate whether wheat seedlings could be grown in pipette tips. Wheat seeds were sown in P 1000 pipette tips with 5mm removed from the tip and placed 3cm deep into damp soil. During these initial growth trials, a few

problems arose that needed to be solved in order to get a high germination rate and normal growth. Firstly, germination rates were very low as the seeds dried out in the pipette tips this was solved by using a spay bottle to lightly mist the seeds once planted in the pipette tip to increase the humidity around the seeds to encourage germination. Later, seeds became mouldy in the pipette tips which severely inhibited the seedlings growth. This was probably caused by over misting and allowing the seeds to sit in droplets of water for long periods of time. Another problem which arose was the shoots growing down the pipette tip and into the soil rather than up. The shoot growing down into the soil would disrupt an uprooting assay by disrupting the root-soil matrix and creating added friction against the soil. This was solved by orienting the seed with the hairy end, the brush, facing up in the pipette tip before planting. Trouble shooting table of the problems which arose and potential solutions is presented in the appendix.

Determining Appropriate Uprooting Anchor

This assay attempted to use pipette tips as an anchor to assist in uprooting wheat seedlings. Two different shaped brands of pipettes were used, Greiner Bio-one Tip 1000 μl and Sarstedt P1000 pipette tips and Eppendorf tubes. The pipettes were modified by cutting off 5 mm and 10 mm and a hole was made in the bottom the Eppendorf tubes using a 1.2 mm x 40 mm blunt fill needle heated with a Bunsen burner. Stratified wheat seeds were placed in modified Eppendorf tubes and P1000 pipette tips. Then the modified tips and tubes were placed in the centre of 550 ml pots containing sandy-loam soil at a depth of approximately 3-4 cm. After seven days, the germination rate and uprootability were determined for the different growth conditions. Uprootability was calculated as the proportion of successfully uprooted seedlings. Successful uprooting was defined as when the seedlings root system came up with the anchor (modified pipette) and the stem did not snap or slip. The seedlings were gently uprooted by hand using the pipette tip or Eppendorf tube as a grip.

Is Wheat Seedling Development Affected by Growth in the Modified Pipette Tips?

Fifty wheat seeds were stratified and 24 were placed, brush side up, in modified Stastedt P1000 pipette tips coated in PTFE lubricant and pushed 3 cm into 550 ml pots of sandy-loam soil. As a control, another 24 seeds were placed brush side up in 3 cm deep holes in 550 ml pots of soil. The holes were created by pushing a modified Stastedt p1000 pipette tip into the soil. The germination and development of the seedlings was tracked over the next two weeks.

2.3.4 Uprooting Wheat Seedlings

Experimental Design

Wheat seedlings were uprooted at 3 different developmental stages, GS10, GS11 and GS13, which are described growth stages of cereals (AHDB, 2021). Three technical replicates were carried out for GS10 and GS11 and two for GS13. Between 60 and 72 wheat seeds in modified pipette tips were planted for each replicate and between 12 and 24 plants were uprooted for each growth stage. Approximately 20 seedlings can be uprooted in a day, more for the earlier growth stages.

Uprooting

Before uprooting, pots were soaked overnight in trays containing 5 cm excess water to saturate the soil. On the day of uprooting, the plants were carried carefully by hand, in trays, to the tensile testing machine (Instron 3345 and 100 N load cell, Instron, Norwood, Massachusetts, United States). This reduced shaking which caused the soil matrix to collapse. Plants were re-submerged in 5 cm water until uprooting. For plants at growth stage GS13, a hard soil cap had formed on the soil surface, so a spray bottle was used to saturate the surface soil by spraying with tap water 5 times from 20 cm away.

The wires on the modified pipette tips were clamped to the tensile testing machine which vertically pulled the seedlings up at a speed of 10 mm/min until the trace force reached 0 N or it plateaued below 0.2 N for more than 1 min. A schematic of the uprooting set up is displayed in Fig. 2.3 and a picture the uprooting set up of a seedling at GS11 is displayed in Fig. 2.4. Trace forces were measured by a 100 N load cell and collected in the software Bluehill (Instron).

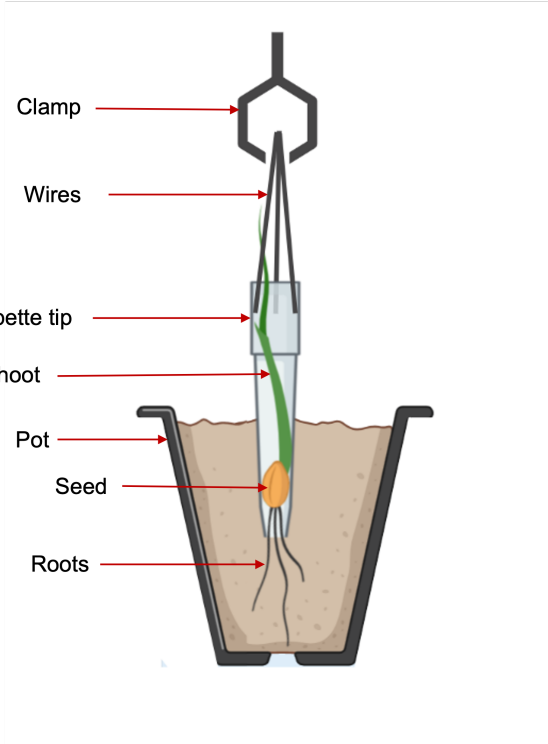

Figure 2.3: Diagram of uprooting set-up. Clamp is attached to instron machine. Not to scale

Root and Soil Processing

After uprooting, the uprooted root samples were cut from the shoot using sharp scissors into a Petri dish, which was then sealed using 3 or 4 layers of para film to prevent the roots from drying out and stored at 4 ^oC. Uprooted samples were cleaned by hand to separate them from any attached soil. The Attached soil was collected in the petri dish. Cleaned roots were placed onto 1% charcoal agar plates, detangled, and photographed with a DSLR Nikon D80 camera. Representatives of roots, from each growth stage, laid out on charcoal agar are shown in fig. 2.3.4. Clean root samples were then transferred to weighing boats for drying. Soil washed from the uprooted roots and cleaned root samples were dried at 60 ^oC overnight to remove all water content. Dried roots and dried soil were then weighed using an analytical balance.

The pots were searched for broken roots by tipping them up into a large sieve and washing the soil through with water. The broken off roots remained in the sieve, were collected, placed in petri dishes and sealed with para film. The broken off roots from the pot were stored at 4 ^oC until they were cleaned, placed on charcoal agar plates

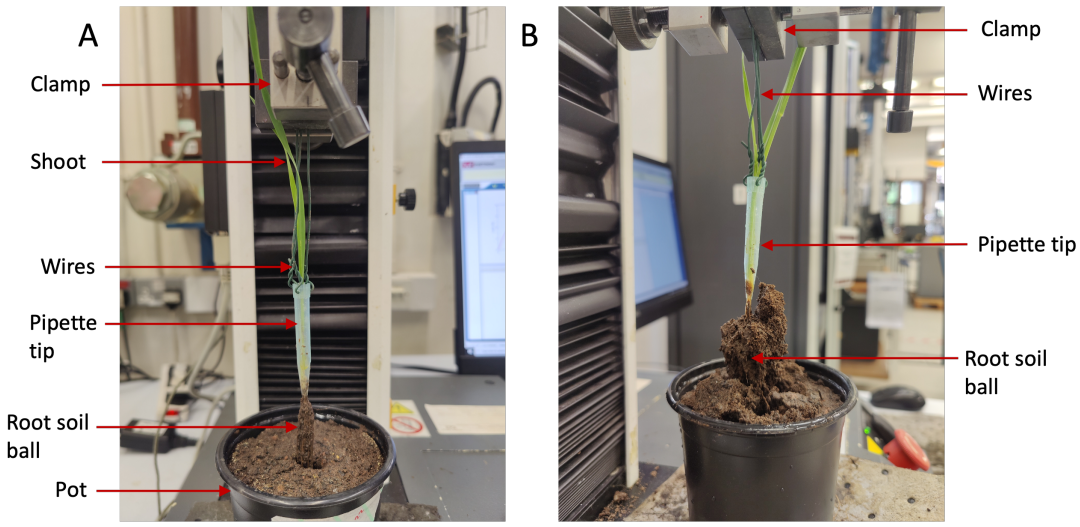

Figure 2.4: Uprooting setup. Front (A) and side (B) view of GS11 wheat seedling being uprooted by the Instron machine

and photographed.

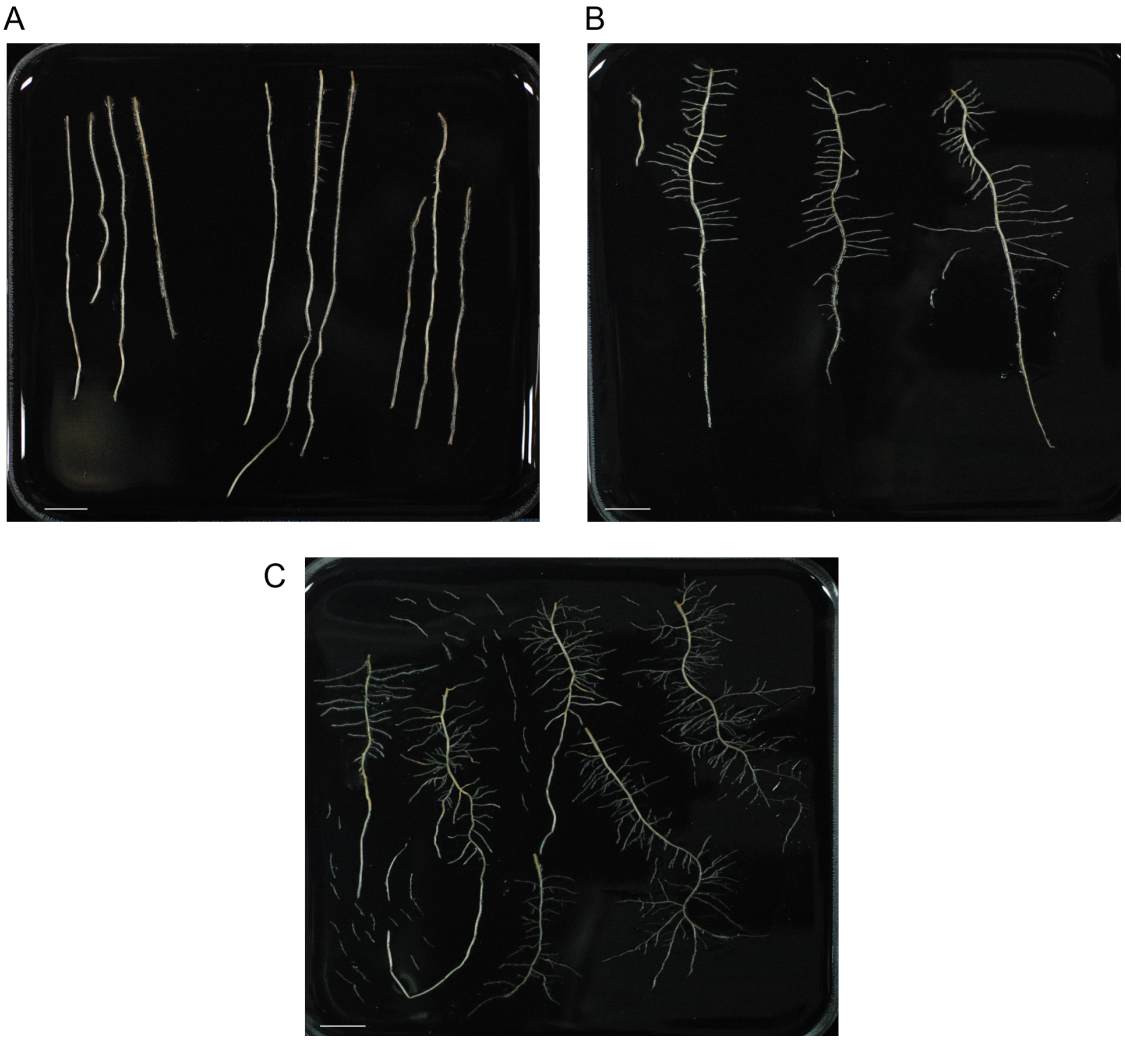

Figure 2.5: Examples of uprooted root samples laid out on charcoal agar. (A) Round 2 GS10, plants 4, 5 and 6. (B) Round 2 GS11 plant 14. (C) Round 2 GS13 plant 10. Scale bars represent 10mm.

Root Image Analysis

Root length was measured from the pictures by tracing the roots using the segmented line tool and the measure function in the image processing software FIJI version 2.3.0/1.53q [68] (fig.2.3.4).

Growth Conditions

For the uprooting assay and preliminary experiments, all Cadenza wheat seedlings were grown in pots containing 500 ml sandy loam soil. Before use, the sandy loam soil was sieved to 2 mm to remove gravel particles and sterilised by baking in autoclave bags at 50 ^oC for at least 3 days. The seeds were imbibed before planting to synchronise germination. This was done by soaking the seeds in tap water at 4 ^oC for 4 days in the dark. The seedlings grew in a controlled environment growth room in constant light, under light : dark cycles of 14 h : 10 h, at 22 ^oC and 60% humidity. Propagator lids were used for the first 3 days of growth and misted using a spray bottle to increase humidity levels around the germinating seeds. Developing seedlings were watered every 2-3 days from below.

Charcoal Agar Plates

Charcoal agar plates were made by adding 8 g charcoal and 8 g agar to 800 ml distilled water in a 1 l bottle. The medium was mixed to suspend the charcoal and agar, and then sterilised by autoclaving. The hot liquid medium was mixed again by swirling the bottle before pouring. A total volume of 70 ml medium was poured into 90 ml square plates using a 50 ml serological pipette in a laminar flow hood. The plates were left to set for at least 20 min at room temperature before they were sealed back into their plastic packaging and stored inverted at 4 ^oC .

Data Analysis

Data collected from the uprooting was collated in Excel. This included plant growth stage, weight of dried uprooted roots, uprooted root length, pot root length and uprooted soil weight. The RLD was calculated as the (uprooted RL + pot RL)/ 500. The uprooted soil per root length was also calculated as uprooted soil mass / uprooted RL. RLD and uprooted soil per root length were calculated for each plant, outliers were excluded, and the data analysed in the statistical graphing software Origin (OriginLab, Northhampton, Massachusetts, USA).

2.4 Cloning *XTH23* and Expression in Model Plant Species

2.4.1 Genotyping of *xth23 A. thaliana* Mutant Line

Genomic DNA Extraction from *A. thaliana*

Leaf samples were taken from 12 young *xth23 A. thaliana* plants thought to be homozygous T-DNA insertion mutants. Each leaf sample was placed in a 2 ml centrifuge tube with a metal ball bearing and frozen in liquid nitrogen. The frozen samples were then ground to a powder using a tissue lyser (QUIAGEN, TissueLyser II 85300)(QUIAGEN, Hilden, Germany) before 400 μl DNA extraction buffer was added to each sample, which were then vortexed for 30 s. The samples were then centrifuged at 21,100 $\times$ g for 5 min, and the supernatant was transferred to clean 1.5 μl centrifuge tubes. The DNA was precipitated by adding 400 μl 100% isopropanol to each sample, which was mixed by inverting six times. The samples were then incubated at -20 ^oC for 30 min and centrifuged at max speed for 10 min to pellet the DNA. The supernatant was removed, and the pellet dried by inverting the tubes over a paper towel for 2 min. The pellets were then resuspended in 50 μl nuclease free water by pipetting. The extracted DNA samples were stored at -20 ^oC until further use.

Genotyping of *xth23 A. thaliana* Mutant Line by PCR

To genotype the *xth23* mutant line, three PCR reactions were run for each individual using a combination of *AtXTH23* and T-DNA insert specific primers. The forward and reverse primers used are presented in table 2.12. For each *xth23* individual and a WT Col-0 gDNA control , three 25 μl PCR reactions were set up (table 2.13). The first reaction used the forward and reverse primers specific to *AtXTH23* (table 2.14), the second using the forward and LB (left border) primer, which is specific to the T-DNA insert, and the third reaction used the reverse primer and the LB primer. The water control contained no gDNA.

Table 2.12: Primers used to genotype *A. thaliana xth23* mutants.

Primer name	F / R	Sequence 5'-3'	Product length
AtXTH23 F	F	CTGGAACTGTCACCGCTTACTATG	1200 bp
AtXTH23 R	R	ACTTTTCGTTGAGGTCTATGAC	

F = forward, R = Reverse and Product length = expected PCR product length.

Table 2.13: Components of one PCR reaction used to amplify *AtXTH23* from gDNA for genotyping xth23 plants

Component	Volume (ml)
gDNA	1.5
2X Go Taq hot start green	12.5
Forward primer/ Reverse primer	1
Left border primer	1
Sterile water	9

Table 2.14: PCR conditions for genotyping of xth23 individuals

Step		Temperature (°C)	Time
Initial denaturation		95	2 min
Denaturation		95	30 s
Annealing	X30	60	30 s
extension		72	1min
Final extension		72	5min
hold		4	-

Gel Electrophoresis

A volume of 8 μl for each PCR reaction product was run on a 1% (w/v) agarose 1X TAE buffer gel for 50 min at 90 V with 5 μl 1 kb DNA ladder in the first well.

2.4.2 RT-PCR of *xth23* Mutant Line

Seed Sterilisation and Stratification

Approximately 100 seeds of *xth23* and Col-0 were aliquoted into microfuge tubes before 1 ml 20% bleach solution was added for 15 min with regular shaking every 3-5 min. The tubes were briefly spun in a centrifuge to collect the seeds and the bleach solution removed by pipetting under a laminar flow hood. The seeds were then rinsed with 1 ml sterile water four times and suspended in a final volume of 1 ml. The tubes were wrapped in tin foil and the seeds were stratified at 4 ^oC for 48 h.

Growth Media, Seed Plating and Collection

Sterile stratified seeds were plated onto 0.5X MS (Murashige and Skoog) square plates and grown vertically at approximately 80^oC angle in a controlled environment growth room. After 5 days, two samples of 50 seedlings were collected for Col-0 and xth23

lines. The samples were flash frozen in liquid nitrogen with two ball bearings and stored at -80 ^oC. 0.5X MS plates were 1% agar, 0.5X MS and 1% sucrose.

Total RNA Extraction and DNase Treatment

Total RNA extraction was carried out on frozen samples of *xth23* and Col 0 seedlings using the Spectrum Plant Total RNA kit (Sigma Aldrich, Missouri, USA). Prior to use, the samples were ground to a powder using a tissue lyser at full speed for 1 min. The samples were kept on ice as much of possible throughout the protocol. After grinding, 500 μl lysis solution containing 2mercaptoethanol were added to the tissue samples and vortexed for 30 s before they were incubated at 56 ^oC for 3 min. The resulting cellular debris was removed by centrifugation at 21,100 $\times$ g (max speed) for 3 min and the supernatant was collected. This supernatant was pipetted onto a filtration column and centrifuged at max speed for 1 min. Then, 500 μl binding solution was added to each sample and mixed by pipetting and vortexing. 700 μl each lysate solution was then pipetted onto binding columns and centrifuged for 1 min at max speed. The flow through was discarded, and the centrifugation repeated until all the lysate had run through the column.

The filtration columns were washed with 500 μl wash solution 1 and centrifuged at max speed for 1min. The flow through was discarded and the washing step was repeated twice more with the second wash solution, wash solution 2 . The columns were then dried by further centrifugation at max speed for 1 min.

The Total RNA was eluted from the columns by transferring the column to clean 2 ml Eppendorf tubes and adding 25 μl elution solution, which was incubated on the column for 1 min at room temperature. The samples were centrifuged at max speed for 1 min. This was repeated once more, resulting in a final solution of 50 μl. The RNA concentration and purity of the eluted total RNA were measured using a Nanodrop spectrophotometer. The samples were stored at -80 ^oC until DNase treatment.

To remove potential contaminating DNA, the total RNA extraction samples were DNase treated by adding 2 μl DNase and 2 μl reaction buffer to 16 μl total RNA samples in a microfuge tube. The resulting solution was mixed by gentle flicking and then placed in a water bath at 37 ^oC for 30 min. To stop the reaction, the DNase was denatured by adding 2μl stop solution to each sample and incubation at 70 ^oC for 10 min. The samples were then chilled on ice and assessed with a Nanodrop spectrophotometer. Total RNA quality was also assessed by adding 3 μl purple 6X loading dye to 5 μl RNA sample, which was then run on a 1% (w/v) agarose gel at 90 V for 40 min.

cDNA Synthesis

CDNA synthesis was carried out using the Applied Biosystems High-Capacity cDNA Synthesis Kit (Applied Biosystems, Massachusetts, USA). A 2X RT master mix (Table 2.15) was 10 μl aliquots were added to each total RNA sample at a concentration of 1000 $ng/\mu l$. Negative controls were also set up in the same way with one excluding RNA and another excluding reverse transcriptase. Each sample was gently mixed, spun briefly in a mini centrifuge to remove air bubbles, and placed in a thermocycler. The conditions in the thermocycler are provided in table 2.16. The cDNA was stored at -20 ^oC.

Table 2.15: 2X RT Master mix used for cDNA synthesis from total RNA

Component	Volume (ml)
10X RT buffer	12
25X dNTP mix	4.8
10X RT random primers	12
Multiscribe reverse transcriptase	6
RNase inhibitor	6
Sterile water	19.2

Table 2.16: Thermocycler conditions for cDNA synthesis from

Step	Temperature (°C)	Time (min)
1	25	10
2	37	120
3	85	5
Hold	4	-

RT-PCR of *AtXTH23*

For the xth23 and Col-0 cDNA samples and the two negative controls, three 25 μl reactions were set up for RT-PCR using primer sets, 2 and 3 respectively (table 2.17). RT-PCR primers were manually designed from cDNA sequences and one in the set crossed an exon-exon junction to exclude potential contaminating gDNA. $EF1\alpha$ primers were complimentary to the housekeeping gene $EF1\alpha$ and used as an internal expression control. The conditions used are shown in table 2.19. Aliquots of 8 μl cDNA products were run on a 1% (w/v) agarose gel for 60 min at 90 V.

Table 2.17: RT-PCR primers specific to AtXTH23

Primer name	F / R	Sequence 5'-3'	Product length
Primer set 2 AtXTH23	F	ACCCACAACGCATCATATTCTC	501 bp
Primer set 2 AtXTH23	R	ACAGATGTAACCAAACATCAGATAC	
Primer set 3 AtXTH23	F	ACTGTCACCGCTTACTATTTGAA	366 bp
Primer set 3 AtXTH23	R	AGACCAGTCGGTTTTGACGA	

F = forward, R = Reverse and Product length = expected PCR product length

Table 2.18: Components of one RT PCR reaction used to amplify *AtXTH23* from cDNA

Component	Volume (ml)
Template cDNA	5
2X Go Taq hot start green	12.5
Forward primer	2.5
Reverse primer	2.5
Sterile water	2.5

Table 2.19: RT PCR conditions for the amplification of AtXTH23 from cDNA.

Step		Temperature (°C)	Time
Initial denaturation		95	2 min
Denaturation		95	30 s
Annealing	X30	58	30 s
extension		72	1min
Final extension		72	5min
hold		4	-

2.4.3 Stable and Transient Expression of *TaXTH23* in Model Plant Species

Gateway Cloning of *TaXTH23*

PCR amplification of *TaXTH23* with gateway sites Primers for the amplification of *TaXTH23* B homeolog (TraesCS7B02G3277000) from WT Cadenza gDNA were designed manually from a sequence provided by EnsemblePlant (European Bioinformatics institute). The reverse primer excluded the STOP, and attB sites were then added to the primers to make them gateway primers, table 2.20.

Table 2.20: Primers specific to the pDONR207 plasmid used to sequence entry clones pDONR207 *TaXTH23*

Gateway primer	Sequence (5'-3')
Forward	GGGGACAAGTTTGTACAAAAAAGCAGGCTCTATGACGACGGTGGCGATAGGCA
Reverse	GGGGACCATTTGTACAAGAAAGCTGGGTGGCGGAGCTTGCACTCGGCA

Using the Gateway primers, eight 25 μl PCR reactions were set up to amplify *TaXTH23* from WT Cadenza gDNA using the Taq polymerase Q5 High-Fidelity DNA Polymerase (M0491)(New England Biolabs, Massachusetts, USA). The reaction components for one PCR reaction are summarised in table 2.21 and the conditions used are summarised in table 2.22.

Table 2.21: Components of one 25 μl PCR reaction used to amplify *TaXTH23* from WT Cadenza gDNA

Component	Volume (μl)
Template gDNA	2
Q5 Taq polymerase	12.5
Forward primer	1
Reverse primer	1
Sterile distilled water	8.5

BP Reaction The BP reaction combined at the attB sites flanking the *TaXTH23* DNA fragment amplified and the attP in the pDONR207 donor (pDONR) vector to create the entry clone pDONR*TaXTH23*. The reaction contained the components 5 μl attB-*TaXTH23* PCR product, 2 μl pDONR207 donor vector (150 $ng/\mu l$) and 4μl 5X BP clonase. The components were mixed in a 1.5 ml microfuge tube by vortexing. The reaction was incubated at room temperature overnight.

Table 2.22: Gradient PCR conditions for the amplification of *TaXTH23* from Cadenza WT gDNA with Gateway primers.

Step		Temperature (°C)	Time
Initial denaturation		98	30s
Denaturation		98	5s
Annealing	X40	50-58	30s
extension		72	30s
Final extension		72	2min
hold		4	-

LR reaction The LR reaction recombined the attL sites in the entry clone pDONR*TaXTH23* with the attR sites in the destination vector (pB7FWG2 35S GFP) to create the expression clone p35S::*TaXTH23*::GFP. The destination vector pB7FWG2 35S GFP was isolated by plasmid miniprep from glycerol stocks provided by Dr Alice Baillie. The reaction contained the components 2 μl pDONR*TaXTH23*, 2 μl destination vector (pB7FWG2 35S GFP) and 4 μl 5X LR Clonase in a 1.5 ml microfuge tube, which was mixed by brief vortexing. The reaction was then incubated at room temperature overnight. To stop the reaction, 2 μl 2 $\mu g/\mu l$ Proteinase K was added to the reaction and incubated at 37 ^oC for 10 min.

2.4.4 Microbiology Methods

E. coli Transformation

For both the BP and LR reactions TOP 10 electrocompetent cells were used to clone the entry vector and the expression vector. The following method was used; 2 μl each BP/LR reaction was added to an aliquot of Top 10 electrocompetent *E. coli* cells and mixed gently by flicking. The suspension of cells was then incubated on ice for 30 min. The cell suspensions were transferred to 2 ml cuvettes and electroporated on the setting Ec2.

Electroporated cells were allowed to recover by immediately adding 1 ml of ice-cold liquid LB media and then incubated at 37 ^oC for 1 h. The cultures were then spread onto LB selection plates that contained antibiotics using a sterile p20 pipette tip under a laminar flow hood. The pDONR*TaXTH23* potential transformants were spread onto LB + gentamicin plates and p35S::*TaXTH23*::GFP potential transformants were spread onto LB + spectinomycin plates. The plates were sealed with parafilm and incubated overnight at 37 ^oC. Resulting colonies were sampled for colony PCR and colonies positive for the inserted gene were cultured for plasmid miniprep and glycerol stocks.

A. tumefaciens Transformation

Chemocompetent *A. tumefaciens* GV3101 were transformed with the expression clones p35S::*TaXTH23*::GFP, p35S::*AtXTH23*::GFP, p35S::*TaXTH23*::RFP and p35S::*AtXTH23*::RFP. The RPF clones were supplied by Dr Alice Baillie.

Aliquots of frozen chemocompetent *A. tumefaciens* cells were gently thawed on ice. Once thawed, 3 μl expression clone plasmid was added to the cells and mixed by flicking. The cells were then left for 30 min on ice and flash frozen in liquid nitrogen before they were heat shocked in a water bath at 37 ^oC for 5 min. Immediately after heat shock, the cells were transferred into liquid LB, in a 15 ml falcon tube and allowed to recover for 3 h at 28 ^oC with shaking (180 rpm). The cultures were then spread on LB + spectinomycin agar plates and incubated at 28 ^oC for 72 h. Colonies that grew were tested for the expression clone by colony PCR and positive clones were cultured for glycerol stocks.

Microbiological Cultures

Luria-Bertani (LB) broth was made up by adding 8 g LB to 800 ml distilled water. 1% LB agar plates were made by adding 32 g LB + agar to 800 ml distilled water. If the media solidified before use, it was microwaved with regular shaking until it liquified. The media was then poured into petri dishes under a laminar flow hood and left to set for 20-30 min. Plates were stacked and sealed in plastic bags and stored at 4 ^oC until use. All media was autoclaved before use.

Antibiotic plates – After autoclaving or microwaving, the liquid LB agar was cooled to 50 ^oC and the appropriate antibiotics were added. - For LB + gent: 40 μl 10 $\mu g/ml$ gentamicin was added to 800 ml LB + agar - For LB + spec: 800 μl 50 $\mu g/ml$ spectinomycin was added to 800 ml LB + agar.

Glycerol Stocks of Positive Clones

Glycerol stocks of bacteria were made up for long term storage by adding 500 μl overnight culture and 500 μl 50% glycerol to a 1.5 ml cryovial. Samples were then flash frozen in liquid nitrogen and stored at -80 ^oC.

Colony PCR

To test *E. coli* and *A. tumefaciens* colonies for successful transformation, colony PCRs were carried out. Under a laminar flow hood, a small sample of each colony was taken using a sterile pipette tip and placed in PCR tubes containing 20 μl nuclease free water. The bacteria were mixed into the water and placed in a thermocycler for 5 min at 95 ^oC to lyse the bacteria. Then, 12.5 μl GO Taq hot start was added to

each sample of lysed bacteria along with 1 μl forward and reverse primers. The PCR reactions were carried out in the conditions provided in table 2.23. An aliquot 10 μl of each reaction was run on 1% (w/v) agarose gel for 50 min at 90 V.

Table 2.23: PCR conditions for colony PCRs of *E. coli* and *A. tumefaciens*.

Step		Temperature (°C)	Time
Initial denaturation		95	5 min
Denaturation		95	1 min
Annealing	X35	52	1 min
extension		72	2 min
Final extension		72	10min
Hold		4	-

2.4.5 Molecular Biology Methods

PCR Product Purification

Gradient PCR products taken forward for cloning (reactions 3 and 4) were purified using the QIAGEN QIAquick PCR purification kit. PCR products were added into 1.5 ml centrifuge tubes containing 100 μl PB buffer before this solution was transferred to a DNA binding column. The columns were centrifuged at max speed for 1 min and the flow-through was discarded. Next, 750 μl PE buffer was added to the columns, centrifuged again at max speed for 1 min and the flow-through discarded. The columns were dried by further centrifugation at max speed for 1 min. The column was then placed in a clean 1.5 ml centrifuge tube and 50 μl nuclease free water was added, and the column and tube centrifuged again at max for 1 min to elute the DNA. The final eluted DNA solution's absorbance was measured at 260/230 and 260/280 nm using a Nanodrop spectrophotometer to check its concentration and quality.

Miniprep of *E. coli* Plasmids

All plasmid minipreps were carried out using the QIAGEN QIAprep Spin Miniprep Kit, following the manufactures protocol. Firstly, the bacteria were pelleted from overnight cultures by centrifugation at 125 $\times$ g for 3 min and the supernatant was discarded. For each sample, the pelleted bacteria were resuspended in 250 μl P1 buffer and transferred to a 1.5 ml microfuge tube. Then, 250 μl P2 buffer was added, mixed in by inverting, followed by the addition of 350 μl N3 buffer and immediate mixing by inverting the tubes 4 to 6 times. The resulting solution was then centrifuged for 10 min at max speed. 800 μl supernatant was recovered, transferred to a spin column,

centrifuged for 1 min at max speed and the flow-through discarded. This centrifugation was repeated three more times with 500 μl PB buffer, before 750 μl PE buffer was added, and the flow-through discarded. The empty column was centrifuged for 1 min to removed excess liquid. The dry column was placed in a clean 1.5 ml microfuge tube for the collection of the isolated plasmid. 50 μl nuclease free water was added to the column and left for 1 min at room temperature. The column was centrifuged a final time at max speed for 1 min to elute the DNA. The absorbance of each sample was measured at 260/230 and 260/280 nm using a Nanodrop spectrophotometer to check their concentration and quality.

Gel Electrophoresis

All gel electrophoresis was run on 1% (w/v) agarose gels. These were made using the following protocol. Firstly, 1.5 g agarose (Fisher Bioreagents, BP160-500) was mixed with 150 ml 1X TAE buffer in a conical flask and microwaved for 2 min with shaking every 30 s. The liquid gel was cooled to 50 and 6 μl Midori Green (NIPPON Genetics EUROPE MG04) was added and mixed in by swirling the flask, with the exception for the amplification of *TaXTH23* with Gateway primers, when 3 μl ethidium bromide was used instead of Midori Green. The gel was then poured into a gel tray with a comb to create wells, and left to set for 50 min. The first well was loaded with 5 μl 1 kb DNA ladder (Quick-Load Purple 2-Log DNA Ladder, New England Biolabs N3200L). Every gel was run at 90 V for 50 min, imaged by the Blue-LED-Transilluminator, Vilber Fusion Pulse and visualised in the software Evolution Capture.

Sequencing Entry Clones

Two sequencing reactions, one forward and one reverse, were sent off to Eurofins Genomics for sequencing in 1.5 ml microfuge tubes. The reactions contained 15 μl 100 $ng/\mu l$ pDONR-*TaXTH23* and 2 μl of either the forward or reverse primers specific to pDONR207, table 2.24. Sequencing results were aligned using Clustral Omega with default parameters and visualised in Snap Gene.

Table 2.24: Primers for specific to the pDONR207 plasmid used to sequence entry clones pDONR207-*TaXTH23*

Primer	Sequence (5'-3')
pDONR207 Forward	TCGCGTTAACGCTAGCATGGATCTC
pDONR207 Reverse	GTAACATCAGAGATTTTGAGACAC

2.4.6 Transformation of Model Plant Species with *A. tumefaciens*

Transient Transformation of *Nicotiana tabacum* by Agroinfiltration

Two *N. tabacum* plants were agroinfiltrated with the expression clones *p35S::TaXTH23::GFP*, *p35S::AtXTH23::GFP*, *p35S::TaXTH23::RFP* and *p35S::AtXTH23::RFP*. Firstly, four 5ml LB liquid cultures containing 50 µg/ml spectinomycin and 10 µg/ml gentamicin were inoculated with glycerol stocks of *A. tumefaciens* containing the expression clones. The cultures were incubated at 28 ^oC for 48 h with shaking (180 rpm). The cultures were then centrifuged at 125 $\times$ g for 10 min at 4 ^oC to pellet the cells and the supernatant was discarded. The A. tumefaciens cells were rinsed twice by adding 2 ml of ice-cold transformation buffer (50 ml sterile water, 7.5 μl acetyl syringone and 500 μl MgCl2) and resuspended by pipetting. The cells were suspended in a final volume of 1ml transformation buffer and incubated on ice for 2 h. The OD600 of each cell suspension was measured using a spectrophotometer and then diluted with transformation buffer to OD600 = 0.3. These cell suspensions were then used to inoculate two *N. tabacum* plants. This was done by making a small scratch using sharp sterile tweezers on the abaxial side of the leaf and then using a 1 ml syringe to inoculate the leaf with the cell suspension at the site of the scratch. *N. tabacum* plants were then placed in a growth cabinet and well-watered for 3 d before imaging.

Stable Transformation of *Arabidopsis thaliana*

Floral dipping of *A. thaliana* For each transformed *A. tumefaciens* clone containing the expression constructs *p35S::TaXTH23::GFP* and *p35S::AtXTH23::GFP*, two 50 ml overnight cultures were made up in 50 ml falcon tubes with liquid LB media. The bacteria were spun down in a centrifuge for 15 min at 8 ^oC and 47000 rpm. The supernatant for each was discarded and the pellet was resuspended in 50 ml 5% sucrose, 0.05% silwett L-7 solution. The cultures, now suspended in sucrose solution, were poured into two 500 ml plastic pots, one for each construct. *A. thaliana* flowers from the lines Col-0 and *xth23* were dipped into the suspension for 15 – 30 s. A pipette was used to drip the suspension on to the flowers that could not be dipped. The plants were then laid in a tray lined with wet paper towel, covered with cling film and placed in the controlled environment growth room. They were set back upright after 3 days. The dipped plants were allowed to flower and then completely dry out. Their seeds were then collected and stored for 3 weeks in brown paper bags.

Selection of Transformed *A. thaliana* Plants Seeds from the plants that underwent floral dipping were sown on to trays of 3:1 compost to sand. The seedlings

Table 2.25: Summary of *A. thaliana* lines created by floral dipping

		Expression clone	
		p*35S::TaXTH23::GFP*	p*35S::AtXTH23::GFP*
Arabidopsis line	Col-0	WT background +TaXTH23	WT background +AtXTH23
	xth23	TaXTH23 complimented line	AtXTH23 complimented line

were grown for 5 d and then sprayed with a solution of water containing the herbicide BASTA . The seedlings were sprayed with 150 mg/ml BASTA twice more for 3 d. BASTA resistant individuals were selected and transplanted into pots containing 3:1 compost to sand and grown to set seed. Once the plants had set seed they were dried out and the seeds collected and stored.

2.4.7 Microscopy

Samples of transformed Tobacco leaves were viewed under an epifluorescence microscope two to three days after agroinfiltration. Images were visualised in LAS X (Leica Microsystems, Wetzlar, Germany).

2.4.8 Plant Materials, Growth Conditions and Medium

A. thaliana Materials and Growth Conditions

The *A. thaliana xth23* line was a T-DNA insertion mutant obtained from NASC. The seed was bulked from stocks from the Nottingham Arabidopsis stock centre (NASC), line GK-219B02 (stock number N420942). The ecotype Columbia-0 (Col-0) was used as a wild-type control and was also provided by the Grierson lab.

All Arabidopsis plants used were grown in a controlled environment growth chamber with light : dark cycles of 14 h : 10 h, under continuous light (120-145 $\mu mol/m^2/s^1$), at 21-22 ^oC and 60% humidity.

Arabidopsis plants used for genotyping were grown in 3:1 Sinclair compost to sand (J Arthur Bowers horticultural silver sand).

Seedlings used for total RNA extraction were grown on square plates containing 70 ml 0.5X MS (Murashige and Skoog) basal medium, 1% sucrose, and solidified with 1% agar.

Nicotiana tabacum Materials and Growth Conditions

N. tabacum plants were provided by The Grow Dome at the University of Bristol and were grown in William Sinclaire multipurpose compost. Plants were kept in a growth cabinet under constant light conditions (14 h light: 10 h dark) and at 21 ^oC.

Chapter 3

Results

3.1 Breeding of Wheat Mutant Lines

In order to test hypotheses about the role of XTHs and ABC transporters in root-soil cohesion in wheat appropriate mutant line were needed. A representative from each gene family was selected, *TaXTH23* for XTHs and *TaATH6* for ABC transporters. To understand their function a reverse genetic approach was taken using mutant lines from the TILLING (Targeting Induced Local Lesions IN Genomes) line collection for *TaATH6* and deletion line collection for *TaXTH23*(SeedStor, The John Innes Centre). Deletion lines were selected for *TaXTH23* as there was not appropriate TILLING lines available. TILLING and deletion lines are created by mutagenesis, making use of wheat's resilience to mutation [69, 70]. Sequencing data of mutagenized lines allows the selection of lines with mutations in the genes of interest.

Due to recent polyploidization event in the domestication of hexaploid bread wheat most genes are present in three functional copies, called homeologs [71]. There is often redundancy between homeologs, which has allowed wheat to be highly plastic to changing environments and also resilient to mutagenesis [72, 73]. However, redundancy between homeologs also means that homeologs can mask the knock out of one another. Hence, each homeolog has to be knocked out to create a knock-out mutant phenotype. To account for homeolog redundancy firstly, gene expression data was analysed to check that each homeolog was contributing to the expression of *TaXTH23* and *TaATH6*. Secondly, mutant lines with mutations for each of the homeologs were selected, summarised in the appendix.

Gene Expression Analysis of *TaXTH23* and *ATH6*

As bread wheat has three genomes A, B and D and therefore three homeologs of each gene, sometimes one or two of the homeologs can be switched off or expressed

at lower levels, this is known as homeolog expression bias. To check if *TaXTH23* or *TaATH6* had homeolog expression bias gene expression data was collated from wheatexpression.com. Analysis of gene expression data showed that neither *TaXTH23* or *TaATH6* had extreme homeolog expression bias. Each homeolog of *TaXTH23* contributed between 29 and 36% of the total amount of transcripts (Fig. 3.1 A) and for the *TaATH6* homeologs it was between 41 and 28% (Fig. 3.1 B). If one of the homeologs was not expressed this could have allowed the creation of a mutant line using just mutants for the other two homeologs. This was not the case and therefore all three homeologs needed to be knocked-out to create a mutant line as they were all contributing to the expression of the gene.

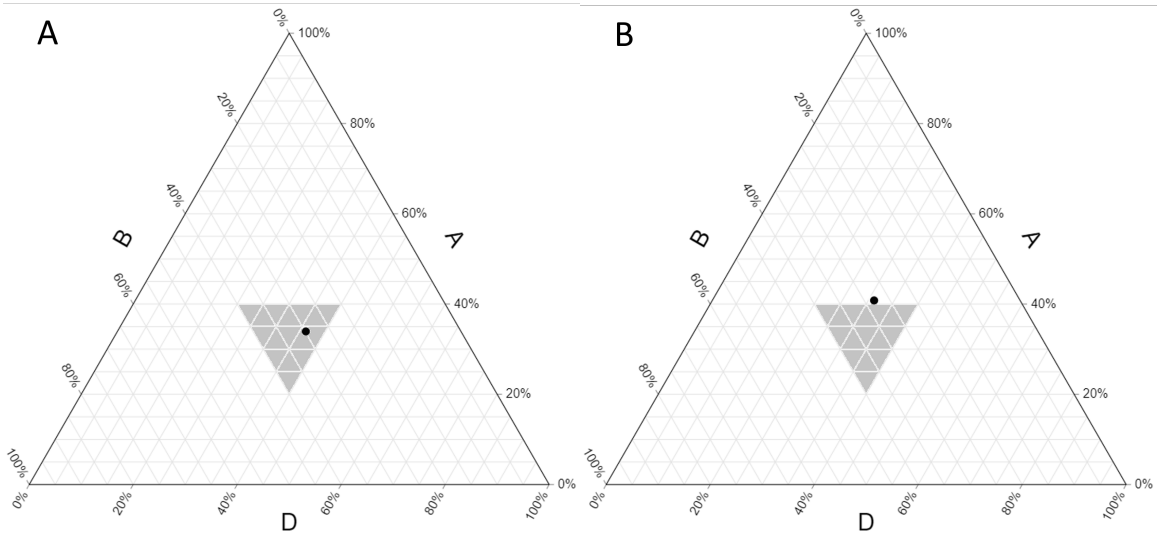

Figure 3.1: Ternary plot showing the percentage contribution of each homeolog A, B and D to the expression of A) *TaXTH23* and B) *TaATH6*. The homeologs analysed were for *TaXTH23* TraesCS7D02G419900, TraesCS7A02G427600 and TraesCS7B02G327700 and for *TaATH6* TraesCS1A02G343000, TraesCS1B02G356200 and TraesCS1D02G345200. The grey area highlights the area were homeolog expression is between 20 and 40% for each homeolog.

3.1.1 Genotyping Deletion Lines by PCR

To confirm that the deletion lines had the expected homeolog of *TaXTH23* deleted, each line was genotyped using homeolog specific primers and PCR. PCR reactions of a deletion line expected to lack homeolog X using homeolog X specific primers would not amplify a PCR product whereas the same PCR reaction with a line known

to contain homeolog X (the positive control) would produce a PCR product. Thus, after gel electrophoresis the presence of a band in the positive control and lack of ones for the deletion line individuals indicates that the individuals did not contain the homeolog.

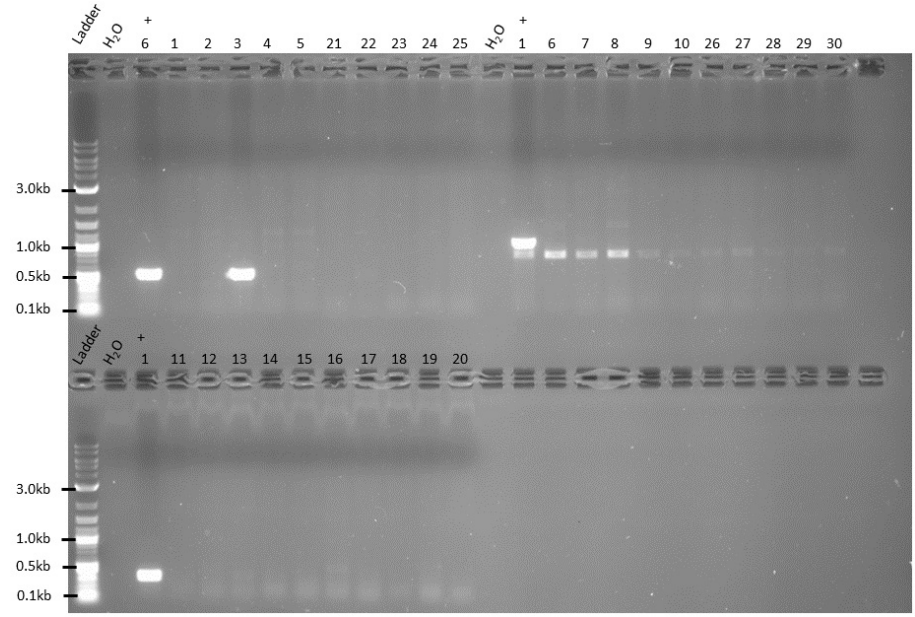

Figure 3.2: Genotyping of the *TaXTH23* deletion lines by PCR. For each of the three homeologs a PCR reaction, with homeolog specific primers, was run for the corresponding mutant lines. Each numbered well indicates a PCR reaction from an individual plant, A homeolog mutant lines J1-72 (plants 6-10) and J8-18 (plants 26-30) had an expected product size of 1000 bp if the A homeolog was present. B homeolog mutant lines J4-64 (plants 1-5) and J3-62 (plants 21-25) had an expected product size of 550 bp if the B homeolog was present and D homeolog mutant lines J5-46 and J3-6 (plants 11-20) had an expected product size of 400 bp if the D homeolog was present.

A Homeolog Mutant Lines

The A homeolog mutant lines were J1-72 (plants 6-10) and J8-18 (plants 26-30) and did not produce bands of the expected size (1000bp) after PCR with A homeolog specific primers (Fig. 3.2 B). The positive control J4-64 (1) produced a band of the expected size indicating that the primers and the PCR conditions both worked. The PCR reactions of the positive control and the deletion lines did produce a faint band of 800bp. This band is probably from the amplification of one of the other homeologs, indicating that the primers were not homeolog specific under the PCR conditions used. However, a band of 1000bp was missing for the deletion lines J1-72 and J8-18 indicating that they were, as expected, lacking the *TaXTH23* A homeolog.

B Homeolog Mutant Lines

The B homeolog mutant lines were J4-64 (plants 1-5) and J3-62 (plants 21-25) and did not produce bands of the expected size (550bp), except for plant 3, after PCR with B homeolog specific primers (Fig.3.2 A). The positive control J1-72 plant 6 produced a band of the expected size indicating that the primers and the PCR conditions both worked. The presence of a band of 550bp for plant 3 indicates that the plant contained the *TaXTH23* B homeolog. This could have come about due to accidental cross pollination of the parental line with a non mutant plant. The rest of the B homeolog mutants did not produce bands and therefore did not to contain the *TaXTH23* B homeolog as expected.

D Homeolog Mutant Lines

The D homeolog mutant lines were J5-46 and J3-6 (plants 11-20) and did not produce bands of the expected size (400bp) after PCR with D homeolog specific primers (Fig. 3.2 C). The positive control J4-64 plant 1 produced a band of the expected size indicating that the plant contained the D homeolog and that the primers and the PCR conditions both worked. Thus, as expected all the D homeolog mutants did not contain the *TaXTH23* D homeolog.

3.1.2 Progeny of Deletion Line Crosses are Double *TaXTH23* Mutants

To generate a knockout mutant for *TaXTH23* mutations in each homeolog needed to be combined by crossing. The wheat deletion lines were crossed with the aim of breeding a *TaXTH23* double heterozygote seed (AaBbDD and AABbDd). The crosses made and the resultant progeny are summarised in Table 3.1. All the crosses produced seeds except for plant 8 line J1-72 X plant 5 line J4-64, this may have been

because the lines were not compatible with too many deletions of essential genes. The line J1-72 was much smaller than the other lines and was also infected with powdery mildew which the other lines were not affected by. This lack of fecundity of J1-72 indicates that the line contained deletions of gene/s important for normal function and development.

Table 3.1: Deletion line crosses and the resulting progeny.

Female				Male			Progeny	
Plant Number	Line	Genotype		Plant No*	Line	Genotype	Seeds	Expected genotype
29	J8-18	aaBBDD	x	5,1	J4-64	AAbbDD	12	AaBbDD
27	J8-18	aaBBDD	x	5,1,4	J4-64	AAbbDD	14	AaBbDD
13	J5-46	AABBdd	x	1,4	J4-64	AAbbDD	25	AABbDd
12	J5-46	AABBdd	x	1	J4-64	AAbbDD	27	AABbDd
16	J3-6	AABBdd	x	1	J4-64	AAbbDD	16	AABbDd
8	J1-72	aaBBDD	x	5	J4-64	AAbbDD	0	AaBbDD
15	J5-46	AABBdd	x	4,5	J4-64	AAbbDD	25	AABbDd
25	J3-62	AAbbDD	x	1,4,5	J4-64	AAbbDD	26	AAbbDD

3.1.3 Genotyping *TaATH6* Mutant TILLING Lines

TILLING lines contain thousands of point mutations generated by ethyl methanesulphonate (EMS) mutagensis. They allow the quick and inexpensive acquisition of mutant lines for genes of interest that can be crossed to combine mutant homeologs. The TILLING lines chosen in this study each had a point mutation in the ABC transporter *TaATH6*, which created a premature STOP codon. The parental genotype of these seeds received from SeedStor (The John Innes Centre) was known. To check that homozygous parental lines had produced homozygous F1 plants, and to identify homozygous F1 plants from heterozygous parents the F1 generation for each TILLING line was genotyped. To genotype F1 plants a region around the point mutation needed to be amplified by PCR and the resulting product sequenced.

PCR Amplification of Region Around Point Mutation in *TaATH6* TILLING Lines

To confirm that TILLING lines contained the expected DNA point mutation in *TaATH6*, PCR was carried out using homeolog specific primers, to amplify a region around the point mutation in *TaATH6*. The amplified regions were then purified and Sanger sequenced. The homeolog specific primers were designed with the three prime end complimentary to only the desired homeolog. When annealed to a different homeolog to the one it is specific to the primer is not fully complimentary with the final three prime base mismatched. This causes the DNA polymerase to stall and

detach preventing elongation. All the plants of each TILLING line successfully produced a single PCR band between 500bp and 600bp as expected (Fig.3.3). A single band indicates that the primers were homeolog specific as different homeologs would produce different length products as the homeologs are different.

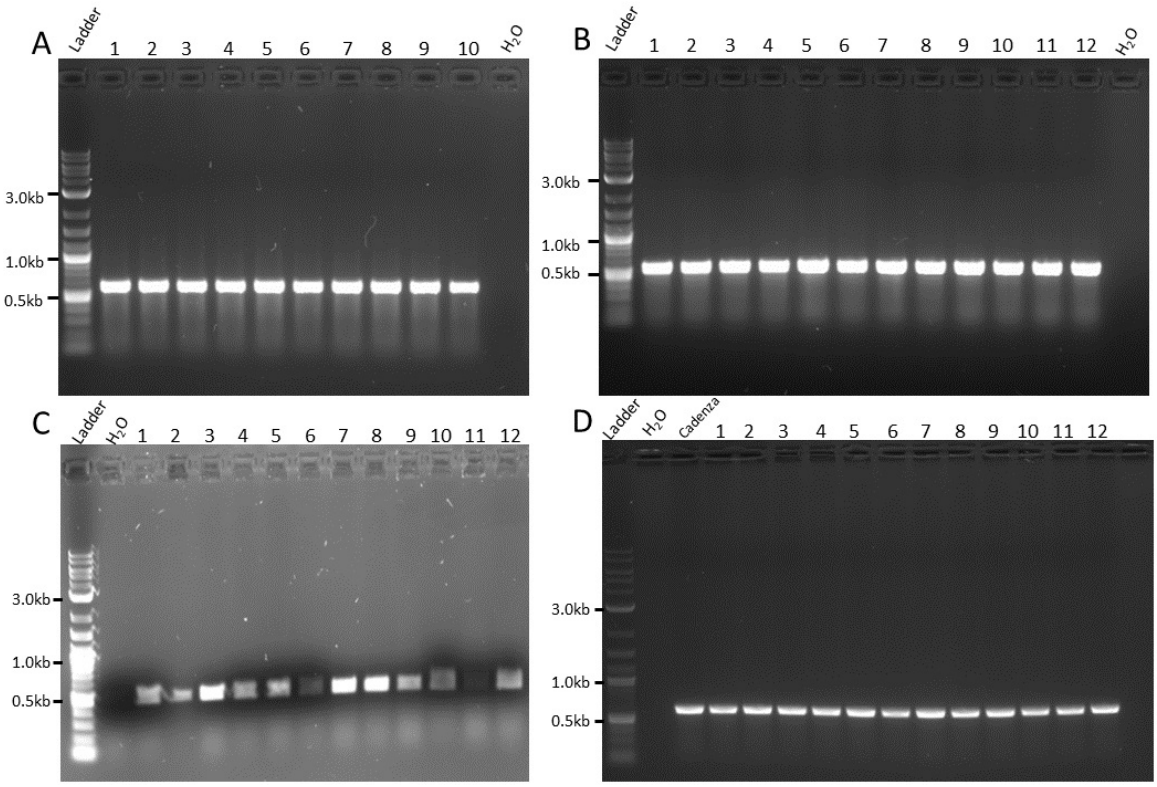

Figure 3.3: TILLING line PCR.(A) Cad0110, predicted PCR product size 611bp. (B) Cad0679, predicted PCR product size 570bp. (C) Cad1704 B homeolog, predicted PCR product size 519bp. (D) Cad1704 D homeolog, predicted PCR product size 628bp.Cadenza is a positive control of WT Cadenza which was used to ensure the PCR conditions and the primers were working.

TILLING Line Sanger Sequencing

The purified TILLING line PCR products were sequenced and the resulting chromatograms used to determine the genotype of each plant. A single peak present at the locus of the mutation indicated the plant was homozygous either for the mutation or WT. To identify homozygous mutants from homozygous WT plants the sequences were compared with WT *TaATH6* homeolog sequences available in Ensembl plant.

If there were two peaks at the at the locus then the plant was heterozygous for the mutation.

For the sequencing of Cad1704 B homeolog both forward and reverse sequencing reactions were carried out. For all the Cad1704 plants, except 2, the forward sequence had a single peak adenine (A) and the reverse had a single peak representing thymine (T) at the locus of the mutation (table 3.2). The bases A and T were complimentary as expected and the single peak indicated that they were homozygous. The presence of A in the forward sequence at the locus of the predicted mutation was the mutant genotype, the WT was guanine (G). The change from G to A results in a premature STOP codon, TGA. This premature STOP codon should stop transcription of the gene early resulting in a truncated protein.

For Cad1704 plant 2, both the forward and reverse sequencing chromatograms had two peaks at the locus of the predicted mutation. These two peaks were for A and G in the forward sequence and T and C in the reverse (Table 3.2). This indicated that the plant is heterozygous for the mutation, which was unexpected as the parent of the plant was homozygous for the mutation. Therefore, there must have either been an accidental cross pollination or less likely a mutation that reverted one of the mutant *ATH6* B homologs back to WT.

Table 3.2: Sequencing results and genotypes of Cad1704 plants for the *ATH6* B homeolog.

Line	Target homeolog	Plant	Base (F)	Base (Rv)	Genotype
Cad1704	B	1	A	T	hom - M
Cad1704	B	2	R (A / G)	Y (T/C)	het
Cad1704	B	3	A	T	hom - M
Cad1704	B	4	A	T	hom - M
Cad1704	B	5	A	T	hom - M
Cad1704	B	6	A	T	hom - M
Cad1704	B	7	A	T	hom - M
Cad1704	B	8	A	T	hom - M
Cad1704	B	9	A	T	hom - M
Cad1704	B	10	A	T	hom - M
Cad1704	B	11	A	T	hom - M
Cad1704	B	12	A	T	hom - M

Base= the Base at the locus of the mutation, F= forward sequence and R= reverse sequence. Genotype, hom= homozygous, het= heterozygous, M = mutant.

The TILLING lines Cad0110, Cad0679 and Cad1704 D homeolog were also genotyped in forward sequencing reactions. All ten Cad0110 plants were homozygous for the mutation with A instead of the WT G (appendix table 5.1). This change from a

G to an A created the premature STOP codon (TGA). All plants being homozygous for the mutation was expected as the parent of this line was also homozygous for this mutation.

The parent of the Cad0679 line was heterozygous for the the mutation and therefore, it was expected that Cad0679 would be 1/4 homozygous WT, 1/2 heterozygous and 1/4 homozygous mutant. The sequencing however showed that all of the Cad0679 plants were homozygous WT (appendix table 5.1). This could have been due to chance, accidental cross pollination or a point mutation in the parent germ line which reverted the mutation back to WT.

The parent of Cad1704 was heterozygous for the D homeolog mutation; thus, it was expected that the line would be 1/4 homozygous WT, 1/2 heterozygous and 1/4 homozygous mutant. Both heterozygous and homozygous plants would have been useful for the breeding of a *ath6* knockout mutant line. Three Cad1704 plants were homozygous for the mutation (plants 1, 7 and 10) and two were heterozygous (plant 11 and plant 8)(appendix table 5.1). Representative chromatograms for each genotpye are show in fig.3.4.

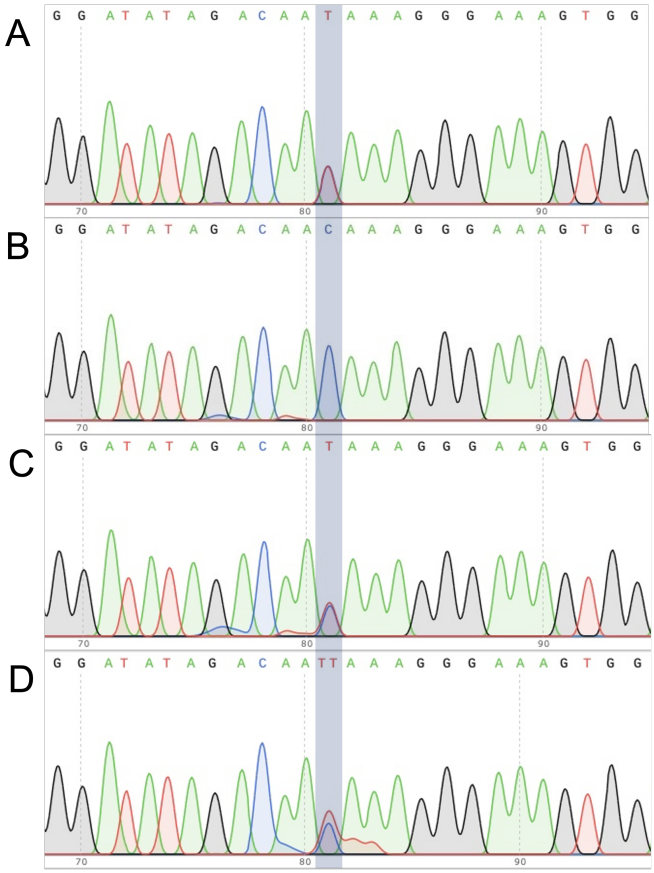

Figure 3.4: Sections of sequencing chromatograms showing the genotype of Cad1704 plants for the *TaATH6* D homeolog. The locus of the mutation is highlighted. A double peak indicates the plant is heterozygous whereas a single indicates they are homozygous. A Thymine (T) at the locus, shown in the consensus sequence above the chromatogram, is the mutant genotype and Cytosine (C) is the WT. (A) plant one homozygous mutant, (B) plant 2 homozygous WT, (C) plant 8 and (D) plant 11 were heterozygous for the mutation.

TILLING Line Crossing Resultant Progeny

The TILLING line Cad0110, which was homozygous mutant for *TaATH6* A homeolog, was crossed with Cad1704 plants 1, 7 and 10, which were homozygous double mutants for the *TaATH6* B and D homeologs. All crosses were successful and produced seed indicating that the parental line does not contain any harmful back ground mutations in important genes Table 3.3. The resulting seeds should all be heterozygous triple mutants AaBbDd for the gene *TaATH6*.

Table 3.3: Summary of TILLING line crosses and the resulting seeds. The emasculated female plants are denoted by Cad1704-plant number.

Female			Male		Progeny	
Line	Genotype		Line	Genotype	Seeds	Expected genotype
Cad1704 - 1	AAbbdd	X	Cad0110	aaBBDD	7	AaBbDb
Cad1704 - 10	AAbbdd	X	Cad0110	aaBBDD	8	AaBbDb
Cad1704 - 7	AAbbdd	X	Cad0110	aaBBDD	35	AaBbDb
Cad1704 - 11	AAbbDd	X	Cad0110	aaBBDD	39	50% AaBbDb : 50% AaBbDD

3.2 Developing a Soil Erosion Assay for Wheat

3.2.1 Soil Composition Analysis

Soil composition can drastically affect root-soil cohesion and soil erosion thus it was important to ensure that the soil acquired for this study was sandy loam and that it was consistent across bags so it would not be a confounding factor between later uprooting experiments. Many previous studies also use sandy loam soil, so to be able to compare this study with their findings it was important to use the same soil type.

To confirm that the soil used in the uprooting experiments was sandy loam, a laser particle analyser was used to estimate the particle size distribution of different soil samples. The mean percentage composition of clay, sand and silt was plotted in the USDA soil texture triangle for each sample to illustrate their composition and classification (fig.3.5)[74, 75]. All the soil samples and the mixed sample had a composition of sandy loam (fig.3.5). The particle size composition of the mixed sample was 4.6% clay, 35.5% silt and 59.9% sand.

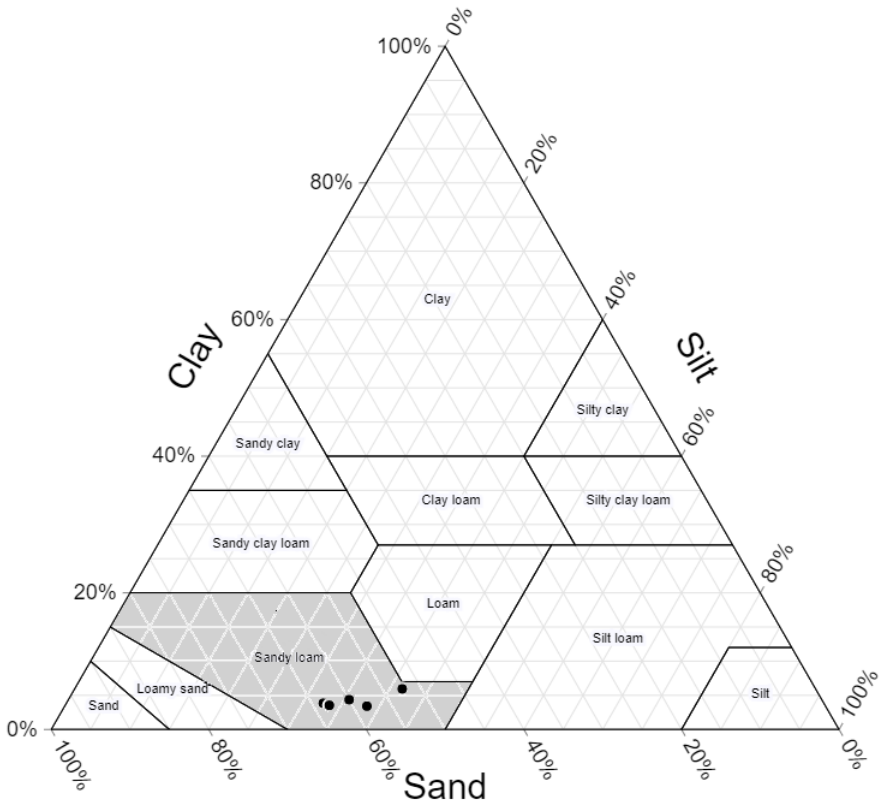

Figure 3.5: USDA Soil Texture Triangle showing the soil composition of six soil samples which are represented as black circles [74, 75].

3.2.2 Development of Uprooting Methods

Growing Wheat Seedlings for Uprooting

It was not know whether wheat seedlings would grow inside pipette tips or whether the pipette tips could act as an anchor to uproot the seedlings with. So, multiple trails were run to investigate. The wheat seeds were sown inside P1000 pipette tips with 5 mm removed from the tip and placed 3cm deep into damp soil. During the initial growth trials a few problems arose which needed to be solved in order to get a high germination rate and normal growth. Firstly, wheat germination rates were very low as the seeds dried out in the pipette tips. This was resolved by using a spray bottle to lightly mist the seeds once places in the pipette tip to increase the humidity around the seeds to encourage germination. Later, seeds became mouldy in the pipette tips, which severely inhibited the seedlings growth. This was probably caused by over misting and allowing the seeds to sit in droplets of water for long

periods of time. Another problem that arose was that the shoots would sometimes grow down into the pipette tip and into the soil rather than upward. Examples of this growth are shown in Fig. 3.6. The shoot growing down into the soil would affect uprooting by disrupting the root-soil matrix and creating added friction against the soil. This was solved by orienting the seed with the hairy, narrow end, called the brush, facing up in the pipette tip before planting.

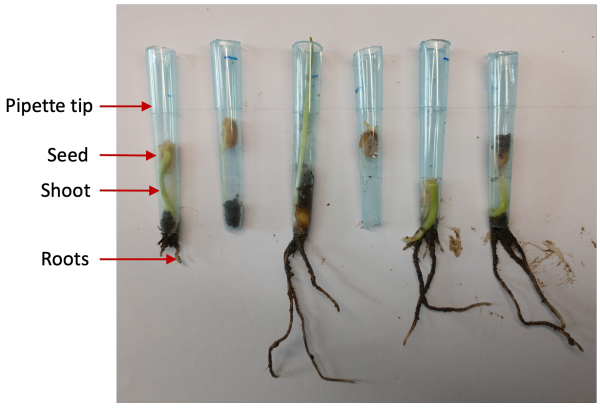

Figure 3.6: Six representatives of 3 d old (GS07) wheat seedlings grown in modified pipette tips from preliminary work. Seedlings A, E and F all showed an undesirable growth strategy with the shoot growing down the pipette tip into the soil. B and D dried out and did not germinate and C is a seedling growing as desired, and suitable for uprooting, with the shoot growing upwards and the roots down into the soil.

Optimal Anchor for Uprooting Wheat Seedlings

After determining that it was possible to grow wheat seedlings in pipette tips, the investigation turned to what the optimal size and shape of pipette tip would be for uprooting the seedlings with. Thus wheat seedlings were grown in different brands of pipette tips with different amounts cut off the end and the percentage of seedlings which germinated, made it to GS11 and could be uprooted was observed and shown in table3.4. GS11 seedlings can be identified as they have their first leaf fully emerged characterised by the presence of a ligule. Out of all the different pipette tips used the Sarstedt p1000 pipette tips with 5mm cut off the end had the highest uprootability (75%) and had a high germination rate (96%). Thus, the Sarstedt p1000 pipette tips with 5mm cut off the end were the most suitable for uprooting experiments and were used for the uprooting of wheat seedlings in the later sections.

Table 3.4: Investigation of the optimal size and shape pipette tip for uprooting wheat seedlings.

	length removed	planted	germination(%)	GS11 (%)	uprootability (%)
Eppendorf		8	50	0	0
Greiner Bio-one Tip 1000	5 mm	22	91	73	20
	10 mm	23	87	70	0
Sarstedt p1000	5 mm	24	96	96	75
	10 mm	24	100	100	0

Does Growth in a Pipette Tip Affect Development?

To test whether the pipette tip affects wheat seedling growth 48 wheat seedlings were planted half in pipette tips (Sarstedt p1000, 5 mm) and the other half sown straight into the soil, normal growth condition, following the methods described in section 2.2.3. The development of the seedlings was tracked over two weeks. For normal growth conditions, 22/24 seeds germinated whereas only 20/24 seeds in pipettes germinated. Following the development of the seedlings over 14 days revealed that the day which all the seedlings reach each growth stage was the same for seedlings grown in a pipette tip and normally (table.3.5). At day 5 all the seedlings for both groups were at GS10, then at day 10 all had reached GS11 and on day 14 all had reached GS13 (table.3.5). Thus, germination rate was slightly lower for wheat seedlings grown in pipette tips but the speed of development from germination to GS13 was not affected.

Table 3.5: Development of wheat seedlings grown in pipette tips and normal growth conditions over 14 days. Numbers are the number of seedlings at each growth stage.

	Pipette tip			Normal		
Age	GS10	GS11	GS13	GS10	GS11	GS13
5 days	20	0	0	22	0	0
6 days	19	1	0		1	0
7 days		4	0		2	0
10 days		20	0		22	0
14 days			20			22

3.2.3 Uprooting Wheat Seedlings at Different Growth Stages

To investigate the potential of uprooting wheat seedlings as an assay to help identify traits which affect root-substrate cohesion in wheat, wheat seedlings were uprooted at three consecutive growth stages. The three growth stages used in this study were GS10, GS11 and GS13. GS10 is characterised by the emergence of the first leaf from

the coleoptile (approximately 5 days after sowing), GS11 by the full emergence of the first leaf and the presence of the ligule (approximately day 7) and GS13 by the full emergence of 3 leaves on the main shoot (approximately day 14). These were used as earlier growth stages cover germination, and have very small roots and later growth stages have very large root systems which become pot bound.

GS10 was the Most Successfully Uprooted Growth Stage

The different growth stages were uprooted using a tensile testing machine, Instron, which was connected to the pipette tips by wires and a clamp. The Instron machine applied a vertical force to the seedling to uproot it. Uprooting was the most successful at GS10 and much less successful at GS11 and GS13, the mean successful uprooting was 88% GS10, 63% GS11 and 62% GS13 (Table 3.6). All the seedlings at GS10 were successfully uprooted and the number of outliers was relatively low in each replicate (R1 2/23, R2 2/18 and R3 2/13). For the other growth stages multiple problems arose which reduced the number of seedlings successfully uprooted to less than 75%. The main problem was the pipette tip slipping off and over the seedling. These failed uprootings decreased the sample size up to half in GS11 and GS13. Other problems were the pot rising with the plant and soil balancing on top of the root soil ball. Any uprooting where a problem arose was excluded from the data set. The issues skew the amount of soil which is actually part of the root soil ball, making the amount of soil stuck to the roots seem much greater than it actually was.

Table 3.6: Summary of the seedlings uprooted and its success rates across the different growth stages. Attempted up rooting refers to the number of wheat seedlings which uprooting was carried out on whereas successful uprooting refers to the number of seedlings which were fully uprooted with out error.

Replicate	Seeds planted	Germinated	Growth stage	Attempted Uprooting	Successful uprooting (%)
1	72	69%	GS10	23	100
			GS11	12	58
			GS13	14	50
2	72	71%	GS10	18	100
			GS11	16	75
			GS13	15	87
3	60	88%	GS11	13	100
			GS13	12	83

The Effect of Wheat Seedling Growth Stage on Uprooted Soil Mass

Figure3.7 shows the uprooted soil mass per root length (RL) for each growth stage and for each replicate (R1, R2 and R3). One way ANOVAs were run to test whether the uprooted soil mass per RL was consistent across replicates for GS10 and GS11 and for GS13 t-test was run instead. The statistical analysis showed that uprooted soil mass per RL was not different across replicates for each growth stage, GS10 $F(2,51)$=1.36, p=0.27, GS11 $F(2,21)$=1.36 p=0.64 and for GS13 $t(17)$=0.34 and p=0.74. The consistent uprooted soil mass per RL for each growth stage indicates that the methods used for uprooting can produce reproducible data across replicates. However, for GS13 the variation did differ largely between replicates, this may mainly be due to a large difference in sample sizes (Table. 3.7).

To test whether the uprooted soil mass per RL differed between growth stages further one way ANOVA analysis was run for R1 and R2. For both replicates growth stage significantly affected uprooted soil mass per RL, R1 $F(2,32)$=33.7, $p < 0.001$ and R2 $F(2,37)$=29.2, $p < 0.001$. For R3 GS10 and GS11 were compared using t-test, this revealed that there was no difference between GS10 and GS11 in R3, $t(20)$=-1.53 and p=0.14. There was also no difference between GS10 and GS11 in R1 and R2, $t(27)$=-1.28 p=0.21 and $t(25)$=-1.56 and p=0.13 respectively. Thus, growth stage does not affect uprooted soil mass per RL until GS13 when it significantly increases (Fig. 3.7).

Relation Between RL and Uprooted Soil Mass

Figure 3.8 shows the relationship between RL and uprooted soil mass at each growth stage for three replicates. At least one replicate for each growth stage showed a positive correlation between RL and uprooted soil mass, $p < 0.05$, (Fig. 3.8) indicating that as root length increases, the soil attached to the roots increases.

Interestingly, for GS10 the smallest sample size ($n = 13$, R3) gave more significant correlation between RL and uprooted soil mass despite R^2 being about the same for each replicate (0.55, 0.58 and 0.56 for R1, R2 and R3 respectively). This may have been due to fewer outliers with a smaller sample size. GS11 only had significant positive correlation for R2, $n = 9$ and not for R1 and R3. This was probably due to the small sample sizes and indicates that a minimum sample size greater than 9 is required to consistently produce significant results for GS11. GS13 however, produced significant correlation for R1 when $n = 6$, p=0.041.

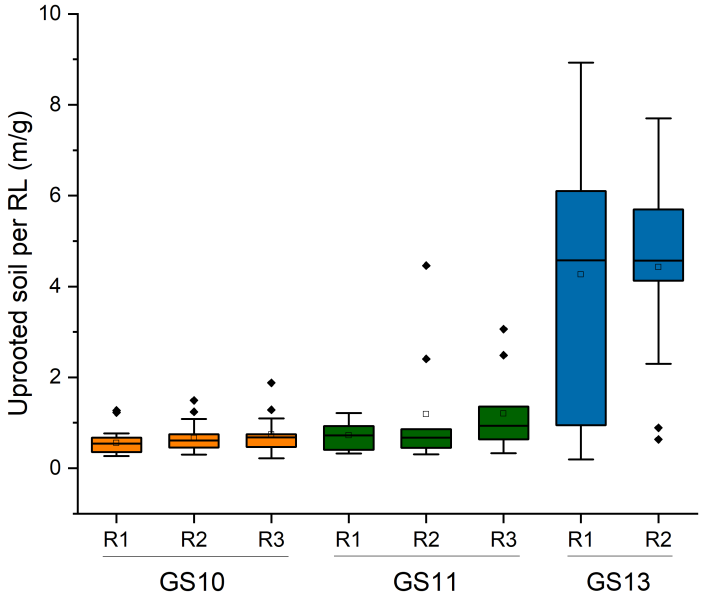

Figure 3.7: The effect of growth stage on uprooted soil mass per RL. GS10, first leaf through the coleoptile: R1 $n = 23$ $\mu = 0.56$, R2 $n = 18$ $\mu = 0.66$, R3 $n = 13$ $\mu = 0.74$. GS11, first leaf unfolded: R1 $n = 6$ $\mu = 0.72$, R2 $n = 9$ $\mu = 1.19$, R3 $n = 9$ $\mu = 1.2$. GS13, three leaves unfolded: R1 $n = 6$ $\mu = 4.82$, R2 $n = 13$ $\mu = 4.42$. Values are to 2 decimal places. Outliers are represented by black diamonds and the mean by an open square.

Relation Between Root Length Density and Uprooted Soil Mass

To investigate whether the roots broken off in the pot effect the soil mass uprooted a regression analyses of root length density (RLD) and uprooted soil mass was carried out for GS11 and GS13 (Fig. 3.9). GS10 plants roots did not break off in the pot and therefore RLD would have been a simple function of RL. Similarly to RL, RLD correlates positively with the mass of soil uprooted in GS11 R3 $p = 0.015$ and GS13 R2 $p = 0.0085$ (Fig. 3.9 C and E). The other replicates did not produce significant correlations between RLD and uprooted soil mass all of which only had a sample size of 6. For GS11 R3 and GS13 R2 RLD accounted for only 43% and 48% of the variation in uprooted soil mass.

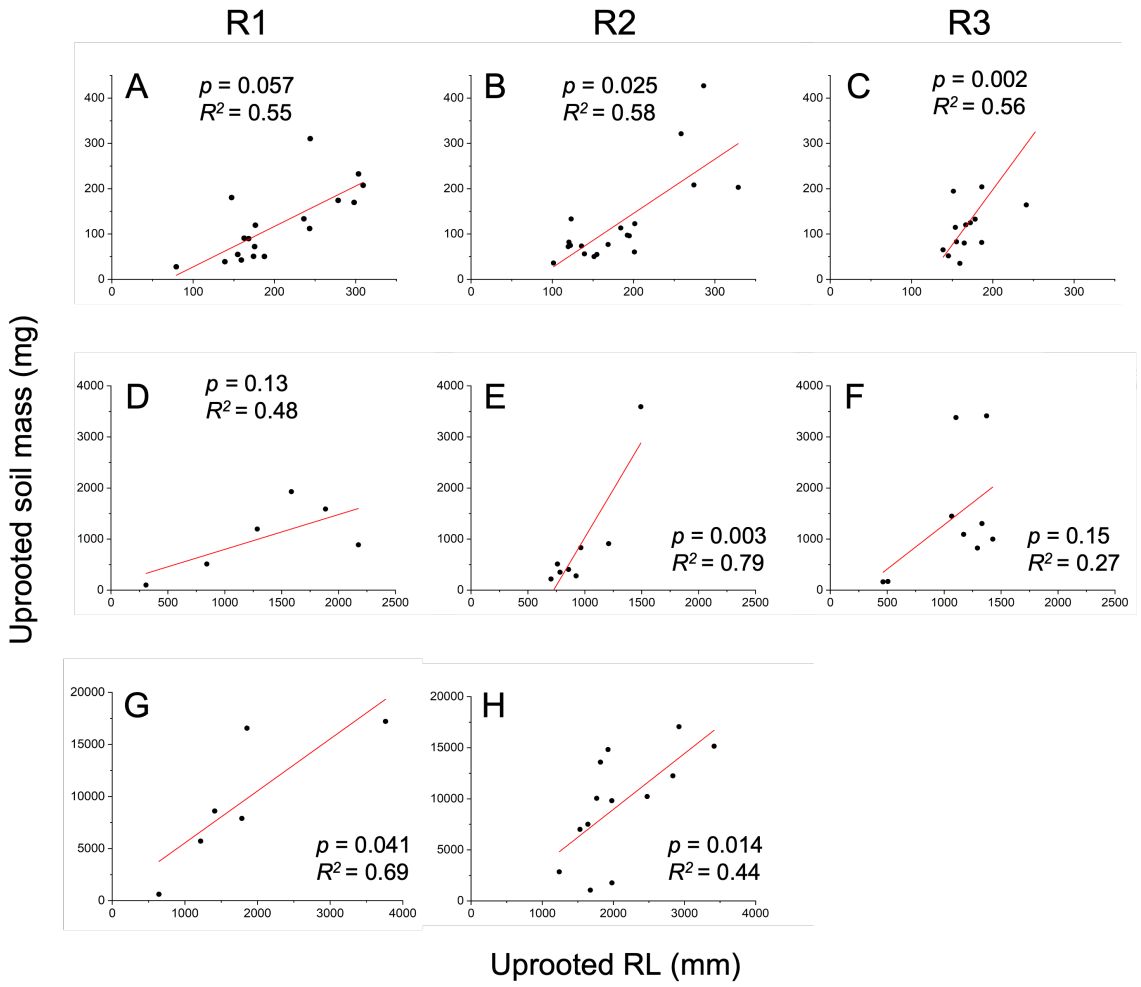

Figure 3.8: The effect of RL on uprooted soil mass at different growth stages. GS10: A, B, and C. GS11: D, E and F. GS13: G and H. Linear regressions are shown as red lines and individual data points are shown as black circles. Values are to 2 d.p. except p which is to 2 s.f.

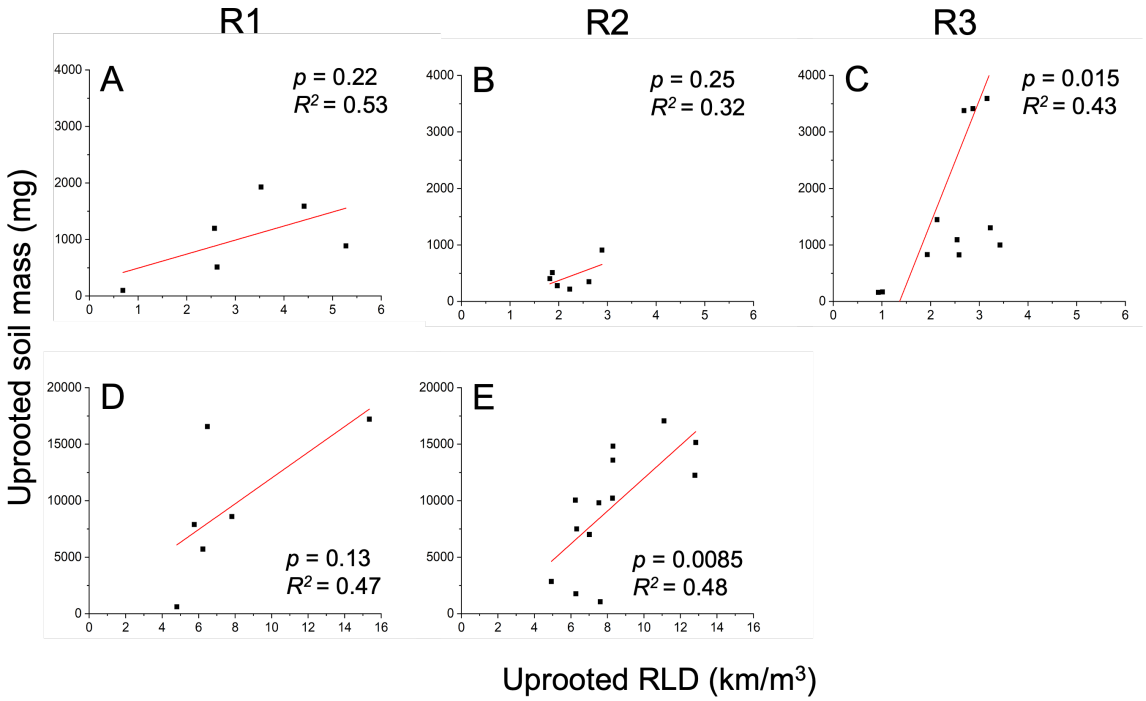

Figure 3.9: The effect of RLD on uprooted soil mass at different growth stages. GS11: A, B and C and GS13: D and E. Linear regressions are shown as red lines and individual data points are shown as black squares. Values are to 2 d.p. except p which is to 2 s.f.

3.3 Stable and Transient Expression of *TaXTH23* in Model Plant Species

3.3.1 Gateway Cloning of *XTH23*

Gradient PCR of *TaXTH23* The coding region of the *TaXTH23* B homeolog, excluding the STOP codon, was amplified using gradient PCR from Cadenza gDNA using gateway primers specific to the B homeolog to add the recombination attB sites to the ends of *TaXTH23* (see table. 2.20). One band was expected of 1100- 1200bp. A single band shows that the primers were homeolog specific at the PCR conditions used. PCR reactions 1 and 2 had two bands one of the expected size and another at <1000bp and is likely an amplification of one of the other homeologs (fig. 3.10). For the rest of the PCR reactions the PCR conditions only allowed the specific homeolog to be amplified as only one band of the expected size was present. The PCR products

from reactions 3 and 4 were taken forward for gateway cloning.

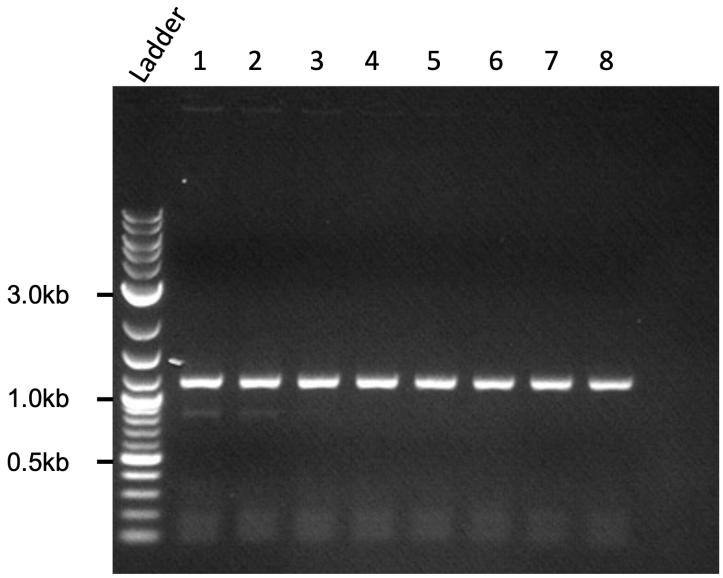

Figure 3.10: Gradient PCR of TaXTH23 with Gateway primers. Temperature increases from well 1 at 50°C to well 8 at 60°C.

Entry clone sequencing results The BP reaction combined the pDONR donor vector with *TaXTH23* by recombination. The resulting entry vector pDONR*TaXTH23* was used to transform *E. coli* (pDONR*TaXTH23* vector map see fig 3.11). Positive *E. coli* colonies were tested for the presence of the entry clone by colony PCR, using the Gateway primers. Sanger sequencing of the entry clones showed that no mutations had occurred in the *TaXTH23* sequence in the entry clone. The expected sequence and the forward and reverse sequencing runs of *TaXTH23* were aligned and this revealed mismatches between them. However, the first mismatch was in the first 100 bps and the rest were in the final 200 bps and none were present in both the forward and reverse sequencing runs. Therefore, the mismatches were highly likely to be down to sequencing error.

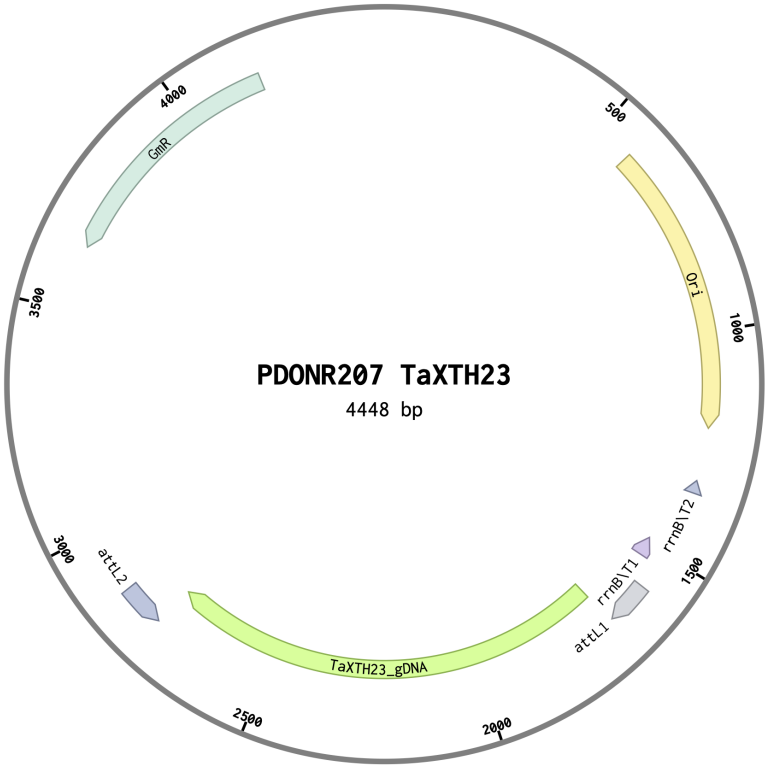

Figure 3.11: Vector map of entry clone pDONR207 *TaXTH23* resulting from the BP reaction. GmR is the gentamicin resistance gene in blue. The recombination sites are attL sites shown in grey and the gene inserted was *TaXTH23* in green. Vector map was constructed in Benchling.

Testing for expression clone positive *E. coli* and *A. tumefaciens* colonies Transformed *E. coli* colonies were tested for the expression clones p35s::*TaXTH23*::GFP, p35s::*AtXTH23*::GFP, p35s::*TaXTH23*::RFP and p35s::*AtXTH23*::RFP using colony PCR with primers specific to the inserts *TaXTH23* and *AtXTH23*. The expression clone p35s::*TaXTH23*::GFP is shown in fig 3.12. *TaXTH23* containing colonies were tested using the Gateway primers and *AtXTH23* containing colonies were tested using *AtXTH23* specific primers. Positive colonies were expected to produce a PCR product bands of 1000bp and 350-400bp for *TaXTH23* and *AtXTH23* respectively. All tested colonies were positive for their expected inserts (Fig. 3.13 and Fig. 3.14). Transformed *A. tumefaciens* colonies were also tested for the inserts using colony

PCR and the same primers. All the tested transformed *A. tumefaciens* were positive for their expected inserts as they showed PCR bands of the expected size (Fig. 3.15).

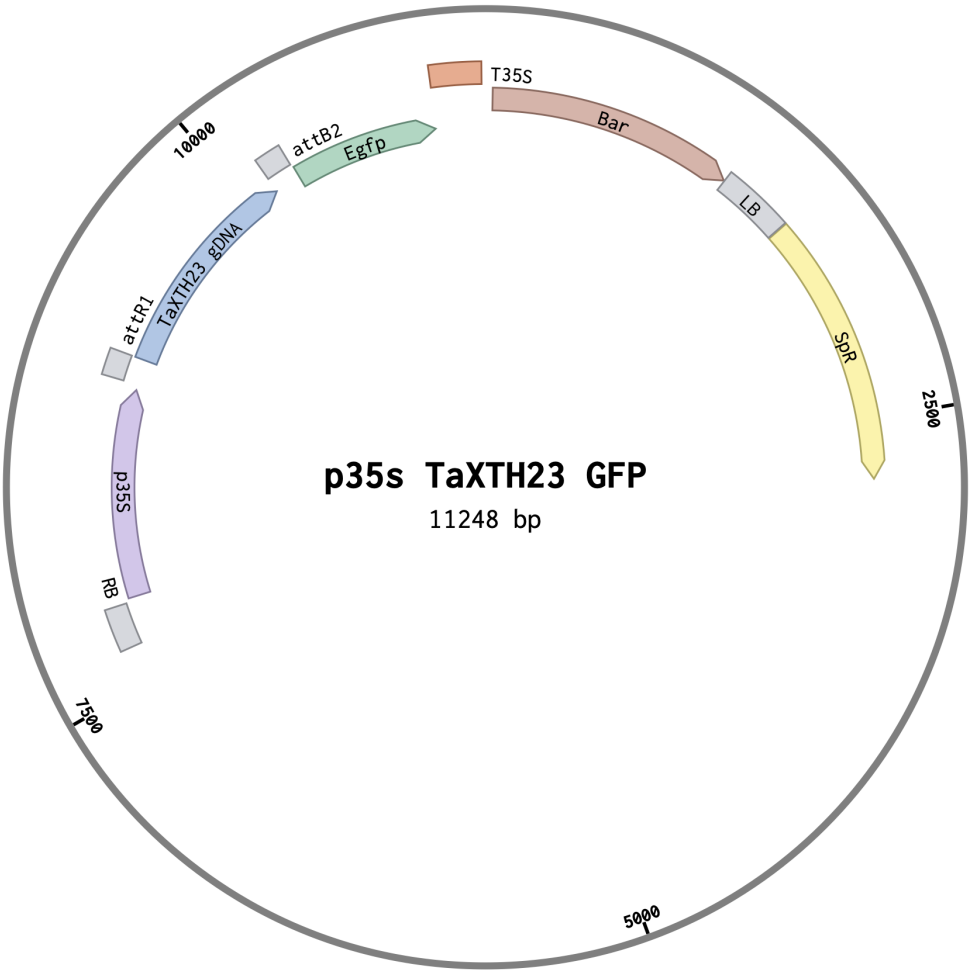

Figure 3.12: Vector map of the expression clone p35S::*TaXTH23*::GFP. The promotor 35S is shown in purple, *TaXTH23* in blue and *GFP* in green. The antibiotic resistance gene SpR in yellow confers resistance to spectinomycin. Vector map was constructed in Benchling. The other expression clones used in this work had the same structure as this expression clone but contained either *AtXTH23* or *RFP* instead.

The resulting expression clones from Gateway cloning contained the Cauliflower Mosaic Virus (CaMV) 35S promoter as it provides strong constitutive expression of transgenes [76]. GFP and RFP were also fused to XTH23 in the expression clone to

ensure that the construct was being expressed in model species and so the localisation of the protein could be determined. The molecular tags GFP and RFP were fused to the XTH23 C terminus, as XTH active site is at the start of the second exon nearer the N terminus and the signal peptide is also at the N terminus, thus reducing the chances of GFP/RFP disrupting the function and localisation of XTH23.

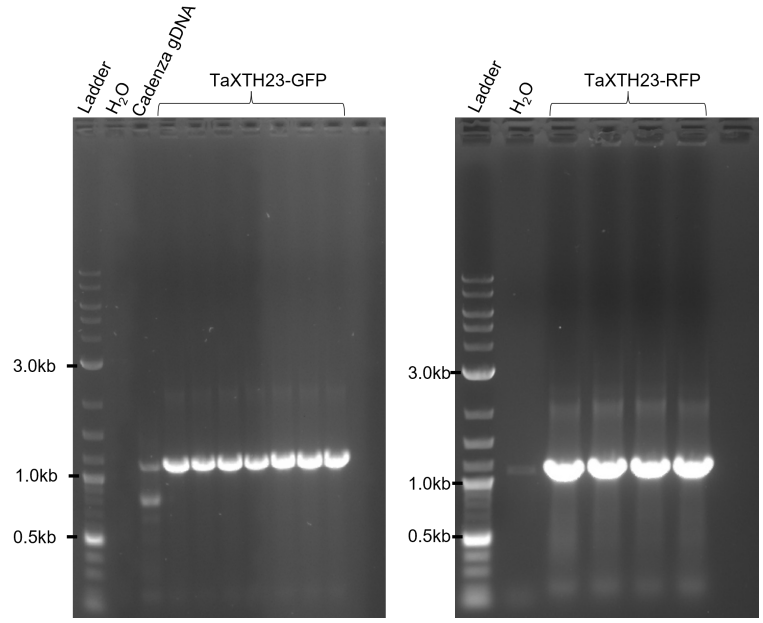

Figure 3.13: Colony PCR of *E. coli* colonies transformed with the expression vectors p35s::*TaXTH23*::GFP and p35s::*TaXTH23*::RFP. Gateway primers were used and the expected band size for a positive colony was 1075bp.

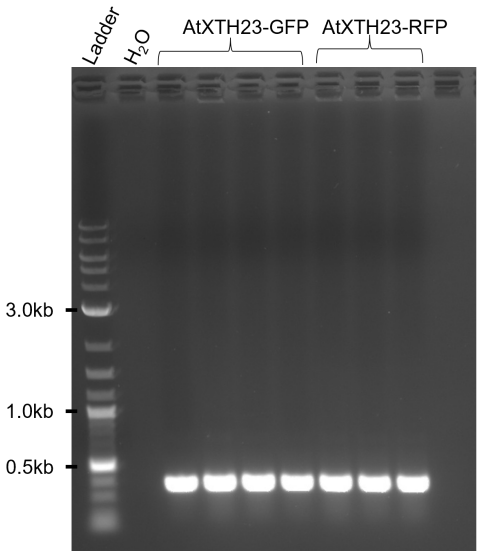

Figure 3.14: Colony PCR of *E. coli* transformed with p35S::*AtXTH23*::GFP and p35S::*AtXTH23*::RFP expression vectors. Positive colonies were expected to produce a band of 350-400bp

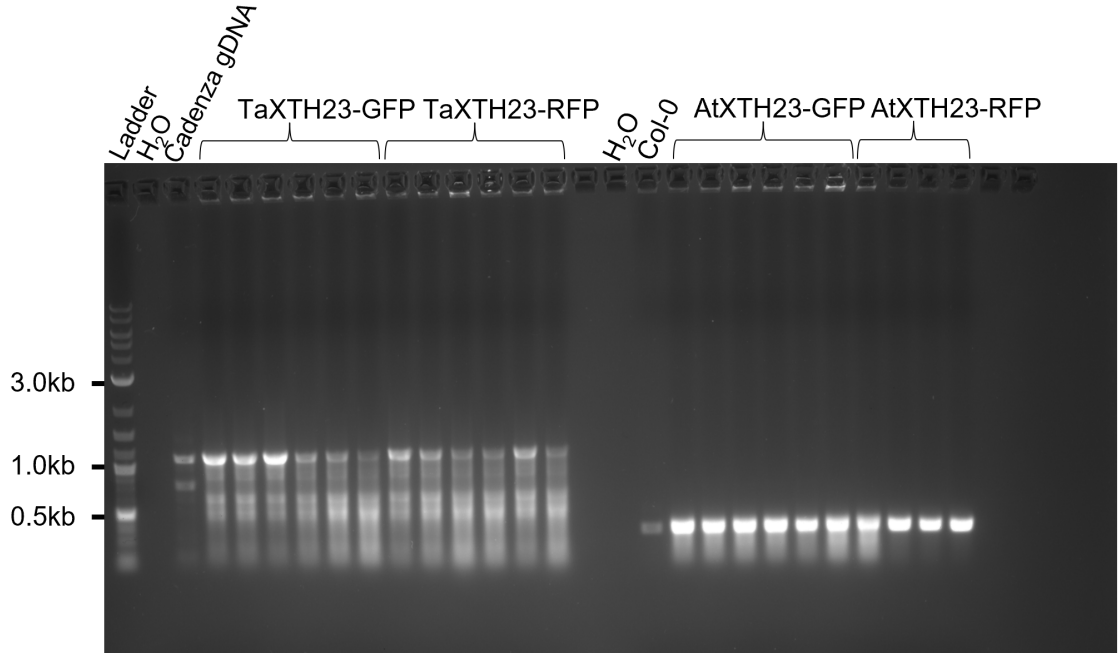

Figure 3.15: Colony PCR of *A. tumefaciens* colonies transformed with the expression clones p35S::*TaXTH23*::GFP, p35S::*AtXTH23*::GFP, p35S::*TaXTH23*::RFP, p35S::*AtXTH23*::RFP. Colonies containing the *TaXTH23* insert were expected to produce a band of approximately 1000bp and Colonies containing the *AtXTH23* were expected to produce a band of 350-400bp.

3.3.2 The *xth23 Arabidopsis thalina* Mutant is Homozygous but not a Knockout

Genotyping *Arabidopsis thalina xth23* Mutants

Twelve *xth23* mutants were genotyped using three PCR reactions with 1. forward + reverse*AtXTH23* specific primers (F+R) 2. forward primer and the T-DNA specific left border primer (LB) (F+LB) and 3. reverse primer and the T-DNA specific LB (R+LB). The position of the primers and the T-DNA insert are represented in fig. 3.16. WT individuals were expected to produce a PCR product only for the F+R PCR reaction. Heterozgyous individuals would produce bands for all three reactions and homozygous for just the F+LB and R+LB. As expected the WT individual tested only produced a band for the F + R PCR reaction (WT band) and not for the F + LB and R + LB (Fig. 3.17). This indicates that the primers and PCR conditions worked and that *XTH23* is present and the T-DNA insert is not as the LB primer is specific to the T-DNA insert. None of the *xth23* mutants produced a WT band as expected indicating that the T-DNA insert is present in both homologs. The mutant individuals, except 2 and 10, produced bands for both the F+LB and R+LB reactions further indicating that they were homozygous for the T-DNA insert. Individual 10 produced no bands probably due to a failed DNA extraction and individual 2 produced a band for only the R+LB reaction this is probably due to a pipetting error. The individual was probably homozygous as well as there was no WT band and there was a R+LB mutant band. In summary the *xth23* mutant line is homozygous for the T-DNA insert.

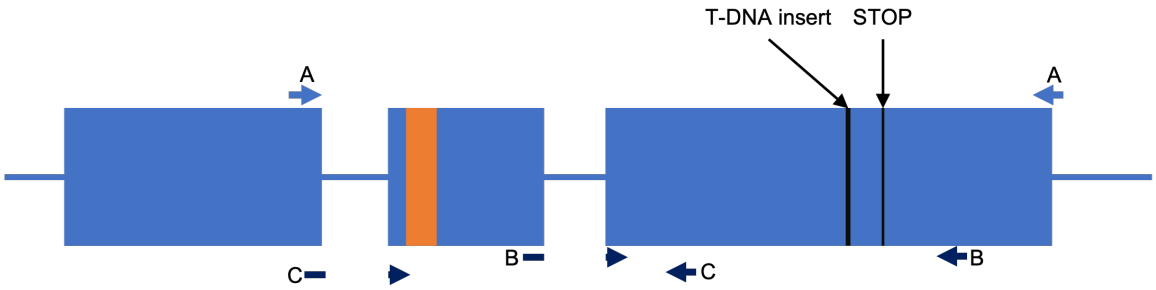

Figure 3.16: *AtXTH23* has three exons represented by blue boxes. The catalytic site is highlighted in orange and the site of the T-DNA insert and STOP codon are also indicated. The forward and reverse primers used for genotyping are shown as arrows and labelled A. The primers used for RT-PCR are represented by darker arrows, with Primer Set 2 labelled B and primer Set 3 labelled C. Diagram is to scale.

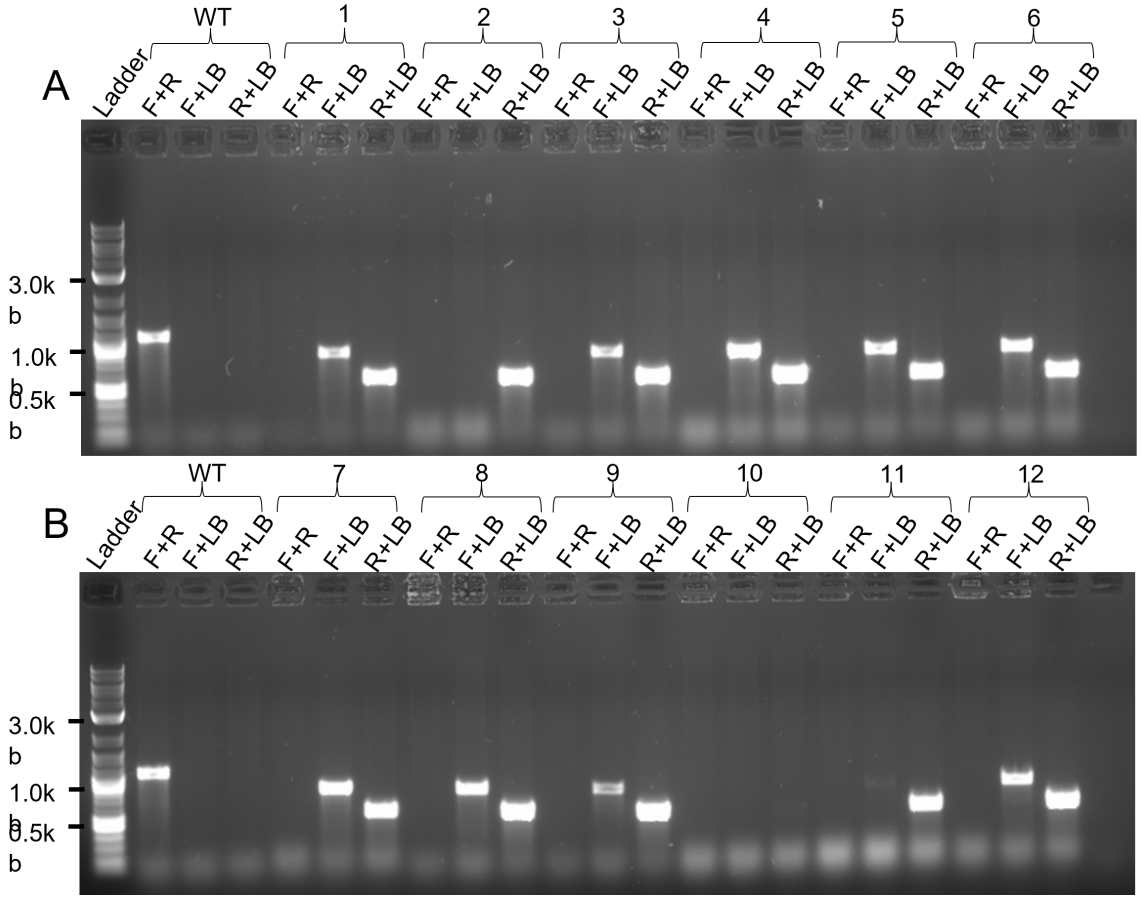

Figure 3.17: Genotyping of xth23 mutants using the forward(F), reverse (R and the T-DNA specific left border (LB) primers. WT F+R had a predicted product length of 1200bp and the F+LB and LB+R should not produce a product. The *xth23* mutant were not expected to produce a product for the F+R reaction but were predicted to produce bands of 800 and 500 bp for the F+LB and LB+R respectively.

RT-PCR of the *Arabidopsis xth23* Mutant Line

RT-PCR was carried out on two samples of *xth23* mutants and two of Col-0 to determine whether the *xth23* mutant line was a knockout. Two primer sets were used and the forward primer in both spanned an exon-exon junction to exclude any contaminating g-DNA. The results are displayed in Fig. 3.18. If the *xth23* mutant line was a knockout it would be expected that *RT*-PCR would not produce a band and Col-0 would. The positive control EF1α was expected to produce bands for all the

samples as EF1α should be expressed in both Col-0 and *xth23*. Both primer set 2 and 3 produced PCR products of the expected sizes, 500bp and 350bp respectively, for all the samples. This indicates that apparently *AtXTH23* transcripts, or equivalent PCR products, possibly from homologues, were present in the knockouts

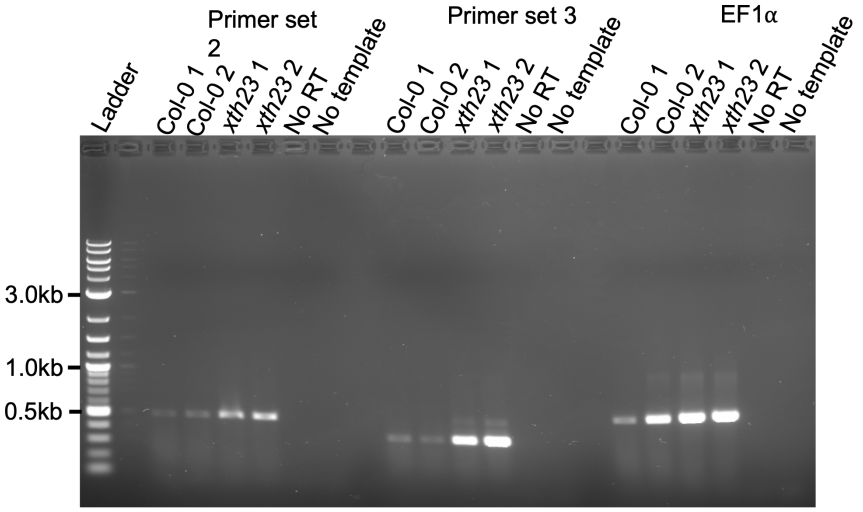

Figure 3.18: *RT*-PCR of *xth23* mutants and Col-0. For primer set 2 the expected band size if transcript was present was 500bp and for primer set 3 it was 350bp. The two negative controls used were no RT which contained no reverse transcriptase and no template which did not contain any CDNA.

XTH23 Arabidopsis Complimentation Lines

To create complimented Arabidopsis lines with the genes *AtXTH23* and *TaXTH23* Col-0 and xth23 mutants were transformed by floral dipping with *A. tumefaciens* containing the constructs p35S::*TaXTH23*::GFP and p35S::*AtXTH23*::GFP. Positive transformants were selected for using the herbicide BASTA, grown to seed and the seeds collected. Resulting Arabidopsis complimentation lines were: Col-0 (p35S::*TaXTH23*::GFP), Col-0 (p35S::*AtXTH23*::GFP), *xth23*(p35S::*TaXTH23*::GFP) and *xth23* (p35S::TaXTH23::GFP).

Transient Expression of *TaXTH23* in Tobacco

To investigate the localisation of *TaXTH23* samples of tobacco leaves agroinfiltrated with the constructs p35S::*TaXTH23*::GFP, p35S::*AtXTH23*::GFP, p35S::*TaXTH23*::RFP

and p35S::AtXTH23::RFP were viewed under an epifluorescence microscope. The transformation rate was very low and the localisation of either XTH23 could not be confidently determined. The low transformation rate and a slow growth rate of the transformed Agrobacterium indicated that the Agrobacterium from the glycerol stocks had been damaged.

Chapter 4

Discussion

4.1 Uprooting of Wheat Seedlings as an Assay for Identifying Traits which Influence Soil Erosion Rates.

To date, little work has been done to identify crop species' root traits, which can increase root-soil cohesion and reduce soil erosion rates. So far work has focused on the model species *A. thaliana* or inter species comparisons. This has identified traits such as root hairs and lateral roots as important in root-soil cohesion but whether these are transferable to crop species such as wheat is unclear [16, 28, 35]. In wheat, studies using hydroponically grown plants have identified polysaccharides in wheat root exudates which can increase soil particle adhesion [32, 34]. Here, I propose a novel uprooting assay for wheat which may be a useful method for measuring the effects of wheat root traits on root-soil cohesion and validate the use of the model species *A. thaliana* in root-soil cohesion studies.

The uprooting of wheat seedlings at different growth stages showed that the uprooted soil per root length stayed the same until GS13 when it drastically increased (fig. 3.7). This matches previous studies into root-soil cohesion which have found an exponential relationship between RLD and uprooted soil or soil erosion in *A. thaliana* [16, 25, 28]. The large increase in uprooted soil per root length at GS13 could reflect the increase in RLD. However, GS11 and GS13 had more similar root architecture, with long lateral roots, than GS10 and GS11 (fig.2.3.4). Hence, changes in root exudate composition rather than architecture could be responsible for the large increase in uprooted soil per RL. In the context of soil erosion, this could suggest that at GS10 and GS11 the soil is much more vulnerable to erosion than at GS13 as the root cannot bind as much soil per RL.

This work also found a positive correlation between RLD and uprooted soil mass at GS11 and GS13 (fig. 3.9), and a positive correlation between RL and uprooted soil mass at GS10 (fig.3.8). This relationship is probably due to seedlings with higher RL and RLD having a longer root system with more root hairs, lateral roots, and surface area for secreting adhesive exudates all of which help to enmesh more soil. The degree to which individual traits contribute to the amount of soil uprooted will require further investigation using mutant lines such as those discussed in section 4.2.

Limitations of the Uprooting Assay

There are a several limitations to the uprooting assay. Uprooting wheat seedlings could provide a useful proxy for determining root-soil cohesion and potentially the effect of roots on soil erosion rates. Whether the amount of soil adhered to the roots in uprooting correlates with soil erosion rates is yet to be tested. This could be confirmed by future field and hydraulic flume experiments. Secondly, the uprooting methods developed are only appropriate for wheat seedlings up to approximately two weeks old as older plants become too large for the anchor and become pot-bound. Therefore, using this assay to assess traits that could reduce soil erosion rates may not transfer to older plants in the field, as root architecture and exudate composition change over the course of the plant's life. However, the soil is particularly vulnerable to erosion during the early stages of wheat growth, when surface cover is the lowest [21]. Thus, an assay which determines wheat seedling root-soil cohesion may be of a higher priority than one that measures it in mature plants, which can reduce soil erosion with their leaves by breaking the fall of raindrops. Thirdly, to maintain consistent soil moisture across pots and replicates, the pots were saturated with water the night before. This may elicit a stress response from the wheat seedlings before uprooting, which may include a change in exudate composition. Changes in exudate composition and XTH activity have been shown to happen under drought conditions and could in turn determine root-soil cohesion [36, 58].

Optimising the Uprooting Assay for Wheat

The relationship between uprooted soil mass RL and RLD were consistent across replicates and previous studies, though did not always produce significant results. This probably reflects the small sample size for some of the replicates and the high amount of background noise. The methods used did reproduce, a positive correlation between RLD and uprooted soil mass and a consistent uprooted soil per root length for each growth stage (fig. 3.9 and fig. 3.7), across replicates the methods may need further optimising to reduce the background noise and the effect of any confounding factors. Root systems are highly sensitive to their environment and plastic. They can

change in response to very small variations in moisture content and soil compaction. These confounding factors are hard to control particularly soil compaction, which may have become varied due to the disturbance caused moving the plants to the Instron machine and attaching the wires to the clamp. Soil moisture could also have varied, particularly at GS13, due to the formation of the soil cap and spraying which may also have altered the soil compaction.

There are a few aspects which could still be optimised for uprooting wheat. Firstly, the success rate of uprooting for GS11 and GS13, as there were a significant number of failed uprooting runs, which reduced the sample sizes. The uprooting success rate did however generally increase over the replicates, suggesting there may have been some level of human practice involved. For maximum throughput, future uprooting experiments could use GS10 which can be uprooted just five days after planting and successfully uproots 100% of the time (Table. 3.6). However, these seedlings have not yet developed lateral roots or a root-soil ball. It is likely that at GS10 just the rhizosheath is being uprooted. This would indicate that the seedlings had not yet established a root-soil matrix beyond the rhizosheath. Thus, in the context of soil erosion, I believe uprooting at later growth stages, GS11 and GS13, when a root-soil matrix has formed are more relevant. To increase successful uprooting for GS11 and GS13 I suggest using larger pots, reducing the amount cut off the end of the modified pipette tip and developing a method to reduce the soil cap at GS13. Reducing the soil cap could be done using a mulch or plastic soil cover.

The second aspect which could be optimised is reducing background noise in the uprooting assay as it was relatively high, indicated by the low R2 values reported in Figures 3.8 and 3.9. The large variation was probably due to the difficulty in getting consistent soil compaction and moisture content across pots. Soil moisture content was particularly an issue at GS13 as the soil had developed a hard dry soil cap which had to be sprayed with water to uproot the plants. Future work could use film or plastic covers over the soil to prevent water from evaporating and thus maintain a more even soil moisture content. I also suggest that the seedlings be transported to the Instron machine the day before uprooting and prior to soaking as the dry soil holds its structure better than soaking wet soil. This would prevent uneven soil compaction between pots and allow all the plants to acclimatise to the new environment at the Instron machine.

Future Application of the Wheat Uprooting Assay

The uprooting assay has many potential applications. These could include 1. studying the effects of different physical influences on root-soil cohesion such as soil type; 2. testing biological determiners of root-soil cohesion such as tensile strength, root architecture and exudate composition; 3. The effects of abiotic and biotic stresses

and 4. application to other cereal crops with similar seedling morphology such as barley. Work by Thomas Denbigh [25], De Baets et al.[16] and Bailey et al.[28] layout methods for the use of uprooting forces, peak force and work done, which can be measured by the Instron machine.

Future work should also determine whether there is a link between root-soil cohesion in uprooting and reduced soil erosion rates. This could be done using the hydraulic flume assay and field trials [13, 16, 21].

4.2 Breeding Mutant Wheat Lines

Mutant lines are very important in characterising the function of genes; by linking a mutation in a gene to a phenotypic change in the mutated organism. There are multiple ways to generate mutant lines: insertional mutagenesis; RNAi, genetic modification using nucleases such as CRISPR, TALENs and zinc finger; and using mutagens. TILLING and deletion lines contain many mutations caused by either chemical or radiation mutagenesis. They are cheap and accessible with known mutations in genes of interest, making them a useful tool in both forward and reverse genetics [69, 77], especially in species where agroinfiltration is not possible. Wheat's large genome and high copy number also make insertions mutagenesis and genetic modification by nucleases inefficient [69, 77, 78]. Other benefits of mutagenesis include, mutations are stable, unlike in RNAi; TILLING lines have a range of mutation types, including a gain of function and it is not classed as genetic modification, which is highly regulated. This work utilised TILLING and deletion line collections of *T. aestivum* to develop mutant lines for the ABC transporter *TaATH6* and the xyloglucan endotransglycosylase *TaXTH23*.

Generating Mutant lines

This work found that neither *TaATH6* nor *TaXTH23* exhibited homeolog expression bias so to generate useful mutant lines all three homeologs needed to be knocked out (Fig. 3.1). The data for the expression plots was taken from across tissues, giving a general idea of each homeologs expression. Given that the expression of each homeolog was similar across all tissues it is highly unlikely that one of the homeologs is not expressed at all in the roots. TILLING lines for *TaATH6* were selected that had mutations in each homeolog and genotyped using Sanger sequencing. This identified double homozygous mutants for the B and D homeologs and a homozygous mutant line for the A homeolog of *TaATH6*. These lines were crossed to generate F2 triple heterozygous seeds (Fig.3.3, Table.3.2, Table.5.1).

As there were no TILLING lines available with STOP gained mutations in all three

TaXTH23 homeologs, deletion lines were used instead. All the lines contained mostly homozygous plants for the expected deletion, except for one individual (Fig. 3.2). The lines were then crossed to produce F2 double heterozygous mutants (Fig.2.2).

Limitations of TILLING and Deletion Lines

The main negative factor against the use of TILLING and deletion lines in determining gene function is the many off-target mutations they contain. In TILLING lines, the average number of mutations was 5000, which is approximately 35-45 per kilobase [79]. However, most of these off-target mutations are missense or silent mutations. Silent mutations change the codon but not the amino acid sequence of the translated protein and therefore will not affect the phenotype, whereas missense mutations will change just one amino acid in the protein sequence which may not change the function of the protein and therefore also not result in a change in phenotype. Nonsense mutations cause an early STOP codon resulting in a truncated protein. Off-target missense and nonsense mutations in TILLING lines can potentially disrupt genes essential in growth and development leading to plants with reduced fecundity. They could also affect genes involved in a similar function to the gene of interest, making it harder to determine the cause of the mutant phenotype. However, redundancy between the multiple copies of genes in the wheat genome is likely to mask the effects of off-targets on the plant's phenotype. Despite the potential interference of off-targets, TILLING lines remain very useful and have aided in the identification of several agronomically important alleles in wheat, including WAXY that influences grain quality and Yr6 which confers resistance to the pathogen yellow rust [69].

Off-targets are much more of a problem in deletion lines than TILLING as whole sections of chromosomes are missing, meaning that many genes are simply not present. The complete lack of so many genes in deletion lines often results in progeny with reduced fecundity. Deletion lines are also useful in locating genes on the chromosome as it reduces the size of the chromosome and hence the number of potential candidates [77]. Deletions can also result in the removal of closely related genes which have some redundancy with the gene of interest. For instance, in this work, the deletion line J4-64 was used, which had *TaXTH23* B homeolog deleted however it also had the gene *TaXTH19* deleted which has also been shown to influence root-substrate cohesion in *A. thaliana* [51]. If there is redundancy between *XTH23* and *XTH19* any resulting mutant phenotype of the lines could be down to the deletion of both or either *TaXTH23* or *TaXTH19*. The successive rounds of crosses and back-crosses though could breed out *TaXTH19*, but the two genes are very close on the chromosome.

The effects of off-targets should be mitigated by using sister lines as controls instead of WT and successive generations of back-crossing with a non-mutant parental line, the mutant lines developed in this work add to a growing number of wheat

mutant lines with altered root traits. So far, in wheat, only a handful of genes involved in root system architecture have been formally identified. These genes include *VERNALIZATION 1*, which influences root angle; Enhanced *GRAVITROPISM 2*, which results in a narrower angle of lateral root growth; *TaARF4*, which determines primary root growth and *TaLAMP1* and *TaTRIP1*, which influence meristem size [80]. The mutant lines developed in this study could add to this list and provide more opportunities for wheat breeders to enhance root traits for reduced soil erosion. However, more crossing is needed to generate full knockout mutants.

Future Work: Breeding Wheat Mutant Lines

Full knockout wheat lines for the genes *TaATH6* and *TaXTH23* are still a few generations away. For *TaATH6* the next step is to sow the F1 seeds collected in this study, which should be triple heterozygotes, and allow them to self-pollinate (Fig. 2.1). The progeny, F2, should be 1/64 triple homozygous knockout mutant for *TaATH6*. To identify these individuals, the F2 generation will need to be genotyped by sequencing, using the primers and conditions laid out in this work (section 2.1.3).

As TILLING lines contain many background mutations outside of the gene of interest, which may affect the plant's phenotype, the background mutation load needs to be lowered or accounted for. This can be done by 1. using multiple independent lines; 2. back-crossing with a non-mutagenized parent; 3. selecting isogenic sibling lines to use as a comparison in phenotyping rather than a non-mutagenized parent [71]. It is recommended, for mutations with subtle phenotypic effects, that lines should be back-crossed to a non-mutagenized parent at least twice [71]. Hence, *Taath6* mutant line should be back-crossed out to reduce the chance that any observed phenotype is due to *Taath6* rather than a background mutation. Further genotyping to screen for triple heterozygous mutants will be needed for each round of back-crossing. The successive back-crossing will lead to the generation of *ath6* near-isogenic lines (NILs) that can be used to investigate the function of *TaATH6*.

This work also identified deletion lines which were lacking one of the *TaXTH23* homeologs and crossed them to produce *TaXTH23* double heterozygous mutants with the genotypes AaBbDD and AABbDd. These two new lines will need to be crossed to produce an F2 segregating population from which AabbDd individuals will need to be identified by genotyping. These individuals can then be left to self-fertilise and should produce 1/16 triple homozygous mutants, aabbdd (fig.2.2). As with the TILLING lines, the deletion lines progeny should also be backcrossed for multiple generations with non-mutagenized plants, to reduce the background mutation load.

As previously discussed, deletion lines can have many genes missing of which some can be essential for plant development. As the different lines contain different background deletions, the progeny of each successive cross accumulates more deletions

increasing the chances of the progeny not functioning normally. Thus, it may not be possible to get a triple homozygous knockout for *TaXTH23* which is not affected by the background deletions and has normal development using deletion lines. In this scenario, double mutants may have to suffice or use different methods to generate a knockout mutant, such as CRISPR.

Future Work: Phenotyping Wheat Mutant lines

Once mutant lines have been fully developed the next step is to phenotype them [69]. Phenotyping the wheat mutant lines may be hard as the effects of the genes cannot be directly observed like genes involved in root architecture. The *A. thaliana* orthologs of *TaXTH23* and *TaATH6* are proposed to influence exudate composition and root-substrate cohesion [35, 51]. Hence phenotyping should focus on determining whether these mutants altered exudate composition and function. Phenotyping the wheat mutant lines may be hard as the effects of the genes cannot be directly observed unlike genes involved in root architecture. However, there is a variety of methods which could be deployed to do this. Firstly, root morphological traits such as root hair density and length, the density of lateral roots and RLD should be examined and compared to WT. This should determine whether the mutants have altered root architecture which affects root-soil cohesion. If there is no difference between WT and the mutants, then any mutant phenotypes in root-soil cohesion are down to exudate composition and not architecture. This is particularly relevant for the *Taxth23* mutant as in *A. thaliana Atxth23* mutants have been shown to have altered lateral root development [63].

The composition of exudates secreted by the mutant plants could be collected from hydroponically grown plants and analysed following methods in Eldridge *et al.*, [35] for *Taath6* lines and Galloway *et al.*[34] for the *Taxth23* lines. The collected exudates could also be used in nitrocellulose sheet-based soil cohesion assays laid out in Akhtar *et al.* [32], and Galloway *et al.*[34] to determine whether the exudates have altered adhesion properties.

Hydroponically growing plants change many of the stresses on roots. In response, plants may change their root architecture and exudates. Thus, whether studies using hydroponically grown plants have any relation to root-soil cohesion in the field is debatable. The uprooting assay, as laid out in this work, uses soil-grown plants and therefore is a better proxy for root-soil cohesion in the field. To investigate whether these *TaXTH23* and *TaATH6* influence root-soil cohesion and soil erosion rates mutant *Taath6* and *Taxth23* lines could be subjected to the uprooting assay and/or the hydraulic flume assay [13, 21].

4.3 Expression of *XTH23* in Model Species

Enhancing crop performance through improved root traits in the cereals has focused on root system architecture (reviewed in [80]). More recently, work is beginning to elucidate the important role of root exudates in a number of functions from microbiome modification, communication, soil stability and water and nutrient uptake. This work aimed to characterise the *A. thaliana* root exudate XTH23 wheat ortholog, *TaXTH23*, as *AtXTH23* has been shown affect root substrate cohesion [51]. To investigate whether the wheat ortholog functioned the same as the *A. thaliana* one, *TaXTH23* was cloned and transiently and stably expressed in model plant species.

Generating Complimentation Lines

Col-0 and *xth23* lines were successfully transformed by agroinfiltration with *p35S::TaXTH23::GFP* and *p35S::AtXTH::GFP*. This generated four new lines; two *xth23* complimented lines with either the wheat or *A. thaliana XTH23* transgene and two over expressing lines, Col-0 background, with either the wheat or *A. thaliana XTH23* transgene. T2 seeds were produced, which should be segregating for the transgenes. Thus, further work is needed to generate fully homozygous populations for each transgene. The T2 seeds should be grown up and genotyped to identify homozygous *35S::XTH23::GFP* plants. The homozygous *XTH23* plants should be selfed and the T3 seeds collected. The T3 generation should all be homozygous for the *XTH23* transgene and should be genotyped to check that no cross pollination has occurred and bulked to generate homozygous transgene *XTH23* populations. Since, *XTH23* has been shown to be involved in lateral root development in *A. thaliana* [63], and lateral roots effect root-substrate cohesion [16, 35], the root phenotypes of the lines should be carefully compared to WT before any assays are undertaken.

Future Work: Localisation of the TaXTH23 Protein

The complimented lines generated could be used to investigate the role of *TaXTH23* in root-substrate cohesion using both the centrifuge assay and the uprooting assay[16, 28, 35]. In both the centrifuge and the uprooting assay, if *TaXTH23* compliments I would expect that the *TaXTH23* transgene would rescue the *xth23* mutant phenotype and the *xth23 TaXTH23* complimented line would have a detachment force and soil adhesion phenotype similar to WT and significantly less than the *xth23* mutant line.

The localisation of *AtXTH23* and *TaXTH23* could also be examined using the complimented lines generated and epi-fluorescent microscopy as both the *XTH23*s have been tagged with GFP. This would also confirm that the transgene constructs are being expressed and are responsible for any changes in phenotype observed. The

localisation of *TaXTH23* has not yet been determined however work by Xu *et al.* [63] used *pro::AtXTH23::GUS* fusions to investigate its role in lateral root development. They found that at an organ level *AtXTH23* is localised in the primary root, lateral root primordium and continues to be expressed in the mature lateral root. If *TaXTH23* is a functional ortholog of *AtXTH23* it would be expected to also be expressed in these organs. To determine the organs *TaXTH23* is expressed in using a reporter gene the constructs developed in this work could not be used as *TaXTH23* has been fused to the constitutive promoter CaMV35S and thus would be expressed in all tissues.

At a cellular level, wheat XTHs localisation has not yet been investigated. Their activity in abiotic stress conditions has been investigated broadly in Iurlaro *et al.* [58]. In *A. thaliana* work by De Caroli *et al.* [81] used *GFP* to tag *AtXTHs*, confirming the final localisation of *XTH11, XTH33* and *XTH29*. These XTHs localised to the cell wall or the plasma membrane. Cell membrane associated *XTHs* had trans membrane domains whereas cell wall ones did not. Gene sequence analysis could determine whether *XTH23* has a trans membrane domain and would therefore, likely be localised to the cell membrane. However, I think this is unlikely as *XTH23* was identified in*A. thaliana* root exudates and so is probably not tethered to the cell membrane.

The transformed *A. tumefaciens* glycerol stocks in this work were slow growing and did not result in high transformation rates of tobacco pavement cells. Therefore, to investigate the localisation of *TaXTH23* in tobacco, the glycerol stocks of *A. tumefaciens* containing the constructs *p35S::TaXTH23::GFP* and *p35S::AtXTH23::GFP* should be streaked out onto selective agar plates containing appropriate antibiotics. Positive colonies can be used for over night cultures to transform tobacco following the methods in section 2.3.6.

Limitations of Transgene Expression

Transient and stable expression of transgenes in model organism is a useful way of determining gene function. However, it only gives a limited scope as gene expression can be highly nuanced. Gene expression is controlled by a multitude of biotic and abiotic factors resulting in specific temporal and spacial expression patterns. By using non-native promoters, such as CaMV35S used in this work, and model organisms the nuanced patterning is lost. Thus, using model species and the CaMV35S promoter can only give limited information about the function and localisation of *TaXTH23*. Furthermore, tagging with GFP or RFP can disrupt the proteins function and trafficking. Future work could transform wheat protoplasts with *p35S::TaXTH23::GFP* using the gene gun to create a better picture of *TaXTH23*'s localisation in wheat. The native promoter could also be used instead of the CaMV35S but this may not give high enough expression levels to visualise the localisation of the protein. Work by

Xu *et al.* [63] however did use *XTH23*'s native promoter and managed to visualises its expression pattern on an organ level using the GUS reporter gene.

Limitation of *A. thaliana xth23* Mutant Line

To ensure that any change in phenotype seen is due to a transgene and not the endemic gene, transgenes complimentation lines should be in a full knockout back ground. This work used T-DNA insertion line GK-219B02, which was thought to be an *xth23* knockout mutant. However, *RT*-PCR revealed that the line was not a full knockout, as it still produced transcript (Fig.3.18). This may be the T-DNA insertion is right at the end of the gene allowing transcription of an almost complete mRNA (Fig. 3.16). Shortened *XTH23* mRNA could potentially lead to the translation of a truncated but functioning *XTH23* protein which would then contribute to the phenotype of the complimentation lines suggested in this work. However, the *xth23* line used still had a strong mutant phenotype in the centrifuge assay [51] and therefore, may produce transcript but not functioning XTH23 protein, resulting in the increased adhesion phenotype of the line. Thus, the complimentation lines generated are useful, despite the presence of *XTH23* transcript, if alternative knockout lines cannot be found or as a preliminary indication of a role for *XTH23* in root-substrate cohesion.

Another issue from the location of the T-DNA insert in GK-219B02 is that it may also disrupt the gene downstream of *XTH23* which happens to be another *XTH* (*XTH14*). Though not yet associated with root-substrate cohesion, *XTH14* may play a role as *XTH*s can have some redundancy between genes. To ensure that the T-DNA insert in GK-219B02 does not disrupt the transcription of *XTH14*, RT-PCR could be carried out on the *xth23* GK-219B02 line using *XTH14* specific primers.

Summary Transgene Expression of XTHs

To date no transgenes from a crop species have been tested in the *A. thaliana* centrifuge or uprooting assays. This work provides complimentation lines which could be used in both and validate them as useful tools in identifying orthologs of genes involved in root soil cohesion in crop species. This work also provides constructs containing both the *AtXTH23* and *TaXTH23* tagged with GFP or RFP and under the constitutive promoter CaMV35s. These constructs can be used to transform model species and wheat protoplasts to investigate the localisation and transport of XTH23.

4.4 Conclusions

In this work I set out to develop a novel root-soil cohesion assay for wheat, develop mutant wheat lines for genes potentially involved in root-soil cohesion and to char-

acterise the wheat gene *TaXTH23*. I succeeded in developing methods to measure root-soil cohesion in wheat by uprooting, which revealed a positive correlation between RL/RLD and uprooted soil mass. The uprooting assay also revealed that uprooted soil per RL is consistent until GS13. Mutant lines were also generated by crossing TILLING and deletion lines. This generated partial knockouts for the genes *TaATH6* and *TaXTH23*. The *TaXTH23* was further investigated and it and its *A. thaliana* ortholog *AtXTH23* were cloned. The expression clones constructed by Gateway cloning can be used to transform model plant species to further investigate *TaXTH23*s function at a cellular level or in the centrifuge assay [35]. The development of the uprooting assay for wheat will help phenotype root-soil cohesion mutants, identifying genes which may aid in reducing soil erosion rates. This has implications for wheat breeders trying to enhance crops and sustainable agriculture through root traits.

Chapter 5

Appendix

Table 5.1: Summary of Sanger sequencing results for Cad0110, Cad0679 and Cad1704 D homeolog.

Line	Target homeolog	Plant	Base	Genotype
Cad1704	D	1	T	hom - M
		2	C	hom - WT
		3	C	hom - WT
		4	C	hom - WT
		5	C	hom - WT
		6	C	hom - WT
		7	T	hom - M
		8	C/A	het
		9	C	hom - WT
		10	T	hom - M
		11	C/A	het
		12	C	hom - WT
Cad0110	A	1	A	hom - M
		2	A	hom - M
		3	A	hom - M
		4	A	hom - M
		5	A	hom - M
		6	A	hom - M
		7	A	hom - M
		8	A	hom - M
		9	A	hom - M
		10	A	hom - M
		11	A	hom - M
		12	A	hom - M
Cad0679	A	1	G	hom - WT
		2	G	hom - WT
		3	G	hom - WT
		4	G	hom - WT
		5	G	hom - WT
		6	G	hom - WT
		7	G	hom - WT
		8	G	hom - WT
		9	G	hom - WT
		10	G	hom - WT
		11	G	hom - WT
		12	G	hom - WT

Base = the nucleotide at the expected mutation locus, Hom= homozygous, het= heterozygous, M= mutant and WT= wild type.

Table 5.2: Trouble shooting, a table of the common problems that occurred in the development of the uprooting assay for wheat and suggested reasons and solutions.

	Problem	Solution
Pre uprooting	Make the hole smaller by cutting less off the tip	Ensure that the brush end of the seed is pointing up when the seed is placed into the pipette tip
		Ensure that the seed is not tightly wedged into the pipette tip by gentley tapping the seed into place.
	Low germination rate - drying out seeds	Imbibe the seeds for 4 days in the dark at 4 degrees celsius
		Use a spray bottle to reguarly mist the seeds before and after they have germinated
	Seedlings going mouldy	The seed is probably in a water droplet, stop or reduce misting
	Roots becoming pot bound	Use larger pots or uproot at an earlier growth stage
	Soil cap formation	Use cling film or a light plastic cover on top of the soil to prevent water evaporating
		Spray soil 6 times with water from a distance of 20cm
Uprooting	Soil colapse	Reduce movement before uprooting, especially any shaking when transporting
		Remove excess water before transport to the Instron machine
	Pot coming up with the plant	The roots are probably pot bound - see roots becoming pot bound
		Use a clamp to hold the pot inplace during uprooting
	Soil balancing ontop of the root ball	Stop uprooting and exclude the run
		This is probably due to the upper layers of soil not being saturated with water
	Plants are not uprooted with the pipette tip	Make the hole for the roots smaller by cutting less off the pipette tip

Bibliography

1. Pimentel, D. & Burgess, M. Soil erosion threatens food production. *Agriculture (Switzerland)* **3.** ISSN: 20770472 (2013).
2. Lal, R. Soil Degradation by Erosion. *Land Degradation & Development* **12,** 519–539 (2001).
3. Ola, A., Dodd, I. C. & Quinton, J. N. Can we manipulate root system architecture to control soil erosion? *Soil* **1,** 603–612. ISSN: 2199398X (2015).
4. Eekhout, J. P. & de Vente, J. Global impact of climate change on soil erosion and potential for adaptation through soil conservation. *Earth-Science Reviews* **226.** ISSN: 00128252 (Mar. 2022).
5. Borrelli, P. *et al.* Land use and climate change impacts on global soil erosion by water (2015-2070). *Proceedings of the National Academy of Sciences of the United States of America* **117.** ISSN: 10916490 (2020).
6. Ray, D. K., Mueller, N. D., West, P. C. & Foley, J. A. Yield Trends Are Insufficient to Double Global Crop Production by 2050. *PLoS ONE* **8.** ISSN: 19326203 (2013).
7. Foley, J. A. *et al.* Solutions for a cultivated planet. *Nature* **478.** ISSN: 00280836 (2011).
8. Rockström, J. *et al.* A safe operating space for humanity. *Nature* **461.** ISSN: 00280836 (2009).
9. Graves, A. R. *et al.* The total costs of soil degradation in England and Wales. *Ecological Economics* **119,** 399–413. ISSN: 09218009 (Nov. 2015).
10. Posthumus, H., Deeks, L. K., Rickson, R. J. & Quinton, J. N. Costs and benefits of erosion control measures in the UK. *Soil Use and Management* **31.** ISSN: 14752743 (2015).
11. Hawkesford, M. J. *et al.* Prospects of doubling global wheat yields. *Food and Energy Security* **2.** ISSN: 20483694 (2013).

12. Zhou, Z. & Shangguan, Z. The effects of ryegrass roots and shoots on loess erosion under simulated rainfall. *CATENA* **70,** 350–355. ISSN: 03418162. https://linkinghub.elsevier.com/retrieve/pii/S0341816206002256 (Aug. 2007).

13. De Baets, S., Poesen, J., Gyssels, G. & Knapen, A. Effects of grass roots on the erodibility of topsoils during concentrated flow. *Geomorphology* **76,** 54–67. ISSN: 0169555X (June 2006).

14. Gyssels, G., Poesen, J., Bochet, E. & Li, Y. Impact of plant roots on the resistance of soils to erosion by water: A review. *Progress in Physical Geography* **29.** ISSN: 03091333 (2005).

15. Wang, J., Zhao, W., Liu, Y. & Jia, L. Effects of plant functional traits on soil conservation: A review. *Shengtai Xuebao* **39.** ISSN: 10000933 (2019).

16. De Baets, S. *et al.* Micro-scale interactions between Arabidopsis root hairs and soil particles influence soil erosion. *Communications Biology* **3.** ISSN: 23993642 (Dec. 2020).

17. Hao, H. x., Qin, J. h., Sun, Z. x., Guo, Z. l. & Wang, J. g. Erosion-reducing effects of plant roots during concentrated flow under contrasting textured soils. *Catena* **203,** 105378. ISSN: 03418162 (2021).

18. Xu, W. x., Yang, L., Bao, Y. h., Li, J. l. & Wei, J. Soil anti-scourability enhanced by herbaceous species roots in a reservoir water level fluctuation zone. *Journal of Mountain Science* **18,** 392–406. ISSN: 19930321 (Feb. 2021).

19. Ennos, A. R. The mechanics of anchorage in wheat. *Journal of Experimental Botany* **42.** ISSN: 00220957 (1991).

20. Edmaier, K., Crouzy, B., Ennos, R., Burlando, P. & Perona, P. Influence of root characteristics and soil variables on the uprooting mechanics of ¡i¿Avena sativa¡/i¿ and Medicago sativa seedlings. *Earth Surface Processes and Landforms* **39,** 1354–1364. ISSN: 01979337. https://onlinelibrary.wiley.com/doi/10.1002/esp.3587 (Aug. 2014).

21. Li, J., Zhang, F., Wang, S. & Yang, M. Combined influences of wheat-seedling cover and antecedent soil moisture on sheet erosion in small-flumes. *Soil and Tillage Research* **151,** 1–8. ISSN: 01671987 (2015).

22. Gao, J., Bai, Y., Cui, H. & Zhang, Y. The effect of different crops and slopes on runoff and soil erosion. *Water Practice and Technology* **15,** 773–780. ISSN: 1751231X (2020).

23. Vannoppen, W., Vanmaercke, M., De Baets, S. & Poesen, J. A review of the mechanical effects of plant roots on concentrated flow erosion rates (2015).

24. Burylo, M., Rey, F., Bochet, E. & Dutoit, T. Plant functional traits and species ability for sediment retention during concentrated flow erosion. *Plant and Soil* **353.** ISSN: 0032079X (2012).

25. Denbigh Thomas. *Root-Soil Cohesion: An Interdisciplinary Approach* PhD thesis (The University of Bristol, Bristol, 2018).

26. ENNOS, A. R. The mechanics of anchorage in seedlings of sunflower, Helianthus annuus L. *New Phytologist* **113.** ISSN: 14698137 (1989).

27. Fogelberg, F. & Dock Gustavsson, A. M. Resistance against uprooting in carrots (Daucus carota) and annual weeds: A basis for selective mechanical weed control. *Weed Research* **38.** ISSN: 00431737 (1998).

28. Bailey, P. H. J., Currey, J. D. & Fitter, A. H. The role of root system architecture and root hairs in promoting anchorage against uprooting forces in Allium cepa and root mutants of Arabidopsis thaliana. *Journal of Experimental Botany* **53,** 333–340 (Feb. 2002).

29. Toukura, Y., Devee, E. & Hongo, A. Uprooting and shearing resistances in the seedlings of four weedy species. *Weed Biology and Management* **6,** 35–43. ISSN: 1444-6162. https://onlinelibrary.wiley.com/doi/10.1111/j.1445-6664.2006.00192.x (Mar. 2006).

30. Burylo, M., Rey, F., Roumet, C., Buisson, E. & Dutoit, T. Linking plant morphological traits to uprooting resistance in eroded marly lands (Southern Alps, france). *Plant and Soil* **324.** ISSN: 0032079X (2009).

31. Mickovski, S. B. *et al.* Material stiffness, branching pattern and soil matric potential affect the pullout resistance of model root systems. *European Journal of Soil Science* **58.** ISSN: 13510754 (2007).

32. Akhtar, J., Galloway, A. F., Nikolopoulos, G., Field, K. J. & Knox, P. A quantitative method for the high throughput screening for the soil adhesion properties of plant and microbial polysaccharides and exudates. *Plant and Soil* **428,** 57–65. ISSN: 15735036 (2018).

33. Galloway, A. F. *et al.* Altered properties and structures of root exudate polysaccharides in a root hairless mutant of barley Research Article, 1–14 (2022).

34. Galloway, A. F. *et al.* Cereal root exudates contain highly structurally complex polysaccharides with soil-binding properties. *Plant Journal* **103,** 1666–1678. ISSN: 1365313X (2020).

35. Eldridge, B. M. *et al.* A Centrifuge-Based Method for Identifying Novel Genetic Traits That Affect Root-Substrate Adhesion in Arabidopsis thaliana. *Front. Plant Sci* **12,** 602486 (2021).

36. Vives-Peris, V., de Ollas, C., Gomez-Cadenas, A. & Perez-Clemente, R. M. Root exudates: from plant to rhizosphere and beyond. *Plant Cell Reports* **39,** 3–17. ISSN: 1432203X (Jan. 2020).

37. Sasse, J., Martinoia, E. & Northen, T. Feed Your Friends: Do Plant Exudates Shape the Root Microbiome? *Trends in Plant Science* **23,** 25–41. ISSN: 13601385 (Jan. 2018).

38. Naveed, M. *et al.* Plant exudates may stabilize or weaken soil depending on species, origin and time. *European Journal of Soil Science* **68,** 806–816. ISSN: 13652389 (Nov. 2017).

39. Schmid, N. B. *et al.* Feruloyl-CoA 6-Hydroxylase1-dependent coumarins mediate iron acquisition from alkaline substrates in Arabidopsis. *Plant Physiology* **164.** ISSN: 15322548 (2014).

40. Ahmed, M. A., Kroener, E., Holz, M., Zarebanadkouki, M. & Carminati, A. Mucilage exudation facilitates root water uptake in dry soils. *Functional Plant Biology* **41.** ISSN: 14454416 (2014).

41. Hu, L. *et al.* Root exudate metabolites drive plant-soil feedbacks on growth and defense by shaping the rhizosphere microbiota. *Nature Communications* **9.** ISSN: 20411723 (2018).

42. Bertin, C., Yang, X. & Weston, L. A. The role of root exudates and allelochemicals in the rhizosphere. *Plant and Soil* **256.** ISSN: 0032079X (2003).

43. Wang, N. Q., Kong, C. H., Wang, P. & Meiners, S. J. Root exudate signals in plant-plant interactions. *Plant Cell and Environment* **44.** ISSN: 13653040 (2021).

44. Galloway, A. F. *et al.* Xyloglucan is released by plants and promotes soil particle aggregation. *New Phytologist* **217,** 1128–1136. ISSN: 14698137 (2018).

45. Pandeirada, C. O., Achterweust, M., Janssen, H. G., Westphal, Y. & Schols, H. A. Periodate oxidation of plant polysaccharides provides polysaccharide-specific oligosaccharides. *Carbohydrate Polymers* **291.** ISSN: 01448617 (Sept. 2022).

46. Chaparro, J. M. *et al.* Root Exudation of Phytochemicals in Arabidopsis Follows Specific Patterns That Are Developmentally Programmed and Correlate with Soil Microbial Functions. *PLoS ONE* **8,** 1–10. ISSN: 19326203 (2013).

47. Fry, S. C. *et al.* Xyloglucan endotransglycosylase, a new wall-loosening enzyme activity from plants. *Biochemical Journal* **282.** ISSN: 02646021 (1992).

48. Nishitani, K. & Tominaga, R. Endo-xyloglucan transferase, a novel class of glycosyltransferase that catalyzes transfer of a segment of xyloglucan molecule to another xyloglucan molecule. *Journal of Biological Chemistry* **267.** ISSN: 00219258 (1992).

49. Ropitaux, M. *et al.* Xyloglucan and cellulose form molecular cross-bridges connecting root border cells in pea (Pisum sativum). *Plant Physiology and Biochemistry* **139,** 191–196. ISSN: 09819428 (June 2019).

50. Huang, Y. *et al.* Nanospherical arabinogalactan proteins are a key component of the high-strength adhesive secreted by English ivy. *Proceedings of the National Academy of Sciences of the United States of America* **113.** ISSN: 10916490 (2016).

51. Palumbo, V. A. *"We were all rooting for you!" Probing for protein exudates that influence root-substrate adhesion in Arabidopsis thaliana* PhD thesis (The University of Bristol, Bristol, 2021).

52. Badri, D. V. *et al.* An ABC transporter mutation alters root exudation of phytochemicals that provoke an overhaul of natural soil microbiota. *Plant Physiology* **151,** 2006–2017. ISSN: 00320889 (2009).

53. Banasiak, J. & Jasinski, M. ATP binding cassette ABC transporters in non model plants. *New Phytologist,* 1–3. ISSN: 0028-646X (2021).

54. Mahony Lucy. *Identifying genes associated with reduced soil erosion phenotypes in wheat* PhD thesis (The University of Bristol, Bristol, 2021).

55. Liu, Y. B., Lu, S. M., Zhang, J. F., Liu, S. & Lu, Y. T. A xyloglucan endotransglucosylase/hydrolase involves in growth of primary root and alters the deposition of cellulose in Arabidopsis. *Planta* **226.** ISSN: 00320935 (2007).

56. Yokoyama, R. & Nishitani, K. A comprehensive expression analysis of all members of a gene family encoding cell-wall enzymes allowed us to predict cis-regulatory regions involved in cell-wall construction in specific organs of Arabidopsis. *Plant and Cell Physiology* **42.** ISSN: 00320781 (2001).

57. Yokoyama, R., Rose, J. K. & Nishitani, K. A surprising diversity and abundance of xyloglucan endotransglucosylase/ hydrolases in rice. Classification and expression analysis. *Plant Physiology* **134.** ISSN: 00320889 (2004).

58. Iurlaro, A. *et al.* Drought and heat differentially affect XTH expression and XET activity and action in 3-day-old seedlings of durum wheat cultivars with different stress susceptibility. *Frontiers in Plant Science* **7,** 1–18. ISSN: 1664462X (2016).

59. Chen, F., Nonogaki, H. & Bradford, K. J. A gibberellin-regulated xyloglucan endotransglycosylase gene is expressed in the endosperm cap during tomato seed germination. *Journal of Experimental Botany* **53.** ISSN: 00220957 (2002).

60. Niraula, P. M., Lawrence, K. S. & Klink, V. P. The heterologous expression of a soybean (Glycine max) xyloglucan endotransglycosylase/hydrolase (XTH) in cotton (Gossypium hirsutum) suppresses parasitism by the root knot nematode Meloidogyne incognita. *PLoS ONE* **15.** ISSN: 19326203 (2020).

61. Witasari, L. D. *et al.* Higher expression of the strawberry xyloglucan endotransglucosylase/hydrolase genes FvXTH9 and FvXTH6 accelerates fruit ripening. *Plant Journal* **100.** ISSN: 1365313X (2019).

62. Vissenberg, K. *et al.* Differential expression of AtXTH17, AtXTH18, AtXTH19 and AtXTH20 genes in Arabidopsis roots. Physiological roles in specification in cell wall construction. *Plant and Cell Physiology* **46,** 192–200. ISSN: 00320781 (2005).

63. Xu, P., Fang, S., Chen, H. & Cai, W. The brassinosteroid-responsive xyloglucan endotransglucosylase/hydrolase 19 (XTH19) and XTH23 genes are involved in lateral root development under salt stress in Arabidopsis. *Plant Journal* **104,** 59–75. ISSN: 1365313X (Sept. 2020).

64. Shi, J. *et al.* Effects of wheat root exudates on bacterial communities in the rhizosphere of watermelon. *Plant, Soil and Environment* **67.** ISSN: 18059368 (2021).

65. Badri, D. V. *et al.* Altered profile of secondary metabolites in the root exudates of arabidopsis ATP-binding cassette transporter mutants. *Plant Physiology* **146,** 762–771. ISSN: 15322548 (2008).

66. Colbert, T. *et al.* High-Throughput Screening for Induced Point Mutations. *Plant Physiology* **126,** 480–484 (2001).

67. Edwards, K., Johnstone, C. & Thompson, C. A simple and rapid method for the preparation of plant genomic DNA for PCR analysis. *Nucleic Acids Research* **19.** ISSN: 03051048 (1991).

68. Schindelin, J. *et al.* Fiji: An open-source platform for biological-image analysis. *Nature Methods* **9,** 676–682. ISSN: 15487091 (July 2012).

69. Kurowska, M. *et al.* TILLING - a shortcut in functional genomics. *Journal of Applied Genetics* **52,** 371–390. ISSN: 12341983 (Nov. 2011).

70. Endo, T. R. & Gill, B. S. The Deletion Stocks of Common Wheat. *Journal of Heredity* **87,** 295–307 (1996).

71. Krasileva, K. V. *et al.* Uncovering hidden variation in polyploid wheat. *Proceedings of the National Academy of Sciences of the United States of America* **114,** E913–E921. ISSN: 10916490 (Feb. 2017).

72. Huang, S. *et al. Genes encoding plastid acetyl-CoA carboxylase and 3-phosphoglycerate kinase of the TriticumAegilops complex and the evolutionary history of polyploid wheat* tech. rep. (2002), 8133–8138.

73. Dubcovsky, J. & Dvorak, J. Genome Plasticity a Key Factor in the Success of Polyploid Wheat Under Domestication. *Science* **316,** 1862–1865. `https://www.science.org` (2007).

74. Barman, U. & Choudhury, R. D. Soil texture classification using multi class support vector machine. *Information Processing in Agriculture* **7,** 318–332. ISSN: 22143173 (June 2020).

75. Dane, J. H. *et al. Methods of Soil Analysis: Part 4 Physical Methods* (2018).

76. Amack, S. C. & Antunes, M. S. CaMV35S promoter: A plant biology and biotechnology workhorse in the era of synthetic biology. *Current Plant Biology* **24,** 100179. ISSN: 2214-6628 (Dec. 2020).

77. Serra, H., Svačina, R., Bartoš, J. & Sourdille, P. Generation of Deletion Lines in Allohexaploid Bread Wheat. *Methods in Molecular Biology* **2484,** 183–199. ISSN: 19406029 (2022).

78. Slade, A. J. & Knauf, V. C. TILLING moves beyond functional genomics into crop improvement. *Transgenic Research* **14,** 109–115. ISSN: 09628819 (Apr. 2005).

79. Mo, Y. *et al.* Mapping causal mutations by exome sequencing in a wheat TILLING population: a tall mutant case study. *Molecular Genetics and Genomics* **293,** 463–477 (2018).

80. Ober, E. S. *et al.* Wheat root systems as a breeding target for climate resilience. *Theoretical and Applied Genetics* **134.** ISSN: 14322242 (2021).

81. De Caroli, M., Manno, E., Piro, G. & Lenucci, M. S. Ride to cell wall: Arabidopsis XTH11, XTH29 and XTH33 exhibit different secretion pathways and responses to heat and drought stress. *Plant Journal* **107,** 448–466. ISSN: 1365313X (2021).